Theoretical Study of Non-Relativistic Electron Dynamics Under Intense Laser Fields

by

Zijian Long

A thesis
presented to the University of Waterloo
in fulfillment of the
thesis requirement for the degree of
Doctor of Philosophy
in
Physics

Waterloo, Ontario, Canada, 2012

I hereby declare that I am the sole author of this thesis. This is a true copy of the thesis, including any required final revisions, as accepted by my examiners.

I understand that my thesis may be made electronically available to the public.

Abstract

Strong field approximation (SFA) is the most important approximation in the analytical theory of intense laser matter interaction. Based on SFA many analytical theories have been developed such that a broad spectrum of strong field physics phenomena can be described. The central idea of SFA-based theories is to approximate the electron propagation in the continuum by the Gordon-Volkov wavefunction - a well studied analytical solution to the time-dependent Schrödinger equation where the electron is driven by the laser field only. This approximation captures some of the essential features of strong-field physics, but at the same time causes several problems in the theory. In this thesis a comprehensive study of the SFA has been presented. We introduce the SFA in both the length gauge and the velocity gauge. The adequacy of SFA has been discussed by comparing the theory to the numerical solution to the time-dependent Schrödinger equation (TDSE). The numerical method of solving TDSE is presented as a separate chapter.

In order to obtain a better understanding of the applicability of SFA-based theory, we tested the major approximations in the theory by using three different models: the zero-range potential, the hydrogen atom and the hydrogen molecular ion. The accuracy of the method of steepest descent (MSD) and other major approximations in the analytical theory have also been examined. Targeting at the generalization of the SFA-based theories, several extensions and improvements of SFA have been proposed. We will review them in detail and bring them into unity.

One of the most successful aspect of the SFA-based theories is to describe and decompose electron dynamics into components such that identification of different physical processes becomes possible. For instance, the direct ionization and non-sequential double ionization bear clear definitions only within the SFA-based framework. The physical interpretation becomes more straight forward due to the fact that there is a close connection between the quantum orbital and classical trajectory. The MSD is a mathematical tool to bridge the quantum orbital and the classical trajectory in an SFA-based theory. We will discuss MSD within a systematic framework so that the higher order asymptotic expansion terms can be obtained in a straight forward way.

After gaining substantial understanding of the SFA and the MSD we developed a graphic user interface (GUI) software that is capable of calculating strong field ionization rates, photo-electron spectra and high harmonic generation spectra. The software interface and algorithms have been presented in the thesis. Sample calculations were done and compared with the previously obtained results.

In the last chapter of the thesis, we further developed the theory to describe a two-laser ionization scheme where one laser is chosen to be resonantly coupled two real states and

the other is a strong few-cycle laser pulse. We demonstrate the periodic dependence of the total ionization on the appearance time of the strong few-cycle laser pulse. In the case of few-cycle pulses with lower intensity, we observed side-bands in the photoelectron spectrum, whose intensity vary periodically with the appearance time of the pulse. We show that our extended theory is able to explain these phenomena adequately.

Acknowledgements

This thesis could not have been written without the patient guidance of Professor Liu. He taught me strong-field physics as well as the rigorous attitude towards scientific research. During the time period of my study, I have been trying to understand the poorly documented theory of strong-field physics and run into many difficulties. Professor Liu offered me his notes on the derivation of the theory. His notes helped me building the missing links so that I can have a thorough understanding of the theory. He taught me self-criticism such that I can always find a way to improve the current result. At the same time I saw a spirit of rigor from his notes. Every step in the derivation should be built on well established mathematical foundation. In addition, Professor Liu patiently proofread my writings and made corrections to the grammar mistakes. He taught me how to organize the paragraphs and sentences. My writing skills have been improved significantly because of him.

I would also like to express my gratitude to Professor Marcel Nooijen. He taught me the fundamentals of quantum chemistry which turns out to be very important to my future research. Most importantly, his passion for science strongly influenced me. During the time period of my research there were several times that I lost motivation. So I joined lunch with him and had conversations about the problems. He helped me finding motivations and suggested new ideas for my research. I feel lucky to have Marcel as my committee member.

I would also like to express my gratitude to Professor Joseph Sanderson. He introduced me to his lab and we collaborated in several projects. Through collaboration, I saw the purpose of theoretical work and learnt many things about experiments. He offered me this good opportunity to do some calculations that are actually measurable in the experiments. He also gave me suggestions so that my theoretical model becomes more realistic.

I would also like to express my gratitude to Professors Zoran Milosevic and Chitra Rangan for patiently going over my thesis.

During the past seven years of my graduate student life I have met many wonderful friends. Sometimes I thought to myself how would my life be if without them. Miserable, it must be. The importance of my friends simply cannot be overestimated. After long time considering what should I thank them for, I found it is actually those little things that filled my memory. I remember watching plays with Poya, having dinner with Tianhua and singing karaoke with Dapeng. I also remember eating sushi with Sergey, cooking meal with Denys and playing board-game with Wuyang. There are too much memories to be listed here. It is these memories that outlined the 10-years of my Waterloo life. I would like to thank my friends who accompany me during my student life.

Dedication

To my beloved family

Table of Contents

List of Tables

List of Figures

List of Acronyms

ATI	Above Threshold Ionization
CREI	Charge Resonance Enhanced Ionization
CW	Continuous Wave
DFT	Density Functional Theory
FFT	Fast Fourier Transform
G2M	Gaussian-2 Model
GF	Green's Fucntion
GUI	Graphic User Interface
HATI	High-energy Above Threshold Ionization
HFCW	High Frequency continuous Wave
HHG	High Harmonic Generation
HOMO	Highest Occupied Molecular Orbital
HOAO	Highest Occupied Atomic Orbital
LCAO	Linear Combination of Atomic Orbitals
LFFC	Low Frequency Few-Cycle
LG	Length Guage
LPEA	Low Photo-electron Energy Approximation
LPEANI	Low Photo-electron Energy Approximation Neglecting Interference
MO	Molecular Orbitals
MSD	Method of Steepest Descent
NSDI	Non-Sequential Double Ionization
PES	Photo-Electron Spectrum
PSD	Path of Steepest Descent
RWA	Rotating Wave Approximation
SAD-RC	SADdle point calculation with Residue Correction
SAEA	Single Active Electron Approximation
SFA	Strong Field Approximation
SFI	Strong Field Ionization
SPA	Saddle Point Approximation
TDSE	Time Dependent Schrödinger Equation
TIP	Two-photon Ionization Peak
VG	Velocity Gauge

Chapter 1

Introduction

Electron is first discovered by British physicist J.J.Thomson in the year of 1897 [1]. It is considered as an elementary particle that has definite mass and charge, but it does not possess any internal degrees of freedom. The electron mass is so tiny such that grouping trillions of trillions of electrons together can not even change the readings on a bathroom scale. The charge it carries is so little that when trillions of electrons passing through your finger tip in a second you can barely feel anything. It is hard to imagine the electron with such an insignificant appearance plays the most significant role in the modern technology. In fact, any further understanding of the electron properties may lead to a technology revolution. For example, in the past several decades people have witnessed the revolution of the electronic industry. The central technology of the revolution - integrated chip, is developed based on the deep understanding of electron transport properties in the semiconductor materials. The rapid development of modern chemical industry is also based on the comprehensive understanding of the electronic structure of the atoms and molecules. Through *ab initio* calculations people start to understand why the atoms bond to form molecules, what information can be retrieved from the atomic molecular spectra and how people can control the chemical reactions by altering the electronic states using light. It is exactly this thorough understanding of the electronic structure that helped people to design new materials that can do the job never could be imagined before, helped biologist to discover the very basic mechanism that life itself depending on, thereby tackling the ancient philosophical questions from a scientific perspective.

The understanding process will never reach an end. Rapid development of light source technologies allow people to access more information in the atomic and molecular level and at the same time gaining substantial controllability of the electron motion. A great leap forward during this time period is the invention by Maiman [2] in 1960 - light amplification

by stimulated emission of radiation, better known as laser. This device provides a unique way of generating intense coherent light radiation which can be used as a tool to probe and control the electron motion. Quantum mechanics is the the theory that describes the interaction. It takes tens of genius minds several decades to sketch the outline of the theory; thousands of diligent scientists have been working on the details and the extensions. As the laser technology becomes more and more advanced, higher laser intensities and shorter pulse length can be achieved, thereby pushing the theory to a region that have never been encountered before. To understand where this trend will lead us, we should first briefly review the history of laser-atom interaction according to an increasing laser-intensity.

In the early days when the laser intensity is low, atoms respond linearly to the external laser fields. First order perturbation theory is commonly used to describe the laser-atom interaction. A generally accepted physical picture behind the theory is given by the following. Electrons initially occupied the field-free orbitals that possess discrete energy levels. When the laser is shone on the atom, the electron will make transition from one orbital to the other by absorbing/emitting one photon from/to the laser field. As a result the electron will be in a superposition of the field-free orbitals hence breaking the spacial symmetry of the charge distribution. Polarization is used to describe the response. In this particular case the polarization of atom can be written as a linear function of the electric field strength: $P(t) = \chi^{(1)}E(t)$, where the linear susceptibility $\chi^{(1)}$ only depends on the atom itself. One year after the invention of laser, Franken *et al.* discovered the second-harmonic generation which can be considered as the milestone that marks the beginning of nonlinear optics [3]. Sum-frequency and difference-frequency generations were observed in the experiments by Harris *et al.* in the late 1967 [4]. These are the second order nonlinear effects which can be described by adding the second order nonlinear susceptibility term to the polarization: $P(t) = \chi^{(1)}E(t) + \chi^{(2)}E^2(t)$. In this new picture, an atom can simultaneously interact with two photons such that coherent adding or subtracting photon frequencies becomes possible. Based on this new discovery people have invented new methods that can alter the laser frequency. For example Ou *et al.* used potassium titanyl phosphate crystal to double the laser frequency such that 85 percent conversion efficiency has been achieved [5]. Since then the laser spectrum can be extended to a much broader regime than before.

In the same year as the discovery of second-harmonic generation, Kaiser and Garret observed two-photon absorption which soon became a useful spectroscopic tool for determining the energy levels that are not accessible through one photon transition [6]. The Kerr electro-optic effect discovered by Scottish physicist John Kerr in 1875 can now be achieved using the laser field itself (optical Kerr effect). These phenomena are known as the third order nonlinear effects which can be fitted into the theoretical picture by adding a third or-

der nonlinear susceptibility term to the polarization $P(t) = \chi^{(1)}E(t)+\chi^{(2)}E^2(t)+\chi^{(3)}E^3(t)$. In the gas phase where the second term vanishes due to symmetry, we can express the total polarization as $P(t) = \chi^{(1)}E(t) + \chi^{(3)}E^3(t)$. The nonlinear refractive index is related to the susceptibilities by

$$n^2 = 1 + 4\pi \left(\chi^{(1)} + 3\chi^{(3)}|E_0|^2\right),$$

where E_0 is the laser field amplitude. Clearly it becomes an intensity-dependent quantity. The intensity-dependent refractive index has led to many interesting physics. Laser self-focusing and self-trapping in the medium were first demonstrated by Lallemand *et al.* in 1965 [7]. This new finding helped Spence *et al.* invent the Kerr-lens mode-locking which can be used to generate ultra-short femtosecond laser pulses; hence higher laser intensity can be achieved ($60fs$ in 1991) [8]. What we can see here is an alternating pattern of progress: a deep understanding of the laser-matter interaction helped people develop better laser technologies and then the improved laser systems can be used to gain further knowledge about laser-matter interaction. Of course this alternating progress will also urge the development in other fields. For example, laser beam filamentation were discovered as a result of irregularities initially present on the laser wavefront. The filamentation can induce fluorescence or breakdown which were proposed to be a potential candidate for remote sensing [9]. The optical bistability first proposed by Szöke *et al.* in 1969 and later observed in experiment by Gibbs *et al.* in 1976 may allow people to create all-optical switching devices for communication and computation [10].

From the theoretical point of view the perturbation theory has been very successful in explaining these nonlinear phenomena. Together with the rapid development of the theoretical methods for calculating the electronic structure, the perturbation theory has been used to predict the values of the nonlinear susceptibilities for varies kinds of materials [11]. However as the laser intensity grows higher ionization becomes significant, the conventional perturbation theory fails to explain the novel phenomena observed in the experiments. For instance the peak suppression phenomenon and the plateau region in the above threshold ionization spectrum clearly indicate the failure of the conventional perturbation theory [12]. Several non-perturbative theories have been proposed. They all have their advantages and disadvantages depending on the laser parameter region and the quantity that need to be calculated. One common feature for all the non-perturbative theories is the consideration of laser field after the electron is promoted to the continuum. This step which is also referred as the dressing of the continuum becomes essential to the theory of strong field physics. Gordon-Volkov solution of the electron in the presence of the external electric field has been discovered by Gordon [13] and Volkov [14] independently. Later in 1964 Keldysh proposed the strong field approximation which can be considered as a very effective way to embed the Gordon-Volkov solution into the quantum mechanical

S-matrix formalism. It is the combination of the Gordon-Volkov solution and the S-matrix formalism that forms the most widely used theory in strong field physics [15]. Because the theory is based on an S-matrix formalism, it has a great flexibility to be extended to other physical processes such as high harmonic generation and non-sequential double ionization.

The change from perturbative to a non-perturbative treatment leads to drastic change of the physical pictures. Because the number of photons involved in each transition becomes large, the quantization phenomena becomes less significant and the system can be considered as more classical-like. Within the transition region, one often finds that two completely different physical pictures may peacefully co-exist without any contradiction. For different parameter regions one can find one interpretation that is superior than the other. The crucial point is to define a proper parameter that will tell people when to use what picture.

In this thesis we will mainly focus on the non-perturbative theory that is based on the strong field approximation (SFA). The organization of the thesis can be summarised as follows:

In Chapter 2 we introduce the SFA-based theories in detail. A formal derivation of the S-matrix expansion is given and followed by the introduction of SFA in the length gauge and the velocity gauge. The comparison between the two gauges clearly indicates that SFA-based theories are gauge dependent. This is the most serious problem caused by SFA that does not have any general solution yet. The other problems caused by SFA are discussed in subsequent sections. First of all the Coulomb correction problem can be partially solved using a semiclassical method. Secondly, the resonance effect or polarization effect can be included by introducing a partition of the Hilbert space. In the end of this chapter we introduce the Lewenstein theory of high harmonic generation which can be considered as the most successful extension of Keldysh's theory to the other strong field physics phenomenon.

In Chapter 3 we focus on the mathematical technique, known as the method of steepest descent (MSD), that plays the central role in calculating the transition amplitude in quantum mechanics. Sometimes it is also referred as the saddle point method (or the saddle point approximation). This technique will be used to evaluate the temporal integrals arisen in the SFA-based theories given by the previous chapter. Distinction has been made between the situation with singularity coincide with the saddle point and the situation without singularity.

In Chapter 4 we test the SFA and the method of steepest descent and other relevant approximations using three models: the zero-range potential atom, the hydrogen atom and the hydrogen molecular ion. Each model represent a characteristic example for a class of

problems in the strong-field ionization. The purpose of the test is to gain some knowledge about the validity of the crucial approximations in the theory, so that for a certain model we can avoid the physical parameter region where the theory becomes inappropriate. This study will be beneficial to the program that we will introduce in the next chapter.

In Chapter 5 we introduce the strong field ionization calculator which is a graphic user interface program written in the MATLAB computing environment. The calculator combines the quantum chemistry softwares such as GAMESS or GAUSSIAN with the SFA-based theories introduced in Chapter 2. It is capable of calculating the strong field ionization rate, the photoelectron spectrum and the high harmonic generation spectrum. The calculator has three major advantages. First of all it is computational less demanding compared to the *ab initio* numerical methods. A laptop computer will be sufficient for all its purposes. Secondly, it makes the SFA-based theories easily accessible through its user friendly graphic interface. All of the complicated formalism is hidden in the background which does not need to be concerned for most of the purposes. Lastly, the fact that this calculator is based on the S-matrix expansion with SFA makes it easily extendible. For instance, we can include Coulomb correction, resonance effect or different gauge calculations. The non-sequential double ionization process can also be included in the program. Despite all the advantages, deficiency of this program is also clear. Because of the SFA, the calculation can only achieve qualitative accuracy in general. Comparison to the *ab initio* calculations is recommended if possible.

In Chapter 6 we introduce the numerical method that has been used to perform the *ab initio* calculations in the thesis. The numerical solution to the time-dependent Schrödinger equation can be considered as the exact result that is used to compare with the SFA-based theories. However, due to its great demand on the computational power we can only use the simplest system with a highly symmetric situation to test the theory.

In Chapter 7 we study a case that has two laser fields with different intensities. This chapter can be considered as an extension of the SFA-based theory to the two-color laser fields interaction. We theoretically investigated the interesting electron dynamics under these two laser fields. Comparison with the numerical calculations has confirmed the predictions by the theory.

In Chapter 8 we conclude this thesis with a discussion of future works.

In Appendix A we discuss Green's function and its relation to the time evolution operator. In Appendix B we present detail derivation of the transition rate. In Appendix C the static tunneling ionization rate of hydrogen atom is derived in the parabolic coordinate system. In Appendix D, detail of the derivation of the analytic formula for the tunneling ionization rate is given.

Chapter 2

Theory of strong field ionization and high harmonic generation

2.1 Introduction

The theory of intense laser atom interaction has been well developed nowadays (see Becker and Faisal [16] or Milosevic, *et al.* [17] for recent reviews). The method can be traced back to the strong field approximation (SFA) proposed by Keldysh in 1964 [15], which is the most successful non-perturbative treatment of strong laser ionization of atoms. Keldysh employed the length gauge in the description of the electromagnetic interaction with an atom. Together with the pioneering work of Faisal [18] and Reiss [19, 20] who used the velocity gauge to describe the atom-laser interaction, their method is also known as the KFR theory. While an exact theory should be gauge independent, the KFR theory, after the introduction of the SFA, become gauge dependent, and it is not clear which gauge would give a more accurate result in general. There is evidence that the length gauge gives better results for negative ions [21] and the nitrogen molecule [22]. One of the major accomplishments of Keldysh was that his theory properly accounts for the two limiting cases of strong field ionization: multiphoton ionization and tunneling ionization, depending on whether the value of an adiabaticity parameter,

$$\gamma = \frac{\omega}{\omega_t}, \qquad \text{where} \qquad \omega_t = \frac{eE_0}{\sqrt{2mI_p}}, \tag{2.1}$$

is larger or smaller than unity. Here ω is the laser frequency, I_p is the atomic ionization potential and E_0 is the laser electric field amplitude. ω_t can be interpreted as the tunneling

frequency. γ is commonly known as the Keldysh parameter. Keldysh's original paper [15] considered only the case of a hydrogen atom, and details of the derivations were not presented. While Keldysh's approach tends to underestimate the total ionization rate [23], a quasiclassical method was developed [24, 25] to treat the correction due to the Coulomb potential. In a series of papers, Perelomov, Popov and Terentev (PPT) [26, 27] extended Keldysh's treatment to the case of a general atom ionized by lasers of both linear polarization and elliptical polarization. In their approach both the Volkov propagator and the quasiclassical propagator were used. The quasiclassical approach allows them to include the Coulomb correction by improving the action in a perturbative way. A matching procedure was proposed to take proper account of the asymptotic behaviour of the initial state of the electron. After the Coulomb correction, a simple analytical ionization rate formula for atoms were derived. It is only until recently, the higher order Coulomb correction is obtained which is believed to be valid in arbitrary values of the Keldysh parameter [28]. See also the recent reviews by Popov on the Keldysh theory [29] and the quasiclassical method [30]. Their formula can be compared to the well-known ADK formula [31] in the tunneling limit $\gamma \ll 1$.

In addition, the KFR theory has been extended to the study of high harmonic generation process (HHG) [32, 33] for the long laser pulse. The essential features of HHG spectrum can be well explained using this theory. The concept of quantum path born naturally in the formalism is shown to be closely related to the classical model known as the simple man's model [34]. The quantum path takes complex values with the real part corresponding to the classical trajectory and the imaginary part is associated with the tunneling nature of electronic wavefunction. An extension of the theory to the HHG by ultra-short laser pulse can be found in reference [35].

Further attempts to extend KFR theory to the molecular case has been made in references [36, 37, 38]. Many phenomena observed in the molecular ionization experiments can be well explained using the extended theory, but there are still some unsettled issues. For instance, the theory predicts a suppression of the ionization yields for the molecules having an anti-bonding symmetry valence orbital [39]. According to this prediction suppression is expected for the F_2 molecule. However this prediction is not confirmed by any experiment [40]. Another example is the charge resonance enhanced ionization (CREI) first predicted theoretically by Zuo *et al.* and later observed in experiments [41, 42]. At the time of writing we have not aware of any SFA-based theory that is capable of describing the CREI properly. Considering all these facts we believe that the extension of the KFR theory to the molecular case is far from complete.

In this chapter we present a detailed derivation of the KFR theory and its extensions. we summarize the formal results for the ionization amplitude based on the Dyson equations for

the evolution operators. We apply the SFA to the exact ionization amplitude and derive expressions for the differential and total ionization rates in term of an SFA transition amplitude $L_n(\mathbf{k})$.

2.2 The formal derivation

The derivation in this section closely follows reference [43]. We shall employ atomic units throughout this thesis ($m = e = \hbar = 4\pi\varepsilon_0 = 1$ so that the charge on an electron is $q = -1$). The Schrödinger equation for the system is

$$i\partial_t|\Psi(t)\rangle = \hat{H}(t)\ |\Psi(t)\rangle. \tag{2.2}$$

For a system interacting with a laser field, the total Hamiltonian can be partitioned according to

$$\hat{H}(t) = \hat{H}_0(t) + \hat{V}(t) \tag{2.3}$$

where the solution to the unperturbed system

$$i\partial_t|\Phi(t)\rangle = \hat{H}_0(t)\ |\Phi(t)\rangle \tag{2.4}$$

is assumed known. The partition in eq.(2.3) is not unique: we may choose different unperturbed Hamiltonians $\hat{H}_0^{(i)}(t)$ for the initial states $|\Phi^{(i)}(t)\rangle$ and $\hat{H}_0^{(f)}(t)$ for the final states $|\Phi^{(f)}(t)\rangle$ of the system [16]. To obtain formal expression for the transition amplitude, it is convenient to express the total wave function $|\Psi(t)\rangle$ in terms of the unperturbed wave function $|\Phi(t)\rangle$. This can be accomplished by using the Green's function method [16], or the evolution operator formalism [17]. We shall employ the evolution operators in this section, and discuss the Green's function technique and its relation to the evolution operators in Appendix A.

The evolution operators can be defined by the solutions to the following initial value problems

$$\left[i\partial_t - \hat{H}(t)\right]\hat{U}(t,t') = 0, \quad \hat{U}(t',t') = \hat{1}, \tag{2.5}$$

$$\left[i\partial_t - \hat{H}_0(t)\right]\hat{U}_0(t,t') = 0, \quad \hat{U}_0(t',t') = \hat{1} \tag{2.6}$$

where $\hat{1}$ is the unit operator. If $|\Psi(t')\rangle$ and $|\Phi(t')\rangle$ are the full wave function and unperturbed wave function, respectively, at t', then

$$|\Psi(t)\rangle = \hat{U}(t,t')|\Psi(t')\rangle, \quad |\Phi(t)\rangle = \hat{U}_0(t,t')|\Phi(t')\rangle \tag{2.7}$$

clearly satisfy the Schrödinger equations (2.2) and (2.4), respectively, and the appropriate initial conditions. Hence $\hat{U}(t,t')$ propagates the wavefunction $|\Psi(t)\rangle$ under the full Hamiltonian eq.(2.3), while $\hat{U}_0(t,t')$ propagates the unperturbed wave function $|\Phi(t)\rangle$ in the absence of the perturbation $\hat{V}(t)$. They obey the group and unitary relations

$$\begin{aligned} \hat{U}(t,t') &= \hat{U}(t,t'')\hat{U}(t'',t'), \quad \hat{U}(t,t') = \hat{U}^\dagger(t',t); \\ \hat{U}_0(t,t') &= \hat{U}_0(t,t'')\hat{U}_0(t'',t'), \quad \hat{U}_0(t,t') = \hat{U}_0^\dagger(t',t). \end{aligned} \tag{2.8}$$

The evolution operators are related by the following Dyson equations (see Appendix A, eqs.(A.10), (A.11), and eq.(A.18)):

$$\hat{U}(t,t') = \hat{U}_0(t,t') - i\int_{t'}^{t} d\tau\ \hat{U}_0(t,\tau)\hat{V}(\tau)\hat{U}(\tau,t') \tag{2.9}$$

$$\hat{U}(t,t') = \hat{U}_0(t,t') - i\int_{t'}^{t} d\tau\ \hat{U}(t,\tau)\hat{V}(\tau)\hat{U}_0(\tau,t'). \tag{2.10}$$

If $\hat{V}(t') \to 0$ as $t' \to -\infty$ so that $\Psi(-\infty) = \Phi(-\infty)$, these Dyson equations together with eq.(2.7) give

$$|\Psi(t)\rangle = |\Phi(t)\rangle - i\int_{-\infty}^{t} d\tau\ \hat{U}_0(t,\tau)\hat{V}(\tau)|\Psi(\tau)\rangle, \tag{2.11}$$

$$|\Psi(t)\rangle = |\Phi(t)\rangle - i\int_{-\infty}^{t} d\tau\ \hat{U}(t,\tau)\hat{V}(\tau)|\Phi(\tau)\rangle; \tag{2.12}$$

which are equivalent to the Lippmann-Schwinger equations (A.6) and (A.9) in Appendix A.

We can now study the dynamics of the electron based on the above expansion. The initial and final states $|\Phi_i(t)\rangle$ and $|\Phi_f(t)\rangle$ will be the bound and continuum states of the system in the presence of the binding potential of the system but in the absence of the laser field [17, 44] so that they are orthogonal to each other: $\langle\Phi_f(t)|\Phi_i(t)\rangle = 0$. $\hat{V}(t)$ then represents the interaction of the system with the laser, which will be denoted by $\hat{V}_L(t)$ where $\hat{V}_L(t) \to 0$ as $t \to \pm\infty$. The transition amplitude is given by

$$M_{fi} \equiv \lim_{t\to\infty} \langle\Phi_f(t)|\Psi_i(t)\rangle \tag{2.13}$$

where $|\Psi_i(t)\rangle$ is the total wave function evolved from $|\Phi_i(t')\rangle$, $t' \to -\infty$, in the presence of the binding potential with the laser turned on at t'. Using the evolution operator eq.(2.7) to write $|\Psi_i(t)\rangle = \hat{U}(t,t')|\Phi_i(t')\rangle$, $t' \to -\infty$, the Dyson equation (2.10) then gives

$$M_{fi} = -i\lim_{t\to\infty}\int_{-\infty}^{t} d\tau\ \langle\Phi_f(t)|\hat{U}(t,\tau)\hat{V}_L(\tau)|\Phi_i(\tau)\rangle, \tag{2.14}$$

where we note that $\langle\Phi_f(t)|U_0(t,t')|\Phi_i(t')\rangle = \langle\Phi_f(t)|\Phi_i(t)\rangle = 0$. Eq.(2.14) is *exact*. It is sometimes referred to as the "prior" form of the transition amplitude [16, 45].

2.3 Strong field approximation and choice of gauge

Two gauges are commonly used in the theory: The length gauge (LG) and the velocity gauge (VG). In principle the calculation results should be invariant with respect to the change of gauge; however, due to the strong field approximation, the gauge invariance is broken. It is thus important to keep track on both gauges in all the calculations. Sometimes different gauge will even provide us different physical intuitions. There is still no universal rule to clarify the choice of gauge. In the end the result should be compared with the numerical solution of the time-dependent Schrödinger equation and the experiments.

2.3.1 SFA-LG

Keldysh applied the strong field approximation (SFA) to the ionization of the hydrogen atom [15], and his theory can readily be applied to other atoms [46, 47, 48] and molecules [49] under the single-active-electron approximation (SAEA), in which the ionizing electron is assumed to move independently in an effective potential $\hat{V}_a$ in the presence of the laser field. In this case, the total Hamiltonian eq.(2.3) for the active electron can be written as

$$\hat{H} = -\frac{1}{2}\nabla^2 + \hat{V}_a + \hat{V}_L(t), \tag{2.15}$$

where

$$\hat{V}_L(t) = \mathbf{r}\cdot\mathbf{E}(t) \tag{2.16}$$

is the interaction of the electron with the electric field $\mathbf{E}(t)$ of the laser under the dipole approximation in the length gauge. Our starting point is the exact equation (2.14), in which the initial state is the single electron ground state $|\Phi_i(t)\rangle = |\psi_i\rangle e^{iI_p t}$ and the final state is the single electron scattering state $|\Phi_f(t)\rangle = |\psi_{\mathbf{k}}(t)\rangle$ specified by momentum $\mathbf{k}$.

The approximations that lead to the Keldysh's result are succinctly summarized by W. Becker, *et al.*[33] The first approximation is to replace the full evolution operator $\hat{U}(t,\tau)$ in eq.(2.14) by the evolution operator $\hat{U}_V(t,\tau)$ for a free electron in the presence of the laser, which satisfies

$$\left[i\partial_t - \hat{H}_L(t)\right]\hat{U}_V(t,t') = 0, \quad \hat{H}_L(t) = -\frac{1}{2}\nabla^2 + \hat{V}_L(t). \tag{2.17}$$

$\hat{U}_V(t,\tau)$ is commonly known as the Volkov evolution operator (or Volkov propagator). The Volkov wave function satisfying the Schrödinger equation

$$i\partial_t|\phi_{\mathbf{k}}^V(t)\rangle = \hat{H}_L(t)\ |\phi_{\mathbf{k}}^V(t)\rangle \tag{2.18}$$

is given in coordinate representation by [50]

$$\phi_{\mathbf{k}}^V(\mathbf{r},t) = \langle\mathbf{r}|\phi_{\mathbf{k}}^V(t)\rangle = e^{i[\mathbf{k}+\mathbf{A}(t)]\cdot\mathbf{r}-iS(t)} = \langle\mathbf{r}|\mathbf{k}+\mathbf{A}(t)\rangle e^{-iS(t)} \tag{2.19}$$

where $\mathbf{A}(t)$ is the vector potential related to the electric field by $\mathbf{E}(t) = -\partial_t\mathbf{A}(t)$, $|\mathbf{k}+\mathbf{A}(t)\rangle$ denotes a plane wave state with momentum $\mathbf{p} = \mathbf{k}+\mathbf{A}(t)$, and

$$S(t) = \frac{1}{2}\int^t [\mathbf{k}+\mathbf{A}(t')]^2\, dt' \tag{2.20}$$

is the classical action. The Volkov evolution operator is given in terms of the Volkov functions eq.(2.19) by

$$\hat{U}_V(t,t') = \int \frac{d^3\mathbf{k}}{(2\pi)^3}\left|\phi_{\mathbf{k}}^V(t)\right\rangle\left\langle\phi_{\mathbf{k}}^V(t')\right|. \tag{2.21}$$

It can readily be verified that eq.(2.21) satisfies the definition (2.17) using eq.(2.18); furthermore the completeness of the plane wave states gives the initial condition $\hat{U}_V(t',t') = \hat{1}$, as required by eq.(2.6). The transition amplitude eq.(2.14) then takes the form

$$M_{fi} \simeq -i\lim_{t\to\infty}\int_{-\infty}^t d\tau\ \langle\psi_{\mathbf{k}}(t)|\,\hat{U}_V(t,\tau)\hat{V}_L(\tau)\,|\psi_i\rangle\, e^{iI_p\tau}. \tag{2.22}$$

Recall that the exact expression of the transition amplitude eq.(2.14) was obtained by choosing $\hat{V}(\tau) = \hat{V}_L(\tau)$ in the Dyson equation for $\hat{U}(t,t')$. Other choice for $\hat{V}(\tau)$ is possible in further application of the Dyson equation. Thus the result of eq.(2.22) can be considered to be the first term of a perturbation series [51] obtained by applying the Dyson equation eq.(2.10) with $\hat{V}(\tau) = \hat{V}_a$ to the full evolution operator $\hat{U}(t,\tau)$ in eq.(2.14). Eq.(2.22) represents the "direct" ionization process in which the electron detached from the atom escapes without further interaction with the atomic core. Higher order terms give rise to additional interaction of the ionizing electron with the ion core, leading to "rescattering effects" [32, 51, 52]. We shall only be concerned with direct ionization in this thesis.

To obtain the final Keldysh result, a second approximation is introduced where the scattering state $|\psi_{\mathbf{k}}(t)\rangle$ in eq.(2.14) is replaced by the plane wave state $|\phi_{\mathbf{k}}(t)\rangle = |\mathbf{k}\rangle e^{-ik^2t/2}$, which amounts to neglecting the spherical wave of the scattering state. In this case, for

a laser adiabatically turned on at $t' \to -\infty$ and turned off at $t \to \infty$, $\langle\psi_{\mathbf{k}}(t)|\hat{U}_V(t,\tau) \simeq \langle\phi_{\mathbf{k}}(t)|\hat{U}_V(t,\tau) = \langle\phi^V_{\mathbf{k}}(\tau)|$ as $t \to \infty$, giving the Keldysh amplitude

$$\begin{aligned} M_{fi} &\simeq -i\int_{-\infty}^{\infty} d\tau \ \left\langle\phi^V_{\mathbf{k}}(\tau)\right| \hat{V}_L(\tau)\,|\psi_i\rangle\, e^{iI_p\tau} \\ &= -i\int_{-\infty}^{\infty} dt \int d^3\mathbf{r}\ e^{-i[\mathbf{k}+\mathbf{A}(t)]\cdot\mathbf{r}+iS(t)}\ \mathbf{r}\cdot\mathbf{E}(t)\ \psi_i(r)e^{iI_pt} \\ &= -i\int_{-\infty}^{\infty} dt\ e^{iS_p(t)}\ \langle\mathbf{k}+\mathbf{A}(t)\,|\mathbf{r}\cdot\mathbf{E}(t)|\,\psi_i\rangle \end{aligned} \tag{2.23}$$

where we have used the Volkov function eq.(2.19) and the dipole interaction eq.(2.16), and we define the combined action by

$$S_p(t) = S(t) + I_pt. \tag{2.24}$$

Now the laser field is assumed to be linearly polarized

$$\mathbf{E}(t) = \mathbf{E}_0\cos\omega t \tag{2.25}$$

where $\mathbf{E}_0$ is a constant vector. This electric field is derivable from the vector potential

$$\mathbf{A}(t) = -\frac{\mathbf{E}_0}{\omega}\sin\omega t. \tag{2.26}$$

The action eq.(2.20) can then be evaluated to give

$$S_p(t) = S(t) + I_pt = \left(\frac{k^2}{2} + U_p + I_p\right)t + \left(\frac{kE_0\cos\theta}{\omega^2}\cos\omega t - \frac{U_p}{2\omega}\sin 2\omega t\right), \tag{2.27}$$

where θ is the angle between $\mathbf{k}$ and $\mathbf{E}_0$, and $U_p = \dfrac{E_0^2}{4\omega^2}$ is the pondermotive potential which is the time-average kinetic energy of a free electron in the laser field. Thus the integrand of the transition amplitude eq.(2.23) contains the following factor periodic in time with period $T = \dfrac{2\pi}{\omega}$, which can be expanded in a Fourier series

$$e^{i\left(\frac{\mathbf{k}\cdot\mathbf{E}_0}{\omega^2}\cos\omega t - \frac{U_p}{2\omega}\sin 2\omega t\right)}\ \langle\mathbf{k}+\mathbf{A}(t)\,|\mathbf{r}\cdot\mathbf{E}(t)|\,\psi_i\rangle = \sum_{n=-\infty}^{\infty} L_n(\mathbf{k})e^{-in\omega t}, \tag{2.28}$$

with Fourier coefficients

$$L_n(\mathbf{k}) = \frac{1}{T}\int_0^T dt\; e^{in\omega t}\left[e^{i\left(\frac{\mathbf{k}\cdot\mathbf{E}_0}{\omega^2}\cos\omega t - \frac{U_p}{2\omega}\sin 2\omega t\right)}\;\langle \mathbf{k}+\mathbf{A}(t)\,|\mathbf{r}\cdot\mathbf{E}(t)|\,\psi_i\rangle\right]. \tag{2.29}$$

Substituting eqs.(2.27) and (2.28) into eq.(2.23) and evaluate the integral over t, the transition amplitude can be expressed in term of $L_n(\mathbf{k})$ as

$$M_{fi} = -2\pi i\sum_{n\geq n_0}^{\infty} L_n(\mathbf{k})\;\delta\left(\frac{k^2}{2}+U_p+I_p-n\omega\right), \tag{2.30}$$

where n are integers and $n_0\omega = U_p+I_p$. Taking advantage of the delta function in eq.(2.30) to write $n\omega t = \left(\frac{k^2}{2}+U_p+I_p\right)t$, the Fourier coefficients of eq.(2.29) can be simplified as

$$L_n(\mathbf{k}) = \frac{1}{T}\int_0^T dt\; e^{iS_p(t)}\;\langle \mathbf{k}+\mathbf{A}(t)\,|\mathbf{r}\cdot\mathbf{E}(t)|\,\psi_i\rangle \tag{2.31}$$

$$= -\frac{1}{T}\int_0^T dt\;\;\left\langle \mathbf{k}+\mathbf{A}(t)\,\middle|\psi_i\right\rangle S_p'(t)\;e^{iS_p(t)}\;\;, \tag{2.32}$$

where the second form of $L_n(\mathbf{k})$, eq.(2.32), is obtained by noting that

$$\langle \mathbf{k}+\mathbf{A}(t)\,|\mathbf{r}\cdot\mathbf{E}(t)|\,\psi_i\rangle = \int d^3\mathbf{r}\; e^{-i[\mathbf{k}+\mathbf{A}(t)]\cdot\mathbf{r}}\mathbf{r}\cdot\mathbf{E}(t)\psi_i(r) = -i\int d^3\mathbf{r}\;\partial_t\{e^{-i[\mathbf{k}+\mathbf{A}(t)]\cdot\mathbf{r}}\}\;\psi_i(r).$$

Integrating by parts with respective to t gives the desired result since the integrated term vanishes due to its periodicity [53]. $L_n(\mathbf{k})$ can be interpreted as the transition amplitude of an electron into a continuum state with momentum $\mathbf{k}$ after absorbing n photons. The rate of ionization into the momentum state $|\mathbf{k}\rangle$ is given by [19, 20, 16]

$$\Gamma_{fi} = \lim_{t\to\infty}\frac{1}{t}\,|M_{fi}|^2 = 2\pi\sum_{n\geq n_0}^{\infty}\delta\left(\frac{k^2}{2}+U_p+I_p-n\omega\right)|L_n(\mathbf{k})|^2\,, \tag{2.33}$$

a result derived in Appendix B. The total ionization rate is

$$\Gamma_T = \int\frac{d^3\mathbf{k}}{(2\pi)^3}\;\Gamma(\mathbf{k}) = \sum_{n\geq n_0}^{\infty}\int_0^{\pi} d\theta\;\Gamma_n(\theta), \tag{2.34}$$

where the differential ionization rate is defined by

$$\Gamma_n(\theta) = \frac{k_n}{2\pi}\,|L_n(\mathbf{k}_n)|^2\sin\theta \tag{2.35}$$

and $k_n^2 = 2(n\omega - U_p - I_p)$. Thus the amplitude $L_n(\mathbf{k})$ of eq.(2.31) or eq.(2.32) is the central quantity of interest in the SFA calculation of strong field ionization [15, 26, 54, 44, 16, 17, 55, 56].

For low laser frequency excitation, the change in the electric field during the tunneling of the electron through the barrier will be negligible, and the tunneling ionization rate for an electron in a static field E, given to exponential order by [57, 58, 31]

$$w_{stat}(E) \sim \exp\left\{-\frac{2(2I_p)^{\frac{3}{2}}}{3E}\right\}, \tag{2.36}$$

would be applicable. In fact PPT [26] suggested that in the adiabatic limit $\gamma \ll 1$, the total ionization rate for plane polarized laser excitation eq.(2.25) can be calculated from

$$\Gamma_{qs} = \left[\frac{3E_0}{\pi(2I_p)^{\frac{3}{2}}}\right]^{\frac{1}{2}} w_{stat}(E_0), \tag{2.37}$$

where the first factor results from averaging the rate (2.36) over a period of $E(t) = E_0 \cos\omega t$ [26, 29, 59]. The quasi-static theory and its generalization [31] have proven to be very successful in analyzing tunneling ionization by intense 10.6 μm lasers [60, 61]. We shall compare the adiabatic limits of the total rate Γ_T of eq.(2.34) with the quasi-static result of eq.(2.37) for various models in the chapter4.

2.3.2 SFA-VG

Faisal and Reiss first introduced the SFA in the velocity gauge [18, 19, 62]. Their approach can be summarized as the following. The total Hamiltonian of the single active electron reads

$$\hat{H} \;=\; -\frac{1}{2}\nabla^2 + \hat{V}_a + \hat{V}_L(t), \tag{2.38}$$

where

$$\hat{V}_L(t) = -i\nabla\cdot\mathbf{A}(t) + \frac{1}{2}A^2(t) \tag{2.39}$$

is the interaction of the electron with the electric field of the laser under the dipole approximation. The vector potential is related to the electric field by $\mathbf{E}(t) = -\partial_t\mathbf{A}(t)$, where in this derivation it takes the explicitly form of eq.(2.26). In the transition amplitude

eq.(2.14), the ground state ψ_i of the unperturbed Hamiltonian is used as the initial state and the final state is approximated by the free electron state. In the SFA, again we replace the the full time evolution operator by the Volkov evolution operator

$$\hat{U}_V^{VG}(t,t') = \int \frac{d^3\mathbf{k}}{(2\pi)^3} \left|\phi_{\mathbf{k}}^{V,VG}(t)\right\rangle \left\langle\phi_{\mathbf{k}}^{V,VG}(t')\right|, \tag{2.40}$$

where $|\phi_{\mathbf{k}}^{V,VG}(t)\rangle$ is the Volkov state in the velocity gauge whose coordinate representation is given by [63]

$$\phi_{\mathbf{k}}^{V,VG}(\mathbf{r},t) = \langle\mathbf{r}|\phi_{\mathbf{k}}^{V,VG}(t)\rangle = e^{i\mathbf{k}\cdot\mathbf{r}-iS(t)} = \langle\mathbf{r}|\mathbf{k}\rangle e^{-iS(t)}. \tag{2.41}$$

The action $S(t)$ takes the same form as in eq.(2.20). Substitute eq.(2.40),(2.41) into eq.(2.14) we can write the transition amplitude as

$$\begin{aligned}
M_{fi}^{VG} &\simeq -i\int_{-\infty}^{\infty} d\tau \left\langle\phi_{\mathbf{k}}^{V,VG}(\tau)\left|\hat{V}_L(\tau)\right|\psi_i\right\rangle e^{iI_p\tau} \\
&= -i\int_{-\infty}^{\infty} dt \int d^3\mathbf{r}\; e^{-i\mathbf{k}\cdot\mathbf{r}+iS(t)}\left(-i\nabla\cdot\mathbf{A}(t)+\frac{1}{2}A^2(t)\right)\psi_i(r)e^{iI_pt} \\
&= -i\int_{-\infty}^{\infty} dt\; e^{iS_p(t)}\left\langle\mathbf{k}\left|\left(-i\nabla\cdot\mathbf{A}(t)+\frac{1}{2}A^2(t)\right)\right|\psi_i\right\rangle \\
&= -i\int_{-\infty}^{\infty} dt\; e^{iS_p(t)}\left[\mathbf{k}\cdot\mathbf{A}(t)+\frac{1}{2}A^2(t)\right]\langle\mathbf{k}|\psi_i\rangle\,,
\end{aligned} \tag{2.42}$$

where $S_p(t)$ is given by eq.(2.27). Noting that

$$i(\mathbf{k}\cdot\mathbf{A}(t)+\frac{1}{2}A^2(t))e^{i\left(\frac{\mathbf{k}\cdot\mathbf{E}_0}{\omega^2}\cos\omega t-\frac{U_p}{2\omega}\sin 2\omega t+U_pt\right)} = \frac{\partial}{\partial t}e^{i\left(\frac{\mathbf{k}\cdot\mathbf{E}_0}{\omega^2}\cos\omega t-\frac{U_p}{2\omega}\sin 2\omega t+U_pt\right)}, \tag{2.43}$$

and use integration by parts we can further simplify eq.(2.42) and obtain

$$M_{fi}^{VG} \simeq -i\left(\frac{k^2}{2}+I_p\right)\langle\mathbf{k}|\psi_i\rangle\int_{-\infty}^{\infty} dt\; e^{i\left(\frac{k^2}{2}+U_p+I_p\right)t+i\left(\frac{kE_0\cos\theta}{\omega^2}\cos\omega t-\frac{U_p}{2\omega}\sin 2\omega t\right)}. \tag{2.44}$$

Recognizing the generating function of the generalized Bessel function [64]

$$e^{i\left(\frac{kE_0\cos\theta}{\omega^2}\cos\omega t-\frac{U_p}{2\omega}\sin 2\omega t\right)} = \sum_n e^{-in\omega t}J_n\left(\frac{kE_0\cos\theta}{\omega^2},\frac{U_p}{2\omega}\right), \tag{2.45}$$

where the generalized Bessel function $J_n(u,v)$ is expressed in terms of the Bessel functions $J_n(u)$ as

$$J_n(u,v) = \sum_{k=-\infty}^{\infty} J_{n-2k}(u) J_k(v), \tag{2.46}$$

we can re-write eq.(2.44) as

$$M_{fi}^{VG} \simeq \tag{2.47}$$
$$-i2\pi \sum_n J_n\left(\frac{kE_0\cos\theta}{\omega^2}, \frac{U_p}{2\omega}\right)\left(\frac{k^2}{2}+I_p\right)\langle \mathbf{k}|\psi_i\rangle\, \delta\left(\frac{k^2}{2}+U_p+I_p-n\omega\right).$$

Following the same procedure as before we can obtain the differential ionization rate as

$$\Gamma_n(\theta) = \frac{k_n}{2\pi}\left|J_n\left(\frac{kE_0\cos\theta}{\omega^2}, \frac{U_p}{2\omega}\right)\langle \mathbf{k}_n|\psi_i\rangle\right|^2 \left(\frac{k_n^2}{2}+I_p\right)^2. \tag{2.48}$$

In the tunneling region one can show that the velocity gauge total ionization rate is also given by eq.(2.36) to exponential accuracy; however, the pre-exponential factor is different from the LG calculation [20].

2.4 Semiclassical theory and the Coulomb correction to the SFA

One of the major problems of SFA is that it neglects the long range Coulomb tail of the residue ion once the active electron is promoted to the continuum by the intense laser field. On the other hand, based on WKB approximation, Ammosov, Delone and Kranov derived the static strong field ionization rate for atoms [31]. The ADK-formula is proven to be reliable for the calculation of the tunneling ionization rate in the atomic cases [60]; however, the theory is intrinsically time independent which can only describe the limiting case of the tunneling ionization. Multi-photon ionization picture is completely absent. Perelomov, Popov and Terent'ev introduced SFA using a semiclassical propagator such that both the time dependent effect and the long range Coulomb tail can be incorporated [27]. This method which is called the imaginary time method can be viewed as a bridge connecting the WKB method and the Keldysh's approach. By comparing the Keldysh theory to the semiclassical calculation a better understanding of the action (eq.(2.24)) may be obtained, hence rendering the possibility of introducing a Coulomb correction to the SFA.

Following the derivation in references [26, 27] we write the wavefunction as

$$|\Psi_i(\mathbf{r},t)\rangle = -i\int_{-\infty}^{t} dt' \int d^3\mathbf{r}' G(\mathbf{r},\mathbf{r}';t,t')V_b(\mathbf{r}')|\psi_i(\mathbf{r}',t')\rangle, \tag{2.49}$$

where $G(\mathbf{r},\mathbf{r}';t,t')$ is the semiclassical propagator, $V_b(\mathbf{r}')$ is the binding potential and $|\psi_i(\mathbf{r}',t')\rangle$ is the initial state. We restrict our discussion to exponential accuracy so the time evolution propagator in the semiclassical limit can be written as

$$G(\mathbf{r},\mathbf{r}';t,t') \sim e^{iS_0(\mathbf{r},\mathbf{r}';t,t')}, \tag{2.50}$$

where the action $S_0(\mathbf{r},\mathbf{r}';t,t')$ is calculated along the classical trajectory $\mathbf{r}_c$ starting from $\mathbf{r}',t'$ ending at $\mathbf{r},t$ and given by

$$S_0(\mathbf{r},\mathbf{r}';t,t') = \int_{t'}^{t} \left\{L\left(\dot{\mathbf{r}}_c,\mathbf{r}_c,\tau\right)\right\} d\tau, \tag{2.51}$$

where $L\left(\dot{\mathbf{r}}_c,\mathbf{r}_c,\tau\right)$ is the Lagrangian. Substituting the semiclassical propagation into eq.(2.13) the transition amplitude becomes

$$M_{fi} \sim \lim_{t\to\infty} \int dt' \int d^3\mathbf{r}' \langle\phi_f(\mathbf{r},t)|V_b(\mathbf{r}')e^{iS_0(\mathbf{r},\mathbf{r}';t,t')}|\psi_i(\mathbf{r}',t')\rangle_{\mathbf{r}}. \tag{2.52}$$

To calculate the ionization rate one can approximate the the final state by a free electron wave function. Hence the inner product becomes the Fourier transform of the propagator

$$M_{fi} \sim \lim_{t\to\infty} \int dt' \int d^3\mathbf{r}' \int d^3\mathbf{r} e^{i\mathbf{k}\cdot\mathbf{r}} e^{iS_0(\mathbf{r},\mathbf{r}';t,t')} e^{iI_p t'} V_b(\mathbf{r}')\psi_i(\mathbf{r}'). \tag{2.53}$$

Recall the method of steepest descent (MSD) according to which the integral can be approximated by the saddle point formula [65]

$$\int d^3\mathbf{r} e^{f(\mathbf{r})} g(\mathbf{r}) \sim e^{f(\mathbf{r}_s)} g(\mathbf{r}_s), \tag{2.54}$$

where the saddle point is given by

$$\nabla_{\mathbf{r}} f(\mathbf{r}_s) = 0. \tag{2.55}$$

Applying MSD to the Fourier transform we can obtain the saddle point equation

$$\nabla_{\mathbf{r}} S_0(\mathbf{r},\mathbf{r}';t,t') - \mathbf{k} = 0. \tag{2.56}$$

The equation has the formal solution

$$\begin{aligned}
\mathbf{k} &= \nabla_{\mathbf{r}} S_0(\mathbf{r}, \mathbf{r}'; t, t') \\
&= \frac{\delta S_0}{\delta \mathbf{r}_c} \\
&= \int_{t'}^{t} \left\{ \frac{\partial L}{\partial \mathbf{r}_c} \delta \mathbf{r}_c + \frac{\partial L}{\partial \dot{\mathbf{r}}_c} \delta \dot{\mathbf{r}}_c \right\} \frac{d\tau}{\delta \mathbf{r}_c}, \\
&= \int_{t'}^{t} \left\{ \dot{\mathbf{p}}_c \delta \mathbf{r}_c + \mathbf{p}_c \delta \dot{\mathbf{r}}_c \right\} \frac{d\tau}{\delta \mathbf{r}_c}, \\
&= \mathbf{p}, \qquad (2.57)
\end{aligned}$$

where $\mathbf{p}$ denotes the conjugate momentum to the the coordinate $\mathbf{r}$. We drop the subscript of $\mathbf{p}_c$ because the variation is made at the end point ($\mathbf{r}$ t). In the velocity Gauge, which we will use in the subsequent section, the canonical momentum is conserved in time. At the saddle point the exponent in eq.(2.53) can be written as

$$W_0(\mathbf{p}, \mathbf{r}'; t, t') = S_0(\mathbf{r}, \mathbf{r}'; t, t') - \mathbf{p} \cdot \mathbf{r}, \qquad (2.58)$$

which is recognized as the Legendre transformation of the classical action. Finally we can write the transition amplitude as

$$M_{fi} \sim \lim_{t \to \infty} \int dt' \int d^3\mathbf{r}' e^{iW_0(\mathbf{p}, \mathbf{r}'; t, t')} e^{iI_p t'} V_b(\mathbf{r}') \psi_i(\mathbf{r}'). \qquad (2.59)$$

The integration in eq.(2.59) can be evaluated using the method of steepest descent. The saddle points are found by solving the saddle point equations

$$\frac{\partial W_0(\mathbf{p}, \mathbf{r}'; t, t')}{\partial t'} + I_p = 0 \qquad (2.60)$$

$$\nabla_{\mathbf{r}'} W_0(\mathbf{p}, \mathbf{r}'; t, t') = 0. \qquad (2.61)$$

Recall the total time derivative of the action can be written as

$$\begin{aligned}
\frac{dW_0(\mathbf{p}, \mathbf{r}'; t, t')}{dt'} &= \frac{\partial W_0(\mathbf{p}, \mathbf{r}'; t, t')}{\partial t'} + \dot{\mathbf{r}}' \cdot \nabla_{\mathbf{r}'} W_0(\mathbf{p}, \mathbf{r}'; t, t') \\
&= -L\left(\dot{\mathbf{r}}', \mathbf{r}', t'\right). \qquad (2.62)
\end{aligned}$$

Hence we can write eq.(2.60) as

$$\begin{aligned}
\dot{\mathbf{r}}' \cdot \mathbf{p}' - L\left(\dot{\mathbf{r}}', \mathbf{r}', t'\right) + I_p &= 0 \\
H(\mathbf{p}', \mathbf{r}', t') + I_p &= 0, \qquad (2.63)
\end{aligned}$$

where $H(\mathbf{p}', \mathbf{r}', t')$ is the Hamiltonian. The solutions of the above equation in general will have complex values for the case of bound state where $I_p = -E_b > 0$. Hence the trajectories will be complex which reflect the tunneling nature of the electron dynamics. One can consider the total transition amplitude eq.(2.59) reducing to a summation over the amplitudes of several complex-valued classical trajectories. They are still called classical trajectories because the Newtonian equation of motion is satisfied. Eq.(2.63) determines the saddle time t'_s that can be considered as the starting time of the electron sub-barrier motion. In addition, the electron is assumed to be starting at the origin so

$$\mathbf{r}_c(t'_s) = \mathbf{r}_0 = \mathbf{0} + i\mathbf{r}_{img}. \tag{2.64}$$

Note the imaginary part is added to ensure the electron trajectory to be real in real time.

2.4.1 The leading order approximation - SFA

To proceed further we first consider the leading order approximation of the Lagrangian in velocity gauge given by

$$L\left(\dot{\mathbf{r}}_c, \mathbf{r}_c, \tau\right) = \frac{1}{2}\dot{\mathbf{r}}_c^2 - \dot{\mathbf{r}}_c \cdot \mathbf{A}, \tag{2.65}$$

where $\mathbf{A}(\tau)$ is the same laser vector potential defined in eq.(2.19). The Coulomb binding potential is neglected. Consequently we can write eq.(2.63) as

$$\frac{1}{2}\left[\mathbf{p}' + \mathbf{A}(t'_s)\right]^2 + I_p = 0, \tag{2.66}$$

where $\mathbf{p}'$ is the canonical momentum which is a conserved quantity. The saddle point equation is equivalent to the SFA in KFR theory. The Newtonian equation of motion can be written as

$$\ddot{\mathbf{r}}_c(\tau) = -\mathbf{E}(\tau), \tag{2.67}$$

where the $\mathbf{E}(\tau)$ describes the electric field of the laser. Integrate eq.(2.67) we obtain the electron velocity

$$\dot{\mathbf{r}}_c(\tau) = \mathbf{v}(\tau) = \mathbf{p}' + \mathbf{A}(\tau). \tag{2.68}$$

Integrate eq.(2.68) again to obtain the complex trajectory

$$\mathbf{r}_c(\tau) = \mathbf{r}_0 + \mathbf{p}'(\tau - t_s) + \mathbf{x}_c(\tau) - \mathbf{x}_c(t_s), \tag{2.69}$$

where $\partial_\tau \mathbf{x}_c(\tau) = \mathbf{A}(\tau)$.

Finally we write

$$\begin{aligned}\tilde{W}_0(\mathbf{p}, \mathbf{r}_0; t, t_s') &= W_0(\mathbf{p}, \mathbf{r}_0; t, t_s') + I_p t_s \\ &= \int_{t_s}^{t} d\tau \left\{ \frac{1}{2}\dot{\mathbf{r}}_c(\tau)^2 - \dot{\mathbf{r}}_c(\tau) \cdot \mathbf{A}(\tau) \right\} - \mathbf{p} \cdot \mathbf{r} + I_p t_s \\ &= \int_{t_s}^{t} d\tau \left\{ \frac{1}{2}\left[\mathbf{p}' + \mathbf{A}(\tau)\right]^2 - \left[\mathbf{p}' + \mathbf{A}(\tau)\right] \cdot \mathbf{A}(\tau) \right\} - \mathbf{p} \cdot \mathbf{r} + I_p t_s . \quad (2.70)\end{aligned}$$

Eq.(2.61) will give us $\mathbf{p}' = \mathbf{0}$ which means among all the complex trajectories with different canonical momentum $\mathbf{p}'$ only the the one with $\mathbf{p}' = 0$ will contribute the most to the transition probability. In the deep tunneling region when $\gamma \ll 1$ one only needs to consider this trajectory to obtain the total ionization rate. In the next step the canonical momentum is set to be zero $\mathbf{p} = \mathbf{p}' = 0$. Combining eq.(2.66) and (2.68), we can solve the velocity of the electron at the saddle time as a pure imaginary number given by

$$\dot{r}_c(t_s') = \pm i\sqrt{2I_p}, \quad (2.71)$$

together with eq.(2.64) forms the complete initial condition of the complex trajectories. The $\pm$ sign is chosen based on a physical consideration.

We also assume the laser field is given by eq.(2.25) and (2.26) so that

$$\mathbf{x}(\tau) = \frac{\mathbf{E}_0}{\omega_L^2} \cos \omega_L \tau. \quad (2.72)$$

We obtain

$$\mathbf{r}_c(\tau) = \mathbf{r}_0 + \frac{\mathbf{E}_0}{\omega_L^2} \cos \omega_L \tau - \frac{\mathbf{E}_0}{\omega_L^2} \cos \omega_L t_s, \quad (2.73)$$

where t_s can be solved explicitly from eq.(2.66) and given by

$$t_s = \frac{1}{\omega_L} \arcsin\left(i\frac{\kappa\omega_L}{E_0}\right) = \frac{i}{\omega_L} \mathrm{arcsinh}\left(\frac{\kappa\omega_L}{E_0}\right) = i\frac{\tau_0}{\omega_L}, \quad (2.74)$$

and $\kappa = \sqrt{2I_p}$. The velocity of the electron is given by

$$\dot{\mathbf{r}}_c(\tau) = \mathbf{A}(\tau) = -\frac{\mathbf{E}_0}{\omega_L} \sin \omega_L \tau. \quad (2.75)$$

In eq.(2.70) the upper integration limit is a real number and the lower integration limit is a pure imaginary number. Since the Lagrangian is analytic in the complex plane we can choose arbitrary integration path from t_s to t. It is possible to choose a real time $t_0 < t$ such that both the electron trajectory $\mathbf{r}_c$ and velocity $\dot{\mathbf{r}}_c(\tau)$ become real at time t_0 and afterward. this can be done by choosing $\mathbf{r}_{img}$ in eq.(2.64) to be

$$\mathbf{r}_{img} = \frac{\mathbf{E}_0}{\omega_L^2}\cosh\tau_0 \tag{2.76}$$

so that the trajectory can be written as

$$\mathbf{r}_c(\tau) = \frac{\mathbf{E}_0}{\omega_L^2}\cos\omega_L\tau, \tag{2.77}$$

which is real when τ becomes real. Recall that the ionization rate is given by

$$\Gamma = \frac{|M_{fi}|^2}{T} \sim |e^{i\tilde{W}_0}|^2 = e^{-2\Im\{\tilde{W}_0\}}, \tag{2.78}$$

where T is the total interaction time. As we can see only the imaginary part of $\tilde{W}_0$ contributes to the transition rate. The classical action beyond t_0 becomes real so that it does not contribute to the transition probability. We should thus only consider the initial point $\tau = t_s$. Eq.(2.70) can be written as

$$\Im\left\{\tilde{W}_0(\mathbf{p},\mathbf{r}_0;t,t_s')\right\} = -\frac{1}{2}\int_{t_s}^{t} d\tau\left\{\mathbf{A}(\tau)^2\right\} + I_p t_s \tag{2.79}$$

Substitute eq.(2.75) into eq.(2.79) we can obtain

$$\begin{aligned}\Im\left\{\tilde{W}_0(\mathbf{p},\mathbf{r}_0;t,t_s')\right\} &= \frac{1}{2}\frac{E_0^2}{\omega_L^2}\left[t_s - \frac{1}{4\omega_L}\sin 2\omega_L t_s\right] + I_p t_s \\ &= \frac{i}{2}\frac{E_0^2}{\omega_L^3}\left[\tau_0 - \frac{1}{4}\sinh 2\tau_0\right] + iI_p\frac{\tau_0}{\omega_L}\end{aligned} \tag{2.80}$$

The transition rate is given by

$$\Gamma \propto e^{-2\Im\left\{\tilde{W}_0(\mathbf{p},\mathbf{r}_0;t,t_s')\right\}} = e^{(U_p+I_p)\frac{\tau_0}{\omega_L} - \frac{U_p}{2\omega_L}\sinh 2\tau_0}. \tag{2.81}$$

At the limit when the Keldysh parameter $\gamma \to 0$ eq.(2.81) will approach to a simple exponent form given by

$$e^{(U_p+I_p)\frac{\tau_0}{\omega_L} - \frac{U_p}{2\omega_L}\sinh 2\tau_0} \to e^{-\frac{2(2I_p)^{3/2}}{3E_0}} \tag{2.82}$$

Note this exponent is exactly the same as eq.(2.36) obtained in section 2.3 which implies that the semiclassical method proposed by PPT [27] agrees with the Keldysh's theory [15] at least to the exponential accuracy.

2.4.2 The second order approximation - Coulomb correction

In the next step we shall consider the correction of the transition amplitude due to a long range Coulomb potential [26, 27]. We can write the action as

$$\tilde{W}(\mathbf{p}, \mathbf{r}_0; t, t'_s) = \tilde{W}_0(\mathbf{p}, \mathbf{r}_0; t, t'_s) + \tilde{W}_1(\mathbf{p}, \mathbf{r}_0; t, t'_s), \tag{2.83}$$

where $\tilde{W}_1$ is the variation of the classical action due to a binding potential

$$V_b(\mathbf{r}_c(\tau)) = -\frac{Z}{|\mathbf{r}_c(\tau)|}. \tag{2.84}$$

In principle this variation should include both the variations of the classical trajectory $\mathbf{r}_c(\tau)$ and the saddle time t'_s, but as a leading order correction we can assume the trajectory is not changed so that the first order variation can be calculated using the leading order trajectory

$$\tilde{W}_1(\mathbf{p}, \mathbf{r}_0; t, t'_s) = -\int_{t'_s}^{t} V_b(\mathbf{r}_c(\tau))d\tau. \tag{2.85}$$

However there is a fundamental difficulty to evaluate the integral. The Coulomb potential becomes very strong when the electron is near the origin so the perturbation method may not be applicable. The solution suggested in reference [27] is known as a matching procedure. The idea of this matching is to divide the sub-barrier motion into two regions: the near-core region where the Coulomb potential dominates the electron trajectory, and the far-core region where the external electric field dominates the electron trajectory. Consequently the temporal integral in eq.(2.85) can be partitioned as the following

$$\tilde{W}_1(\mathbf{p}, \mathbf{r}_0; t, t'_s) = -\int_{t'_s}^{t_m} V_b(\mathbf{r}_c(\tau))d\tau - \int_{t_m}^{t} V_b(\mathbf{r}_c(\tau))d\tau, \tag{2.86}$$

where the intermediate time t_m is proposed to separate the electron's inner-core motion and the far-core motion. At this stage the choice of t_m on the complex time plane is completely arbitrary but it should be very close to the saddle time t'_s. We can use the asymptotic behaviour of the field-free wave function

$$\psi_i(r) \sim (\kappa r)^{\frac{Z}{\kappa}} e^{-\kappa r} = e^{-\kappa r + \frac{Z}{\kappa}\ln(\kappa r)} \tag{2.87}$$

to identify the divergent part of the action. There should be an agreement between the first term on the right-hand side of the eq.(2.86) and the divergent part of the action of

the asymptotic form of the field-free wave function so that we set them to be equal and written

$$-\int_{t_s'}^{t_m} V_b(\mathbf{r}_c(\tau))d\tau = -i\frac{Z}{\kappa}\ln\kappa r_m, \tag{2.88}$$

where r_m is the electron coordinate at time t_m.

The second term of eq.(2.86) can be evaluated by linearization of equation of motion near the saddle point t_s' where in the tunneling limit $\gamma \to 0$, $\omega_L \to 0$ we can make the approximations:

$$t_s' = \frac{\arcsin(i\frac{\kappa\omega_L}{E_0})}{\omega_L} \to i\frac{\kappa}{E_0}$$

$$\vec{E}(t_s') \to E_0. \tag{2.89}$$

$$\tag{2.90}$$

Then Taylor expand the classical trajectory near the saddle time

$$\mathbf{r}_c(\tau) \approx \frac{1}{2}E_0\left(\tau^2 - t_s^2\right) \approx i\kappa(\tau - t_s). \tag{2.91}$$

Substitute eq.(2.88), (2.91) into eq.(2.86) and evaluate the integral we obtain

$$\tilde{W}_1(\mathbf{p}, \mathbf{r}_0; t, t_s') = -i\frac{Z}{\kappa}\ln\left(\frac{(t_s + t_m)\, i\kappa\,(t_m - t_s)}{t_s - t_m}\right). \tag{2.92}$$

When considering the limit $t_m \to t_s$ we can obtain

$$\tilde{W}_1(\mathbf{p}, \mathbf{r}_0; t, t_s') = -i\frac{Z}{\kappa}\ln\left(-2i\kappa^2 t_s\right) = -i\frac{Z}{\kappa}\ln\left(\frac{2\kappa^3}{E_0}\right). \tag{2.93}$$

Substitute eq.(2.93) into eq.(2.83) we can obtain the total ionization rate

$$\Gamma \propto e^{-2\Im\left\{\tilde{W}(\mathbf{p},\mathbf{r}_0;t,t_s')\right\}} = \left(\frac{E_0}{2\kappa^3}\right)^{-2\frac{Z}{\kappa}} e^{-2\Im\left\{\tilde{W}_0(\mathbf{p},\mathbf{r}_0;t,t_s')\right\}} \tag{2.94}$$

Comparing eq.(2.94) with eq.(2.81) we can see that the Coulomb correction is given by a multiplication factor:

$$Q_c = \left(\frac{E_0}{2\kappa^3}\right)^{-2\frac{Z}{\kappa}}. \tag{2.95}$$

This correction factor has been used to correct the SFA ionization rate in the Keldysh-type theories.

2.5 Including the excited state - the dressed state picture

When atoms or molecules are present in the strong external electric field polarization effect will be induced. The polarization of the electron cloud can be considered as a superposition of the field-free ground state and the excited state; however, the Keldysh theory only considered the ionization from the ground state of the electron. Excited states have been completely ignored. In this section we will introduce a method that is capable of including the dressed states to the Keldysh formalism. Polarization effect comes out as a limiting case of the dressed states when the external field becomes static.

2.5.1 Partition of the Hilbert space

First of all we will follow the discussion in reference [66] and introduce the projection operator defined by partitioning the identity operators $\hat{I}$.

$$\begin{aligned} \hat{I} = & \underbrace{|\phi_g\rangle\langle\phi_g| + |\phi_u\rangle\langle\phi_u|}_{} + \underbrace{\sum_{\epsilon\neq g,u} |\phi_\epsilon\rangle\langle\phi_\epsilon|}_{} \\ \hat{I} = & \qquad\qquad \hat{P}_b \qquad\qquad\qquad\quad \hat{P}_c \end{aligned} \tag{2.96}$$

where $|\phi\rangle$ is a complete set of eigen-states defined by the field-free Hamiltonian. The total Hamiltonian and the wavefunction can be partitioned accordingly

$$\begin{aligned} \hat{I}^\dagger \hat{H} \hat{I} &= \hat{P}_b^\dagger \hat{H} \hat{P}_b + \hat{P}_c^\dagger \hat{H} \hat{P}_c + \hat{P}_b^\dagger \hat{V}_L \hat{P}_c + \hat{P}_c^\dagger \hat{V}_L \hat{P}_b \\ &= \hat{H}_b + \hat{H}_c + \hat{H}_{bc} + \hat{H}_{cb} \end{aligned} \tag{2.97}$$

$$\begin{aligned} \hat{I}\,|\Psi\rangle &= \hat{P}_b\,|\Psi\rangle + \hat{P}_c\,|\Psi\rangle \\ &= |\Psi\rangle_b + |\Psi\rangle_c \end{aligned} \tag{2.98}$$

Substitute eq.(2.97), (2.98) into the time-dependent Schrödinger equation (TDSE) we can obtain

$$\left\{\hat{H}_b + \hat{H}_c + \hat{H}_{bc} + \hat{H}_{cb}\right\}\left\{|\Psi\rangle_b + |\Psi\rangle_c\right\} = i\partial_t\left\{|\Psi\rangle_b + |\Psi\rangle_c\right\}, \tag{2.99}$$

which is completely equivalent to the original TDSE at the moment. The new form of the equation allows us to include dressing to the initial state in the Keldysh theory. To do so

we should first introduce the approximation that will decouple the bound subspace and the continuum subspace. Eq.(2.99) can be written as

$$\left\{\hat{H}_b - i\partial_t\right\}|\Psi\rangle_b + \hat{H}_c|\Psi\rangle_c + \cancel{\hat{H}_{bc}|\Psi\rangle_c} + \hat{H}_{cb}|\Psi\rangle_b = i\partial_t|\Psi\rangle_c\,, \tag{2.100}$$

where the third term on the LHS is neglected because we only want to consider the transition amplitude from the bound state to continuum. We further assume the population change in the bound subspace is negligible we can decouple eq.(2.100) into two equations so that

$$\left\{\hat{H}_b - i\partial_t\right\}|\Psi\rangle_b = 0 \tag{2.101}$$

$$i\partial_t|\Psi\rangle_c - \hat{H}_c|\Psi\rangle_c = \hat{H}_{cb}|\Psi\rangle_b\,. \tag{2.102}$$

Note this approximation is consistent with the SFA in the KFR theory. The decoupling process allows us to solve the bound state dynamics as initial condition first and substitute into Keldysh's formalism to obtain the transition amplitude. Depend on the initial condition and the external field, the electron can be in either a field-free eigenstate representation or in a Floquet eigenstate representation. In the next section we will examine these two representations in more details.

2.5.2 Two-level initial state model

When the external laser field is periodic with period T_p the exact Hamiltonian will also be periodic. Define the Floquet Hamiltonian

$$\hat{H}_{bF} = \hat{H}_b - i\partial_t \tag{2.103}$$

such that one can find corresponding Floqeut eigenstates

$$\hat{H}_{bF}\left|\tilde{\phi}_\pm\right\rangle = \lambda_\pm\left|\tilde{\phi}_\pm\right\rangle, \tag{2.104}$$

where $\left|\tilde{\phi}_\pm\right\rangle$ are functions of time with period T_p. $\lambda_\pm$ denote the two eigenvalues. The solution of eq.(2.101) that describes the initial state can be written as a linear combination of the Floquet eigenstates

$$|\Psi\rangle_b = a_+e^{-i\lambda_+t}\left|\tilde{\phi}_+\right\rangle + a_-e^{-i\lambda_-t}\left|\tilde{\phi}_-\right\rangle, \tag{2.105}$$

which is in a dressed state representation.

In the next step we should find a relation between the two basis. Within two level model the electronic wave function is given by a linear combination of the ground state $\phi_g(R,\mathbf{r}) = \langle \mathbf{r}|\phi_g\rangle$ and the first excited state $\phi_u(R,\mathbf{r}) = \langle \mathbf{r}|\phi_u\rangle$:

$$\Psi_b = \mathcal{F}_g(t)\phi_g(R) + \mathcal{F}_u(t)\phi_u(R), \tag{2.106}$$

where R denotes an adiabatic parameter which in the case of a diatomic molecule can be the internuclear separation whose varying rate is much less than the electronic motion. The coefficients of the field-free states can be obtained by

$$\begin{pmatrix} -I_g(R) & \mu(R,t) \\ \mu^*(R,t) & -I_u(R) \end{pmatrix} \begin{pmatrix} \mathcal{F}_g(R,t) \\ \mathcal{F}_u(R,t) \end{pmatrix} = i\partial_t \begin{pmatrix} \mathcal{F}_g(R,t) \\ \mathcal{F}_u(R,t) \end{pmatrix}, \tag{2.107}$$

where $I_g(R)$ and $I_u(R)$ are the eigenvalues of the ground state and the first excited states respectively. Under dipole approximation the linearly polarized external electric field is given by

$$E(t) = E_0\hat{z}\cos(\omega_L t + \varphi). \tag{2.108}$$

In the length Gauge the off-diagonal term can be written as

$$\mu(R,t) = Z_{gu}E_0\cos(\omega_L t + \varphi), \tag{2.109}$$

where $Z_{gu} = \langle \phi_g(R)|z|\phi_u(R)\rangle$ is the transition dipole moment. Even though in this thesis we are mainly concerning the ionization of atoms adding the parameter R is for our future convenience. Next we can define an unitary transformation

$$\hat{U}_0 = \begin{bmatrix} e^{iI_g t}e^{-i\frac{\Delta}{2}t} & 0 \\ 0 & e^{iI_u t}e^{i\frac{\Delta}{2}t} \end{bmatrix} \tag{2.110}$$

that transforms both the Hamiltonian and the wave function in eq.(2.107).The detuning parameter is given by

$$\Delta = \omega_0(R) - \omega_L = I_g(R) - I_u(R) - \omega_L \tag{2.111}$$

The Floquet Hamiltonian after the transformation and the rotating wave approximation (RWA) takes the simple form

$$\hat{U}_0^{-1}\hat{H}_F\hat{U}_0 = \hat{H}_I = \frac{1}{2}\begin{bmatrix} I_u - I_g + \omega_L & Z_{gu}E_0 \\ Z_{gu}E_0 & I_g - I_u - \omega_L \end{bmatrix}. \tag{2.112}$$

This new Hamiltonian can be diagonalized using another unitary transformation

$$\hat{U}_1^{-1}\hat{H}_I\hat{U}_1 = \begin{pmatrix} \lambda_- & 0 \\ 0 & \lambda_+ \end{pmatrix}, \tag{2.113}$$

where

$$\hat{U}_1 = \begin{pmatrix} \cos\left(\frac{\vartheta}{2}\right) & -\sin\left(\frac{\vartheta}{2}\right) \\ \sin\left(\frac{\vartheta}{2}\right) & \cos\left(\frac{\vartheta}{2}\right) \end{pmatrix}, \tag{2.114}$$

$$\lambda_\pm = \pm\frac{1}{2}\sqrt{\Delta^2 + (Z_{gu}E_0)^2}. \tag{2.115}$$

The Floquet eigenstates (dressed states) are given by

$$\tilde{\phi}_+ = \cos\left(\frac{\vartheta}{2}\right)\mathrm{e}^{\mathrm{i}\left(\mathrm{I_g}-\frac{\Delta}{2}\right)\mathrm{t}}\phi_\mathrm{g} + \sin\left(\frac{\vartheta}{2}\right)\mathrm{e}^{\mathrm{i}\left(\mathrm{I_u}+\frac{\Delta}{2}\right)\mathrm{t}}\phi_\mathrm{u} \tag{2.116}$$

$$\tilde{\phi}_- = -\sin\left(\frac{\vartheta}{2}\right)\mathrm{e}^{\mathrm{i}\left(\mathrm{I_g}-\frac{\Delta}{2}\right)\mathrm{t}}\phi_\mathrm{g} + \cos\left(\frac{\vartheta}{2}\right)\mathrm{e}^{\mathrm{i}\left(\mathrm{I_u}+\frac{\Delta}{2}\right)\mathrm{t}}\phi_\mathrm{u}, \tag{2.117}$$

where

$$\tan(\vartheta) = -\frac{\mathrm{Z_{gu}E_0}}{\Delta} \tag{2.118}$$

When the external laser field is slowly varying we can apply the adiabatic approximation to eq.(2.101). Diagonalize the instantaneous eigenvalue equation

$$\hat{H}_b\left|\Psi\right\rangle_b = \lambda\left|\Psi\right\rangle_b \tag{2.119}$$

is equivalent to diagonalize the Floquet eigenvalue equation (2.104) which will lead to two polarized states expressed in terms of a superposition of the field-free eigenstates. The polarized states are given be eq.(2.116,) (2.117) with $\omega_L = 0$.

Once the bound state dynamics is solved we can use the solution as initial state to solve the ionization problem described by eq.(2.102). For application example, see eq.(7.28) in section 7.3.1.

2.6 The Lewenstein model of HHG

Leweinstein first introduced the strong field approximation to describe the high harmonic generation process [32]. The theory starts from calculating the electron dipole moment:

$$\mu(t) = \langle \Psi(t) | \left(-\mathbf{r}\right) | \Psi(t) \rangle \,, \tag{2.120}$$

where $|\Psi(t)\rangle$ is the exact solution to the single active electron Schrödinger equation in the presence of the laser and the binding potential. Using the Dyson eq.(2.10), replacing the exact time evolution operator by the Volkov operator (eq.(2.21)) and keeping the leading order term, we obtain

$$\mu(t) \simeq i \int_{-\infty}^{t} dt' \left\langle \phi_i(t) \left| \mathbf{r} \hat{U}_V(t,t') \hat{V}_L(t') \right| \phi(t') \right\rangle + c.c. \tag{2.121}$$

In the length gauge and under dipole approximation we can write

$$\mu(t) \simeq i \int_{-\infty}^{t} dt' \int \frac{d^3\mathbf{k}}{(2\pi)^3} \langle \phi_i \left| \mathbf{r} \right| \mathbf{k} + \mathbf{A}(t) \rangle \langle \mathbf{k} + \mathbf{A}(t) \left| \mathbf{r} \right| \phi_i \rangle \cdot \mathbf{E}(t') e^{iS_p(\mathbf{k},t,t')} + c.c., \tag{2.122}$$

where the action is given by

$$S_p(\mathbf{k}, t, t') = \int_{t'}^{t} dt'' \left\{ \frac{1}{2} \left[\mathbf{k} + \mathbf{A}(t'') \right]^2 + I_p \right\}. \tag{2.123}$$

The numerical evaluation of the four dimensional integral in eq.(2.122) is computationally demanding; however, one can approximate the momentum integral using the method of steepest descent. According to this method the saddle point which contributes the most to the integral is given by the equation

$$\nabla_{\mathbf{k}} S_p(\mathbf{k}, t, t')|_{\mathbf{k}=\mathbf{k}_s} = 0. \tag{2.124}$$

Assume the vector potential of the laser field is known, we can write the solution of eq.(2.124) as

$$\mathbf{k}_s = \frac{\int_{t'}^{t} \mathbf{A}(t'') dt''}{t' - t}. \tag{2.125}$$

Making a Taylor expansion of $S_p(\mathbf{k}, t, t')$ around $\mathbf{k} = \mathbf{k}_s$ we obtained

$$S_p(\mathbf{k}, t, t') \approx \int_{t'}^{t} dt'' \left\{ \frac{1}{2} \left[\mathbf{k}_s + \mathbf{A}(t'') \right]^2 + I_p \right\} + (t - t')\mathbf{k}^2 + \mathcal{O}(\mathbf{k}^3). \tag{2.126}$$

Note the linear term in $\mathbf{k}$ is absent due to the eq.(2.124). We further approximate the pre-exponential terms by the leading order expansion

$$\langle \phi_i \left| \mathbf{r} \right| \mathbf{k} + \mathbf{A}(t) \rangle \langle \mathbf{k} + \mathbf{A}(t) \left| \mathbf{r} \right| \phi_i \rangle \approx \langle \phi_i \left| \mathbf{r} \right| \mathbf{k}_s + \mathbf{A}(t) \rangle \langle \mathbf{k}_s + \mathbf{A}(t) \left| \mathbf{r} \right| \phi_i \rangle . \tag{2.127}$$

Substitute eq.(2.126), (2.127) into eq.(2.122) we obtained a three dimensional Gaussian integral with complex exponent. By choosing the path of steepest descent we can change the integral to a real Gaussian integral. In this specific case the integration path for each momentum component should be chosen along a vector which is -45^o with respect to the real axis. The Gaussian integral thus can be evaluated analytically and we obtained the dipole moment

$$\begin{aligned} \mu(t) \simeq i \int_{-\infty}^{t} dt' \left[\frac{1}{2\pi \left(\epsilon + i \left(t - t' \right) \right)} \right]^{3/2} & \mathbf{d}^* \left(\mathbf{k}_s + \mathbf{A}(t) \right) \\ & e^{iS_p(\mathbf{k}_s, t, t')} \mathbf{d} \left(\mathbf{k}_s + \mathbf{A}(t') \right) \cdot \mathbf{E}(t') + c.c., \end{aligned} \tag{2.128}$$

where $\mathbf{d} \left(\mathbf{k}_s + \mathbf{A}(t) \right) = \langle \mathbf{k}_s + \mathbf{A}(t) \left| \mathbf{r} \right| \phi_i \rangle$. The convergence factor ϵ is introduced which will be taken in the limit $\epsilon \to 0^+$. In Lewenstein's original paper a change of variable is introduced $\tau = t - t'$ so that eq.(2.128) can be re-written as

$$\begin{aligned} \mu(t) \quad \simeq \quad i \int_{0}^{\infty} d\tau \left[\frac{1}{2\pi \left(\epsilon + i\tau \right)} \right]^{3/2} & \mathbf{d}^* \left(\mathbf{k}_s + \mathbf{A}(t) \right) \\ & e^{iS_p(\mathbf{k}_s, t, \tau)} \mathbf{d} \left(\mathbf{k}_s + \mathbf{A}(t - \tau) \right) \cdot \mathbf{E}(t - \tau) + c.c. \end{aligned} \tag{2.129}$$

According to the principle of classical electromagnetism one should expect the HHG spectrum to be proportional to the Fourier transform of the dipole moment

$$I(\omega) \propto \lim_{T_p \to \infty} \frac{1}{T_p} \left| \int_{-T_p/2}^{T_p/2} \mu(t) e^{i\omega t} dt \right| \tag{2.130}$$

To proceed further we introduce a monochromatic CW laser pulse with linear polarization along the z-axis so $\mathbf{A}(t)$ is given by eq.(2.26). The action can be integrated analytically so we obtain

$$S_p(k_s, t, \tau) = \frac{1}{2} \left[-k_s^2 \tau + 2U_p \left(\tau - \frac{1}{2\omega_L} (\sin 2\omega_L t - \sin 2\omega_L (t - \tau)) \right) \right] + I_p \tau, \tag{2.131}$$

where

$$k_s = \frac{E_0}{\omega_L^2 \tau} \cos \omega_L t - \cos \omega_L (t - \tau). \tag{2.132}$$

Note we have dropped the vector notation because the saddle point eq.(2.125) enforces the photoelectron momentum to be parallel to the laser polarization hence the motion of electron is only restricted in the direction of laser polarization. When substitute eq.(2.131), (2.132) into eq.(2.129) we found the dipole moment becomes a periodic function of t with period $T_p = \frac{2\pi}{\omega_L}$ so that in the frequency domain it will peaked at the integer multiples of ω_L.In the next step we will show that only the odd harmonics will contribute to the spectrum.

The Fourier coefficient defined in eq.(2.130) can also be written as a summation of two integrals

$$\begin{aligned}\int_{-T_p/2}^{T_p/2} \mu(t) e^{in\omega_L t} dt &= \int_{-T_p/2}^{0} \mu(t) e^{in\omega_L t} dt + \int_{0}^{T_p/2} \mu(t) e^{in\omega_L t} dt \\ &= \int_{-T_p/2}^{0} \mu(t) e^{in\omega_L t} dt + \int_{-T_p/2}^{0} \mu(t' + T_p/2) e^{in\omega_L (t'+T_p/2)} dt',\end{aligned} \tag{2.133}$$

where n is an integer. Normally the initial state of the electron wavefunction has definite parity (either even or odd) so the transition dipole matrix element will have the symmetry property given by

$$\mathbf{d}(-\mathbf{k}) = \mp \mathbf{d}(\mathbf{k}), \tag{2.134}$$

where $-$ for even and $+$ for odd parity. In addition, after half a laser cycle the mechanical momentum of the electron will be inverted by the laser field so that

$$\mathbf{d}(\mathbf{k}_s + \mathbf{A}(t))\{t + T_p/2\} \mapsto \mathbf{d}(-\mathbf{k}_s - \mathbf{A}(t)), \tag{2.135}$$

Furthermore, the electric field will change direction and the action in eq.(2.131) remains the same. Putting things together we can conclude that

$$\mu(t' + T_p/2) = -\mu(t') \tag{2.136}$$

If the integer $n = 2m$ is an even number we can write eq.(2.134)

$$\begin{aligned}\int_{-T_p/2}^{T_p/2} \mu(t) e^{i2m\omega_L t} dt &= \int_{-T_p/2}^{0} \mu(t) e^{i2m\omega_L t} dt + \int_{-T_p/2}^{0} \mu(t' + T_p/2) e^{i2m\omega_L (t'+T_p/2)} dt' \\ &= \int_{-T_p/2}^{0} \mu(t) e^{i2m\omega_L t} dt - \int_{-T_p/2}^{0} \mu(t') e^{i2m\omega_L t'} dt' \\ &= 0.\end{aligned} \tag{2.137}$$

Therefore the even harmonics will vanish and only the odd terms contribute to the spectrum.

Chapter 3

The method of steepest descent

3.1 Introduction

The method of steepest descent (MSD) is a powerful technique to find an asymptotic expansion of the exponential type integrals [67]. These integrals usually arise from the calculation of transition amplitudes in quantum mechanics. In the previous chapter we have seen that the transition amplitude in the SFA-based theory can be expressed as temporal integrals which may or may not have singularities in the complex domain. In this chapter we will discuss the application of MSD to these integrals. The usual formula for the leading order asymptotic expansion can be given by

$$I(\lambda) = \int_c g(z) e^{\lambda f(z)} \sim \frac{\sqrt{2\pi} g(z_0) e^{i\phi}}{\sqrt{\lambda f''(z_0)}} e^{\lambda f(z_0)}, \tag{3.1}$$

where λ is a real constant assumed to be large. Both $g(z)$ and $f(z)$ are analytic functions in the complex plane. z_0 is the saddle point defined by equation

$$\frac{df(z)}{dz} = 0 \Big|_{z=z_0}. \tag{3.2}$$

The constant phase ϕ is chosen so that $\frac{1}{2}(z - z_0)^2 f''(z_0)$ must be real. In the following sections we will generalize this formula to higher order expansions.

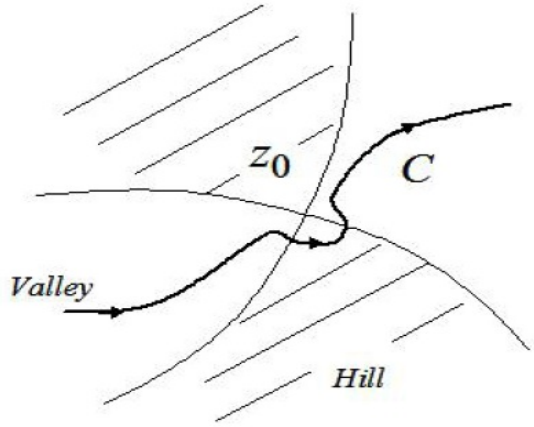

Figure 3.1: Path around the saddle point

3.2 Asymptotic expansion with singularity

The transition amplitude of eqs.(2.32), (2.42), (2.129), (2.53) can be considered to be special cases of the integral

$$I(\lambda) = \int_C g(z) \frac{e^{\lambda w(z)}}{[w'(z)]^\nu} dz \tag{3.3}$$

where $w(z)$ has a simple saddle point at z_0 such that $w'(z_0) = 0$, $w_0'' \equiv w''(z_0) \neq 0$, and the path of integration C can be deformed to lie on the paths of steepest descent (PSD) passing from one valley of $w(z)$ to another, avoiding the singular point z_0 (see Fig.3.1). We assume that $g(z)$ is analytic at z_0. A systematic asymptotic expansion of $I(\lambda)$ can be developed employing the Watson's lemma as the parameter $\lambda \to \infty$ [67]. In the paper [43], we gave the first order term of the asymptotic expansions of a similar integral. Here we derive the second order term of the expansion for eq.(3.3) [68].

Introducing a new integration variable τ by

$$\tau = w_0 - w(z) \tag{3.4}$$

where $w_0 = w(z_0)$, the integral (3.3) becomes

$$I(\lambda) = -\int_L \left[\frac{g(z)}{w'(z)^{\nu+1}} \right]_{z=w^{-1}(w_0-\tau)} e^{\lambda(w_0-\tau)} d\tau \tag{3.5}$$

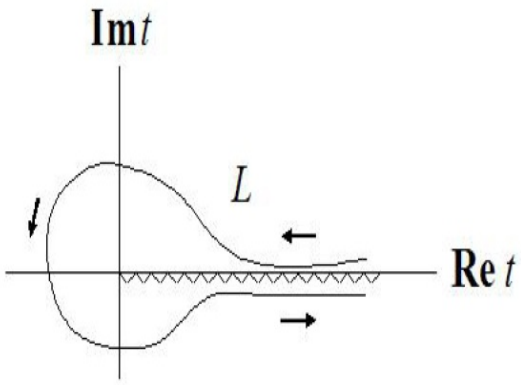

Figure 3.2: The loop path

where it can be shown that eq.(3.4) maps the PSD into the loop path L in the τ-plane [69, 67, 43] (see Fig.3.2). Near the simple saddle point z_0,

$$w(z) = w_0 + \frac{1}{2}w_0''(z-z_0)^2 + \frac{1}{3!}w_0'''(z-z_0)^3 + \cdots, \quad w'(z) = w_0''(z-z_0) + \frac{1}{3}w_0'''(z-z_0)^2 + \cdots. \tag{3.6}$$

With $z - z_0 = \rho e^{i\theta}$, the argument of $z - z_0$ on the PSDs satisfies [67, 43]

$$\theta_1 = -\frac{\alpha}{2} + \frac{\pi}{2}, \quad \text{or} \quad \theta_2 = -\frac{\alpha}{2} + \frac{3\pi}{2}, \tag{3.7}$$

where $w_0'' = |w_0''|e^{i\alpha}$, $0 \le \alpha < 2\pi$, so that $e^{-\lambda w(z)} \simeq e^{-\lambda w_0} e^{-\lambda \frac{1}{2}|w_0''|\rho^2}$. We label the paths of steepest descent from z_0 by D_1 and D_2, corresponding to θ_1 and θ_2, respectively [43]. For simple saddle points, the directions of steepest descent are directly opposite to each other: $\theta_2 - \theta_1 = \pi$. We only need to consider the following two possibilities in deforming the path C to lie along the PSDs [43] (see Fig.3.3):

- Case A: first along the path of steepest *ascent* $-D_1$ towards z_0, avoiding z_0 *counter-clockwise* along a small semicircle, and leaving z_0 along the path of steepest *descent* D_2;

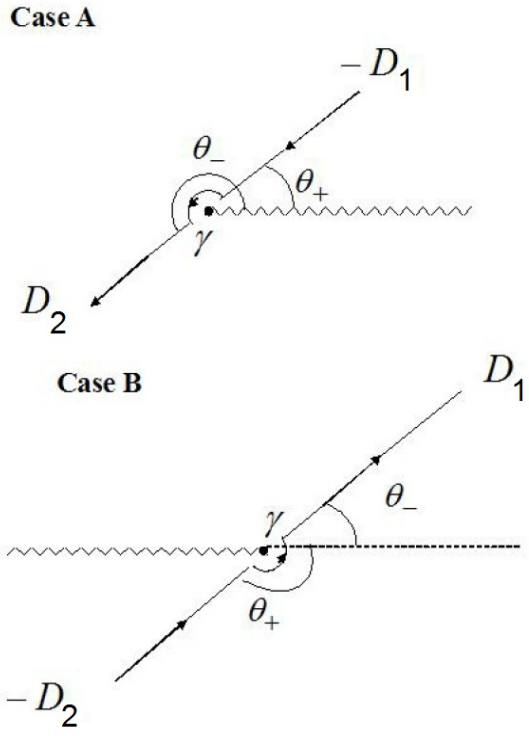

Figure 3.3: Paths of steepest descent

- Case B: first along the path of steepest *ascent* $-D_2$ towards z_0, avoiding z_0 *counter-clockwise* along a small semicircle, and leaving z_0 along the path of steepest *descent* D_1.

The first order mapping is obtained [43] by truncating the series for $w(z)$ in eq.(3.6) to the quadratic term and inverting eq.(3.4):

$$z - z_0 = \left(\frac{2\tau}{w_0''}\right)^{1/2} e^{\pm i\frac{\pi}{2}} \tag{3.8}$$

where $\pm$ correspond to the Cases A and B, respectively. Then eq.(3.8) maps the PSDs in the z-plane to a loop contour in the τ-plane which comes in from ∞ above the cut on the positive real τ axis, loops around the branch point at the origin counterclockwise to below the cut, and return to ∞ below the cut on the positive real τ axis.

With $w'(z)$ given by eq.(3.6), the integrand of eq.(3.5) has a pole of order $\nu + 1$ at z_0, and it can be expanded in a Laurent series as:

$$\frac{1}{w'(z)^{\nu+1}} = \frac{a_1}{(z - z_0)^{\nu+1}} + \frac{a_2}{(z - z_0)^{\nu}} + \cdots, \tag{3.9}$$

where

$$a_1 = \frac{1}{[w_0'']^{\nu+1}}, \quad a_2 = -\frac{(\nu + 1)w_0'''}{3[w_0'']^{\nu+2}}, \cdots. \tag{3.10}$$

We now require a higher order expansion of of the inverse mapping for eq.(3.4): let

$$z - z_0 = \xi(1 + \varepsilon) \qquad \text{where} \qquad \xi = \left(\frac{2\tau}{w_0''}\right)^{1/2} e^{\pm i\frac{\pi}{2}}. \tag{3.11}$$

Substituting eq.(3.11) into eq.(3.4), noting that $-\frac{1}{2}w_0''\xi^2 = \tau$ and ignoring terms $\mathcal{O}(\varepsilon^2)$, we obtain

$$\varepsilon = -\frac{w_0'''}{6w_0''}\xi[1 + \mathcal{O}(\tau^{\frac{1}{2}})], \tag{3.12}$$

where we observe that $\varepsilon = \mathcal{O}(\xi) = \mathcal{O}(\tau^{\frac{1}{2}})$. Since $g(z)$ is analytic at z_0, we can make a Taylor series expansion

$$g(z) = g_0 + g_0'(z - z_0) + \cdots \tag{3.13}$$

where $g_0 = g(z_0)$, $g_0' = g'(z_0)$, etc. Substituting eqs. (3.10), (3.11), (3.12) and (3.13) into the Laurent expansion (3.9) yields an asymptotic expansion in τ:

$$\begin{aligned}\frac{g(z)}{w'(z)^{\nu+1}} &= \frac{g_0}{(w_0'')^{\nu+1}}\left[\left(\frac{w_0''}{2\tau}\right)^{\frac{\nu+1}{2}} e^{\mp i\frac{\pi}{2}(\nu+1)}\right. \\ &\left. -\left(\frac{w_0''}{2\tau}\right)^{\frac{\nu}{2}} e^{\mp i\frac{\pi}{2}\nu}\left(\frac{(\nu+1)w_0'''}{6w_0''}-\frac{g_0'}{g_0}\right)+\mathcal{O}\left(\frac{1}{\tau}\right)^{\frac{\nu-1}{2}}\right]. \qquad (3.14)\end{aligned}$$

Now, Watson's lemma for the loop integral

$$I(\lambda) = \int_L e^{-\lambda\tau} f(\tau) d\tau$$

states that [67] if (i) $f(\tau)$ is analytic in the complex τ-plane except on the cut along the real axis with $\tau = 0$ a branch point, (ii) $f(\tau) = O(e^{a\tau})$ as $|\tau| \to \infty$, a real, for some sector around the real axis, and (iii) $f(\tau) \sim \sum_{m=0}^{\infty} c_m \tau^{r_m}$ as $|\tau| \to 0$, $\arg(\tau) \neq 0$ with $\mathrm{Re}(r_m)$ increasing monotonically to ∞ as $m \to \infty$, then

$$I(\lambda) \sim -2\pi i \sum_{m=0}^{\infty} \frac{c_m e^{i\pi r_m}}{\Gamma(-r_m)\lambda^{r_m+1}} \qquad \text{as} \qquad \lambda \to \infty. \qquad (3.15)$$

Substituting (3.14) into (3.5) and identifying $r_0 = -\frac{\nu+1}{2}$ and $r_1 = -\frac{\nu}{2}$, we can apply Watson's lemma and obtain from eq.(3.15)

$$\begin{aligned}I(\lambda) &= 2\pi i \frac{g_0\, e^{\lambda w_0} e^{-i(\nu+1)(1\pm1)\frac{\pi}{2}}}{[2w_0'']^{\frac{\nu+1}{2}}\ \Gamma(\frac{\nu+1}{2})}\left(\frac{1}{\lambda}\right)^{\frac{1-\nu}{2}}\left[1 \pm \frac{2\Gamma(\frac{\nu+1}{2})}{[2w_0'']^{\frac{1}{2}}\ \Gamma(\frac{\nu}{2})}\left(\frac{1}{\lambda}\right)^{\frac{1}{2}}\left(\frac{(\nu+1)w_0'''}{6w_0''}-\frac{g_0'}{g_0}\right)\right. \\ &\left. +\mathcal{O}\left(\frac{1}{\lambda}\right)\right]. \qquad (3.16)\end{aligned}$$

The first order term has been derived earlier [43]. If there are more than one isolated saddle points, we simply sum up the contributions from each saddle point.

3.3 Asymptotic expansion without singularity

In this subsection we show the derivation of the higher order expansion of the the integral eq.(2.32) along the path of steepest descent when the pre-exponential is not singular at the saddle point. The integral can be written as

$$I^{SAD} = \int_{PSD} dt f(t) e^{iS_p(t)}, \qquad (3.17)$$

where the pre-exponential function $f(t)$ is analytic at the saddle point t_s of the exponential function. This integral basically corresponds to the case $\nu = 0$ in the previous section. To find the higher order expansion of I^{SAD}, we follow the same procedure as before. Using the mapping eq.(3.4), we obtain

$$I^{SAD} = \int_L d\tau \left[\frac{f(t)}{S_p'(t)}\right]_{t(\tau)} e^{iS_p(t_s)} e^{-\tau} \tag{3.18}$$

where L is the loop path of Fig.3.1. The Laurent series expansion of the pre-exponent is given by

$$\frac{f(t)}{S_p'(t)} = \frac{a_{-1}}{t - t_s} + a_0 + a_1(t - t_s) + \ldots, \tag{3.19}$$

where

$$\begin{aligned} a_{-1} &= \frac{f(t_s)}{S_p''(t_s)} \\ a_0 &= \frac{f(t_s)}{S_p''(t_s)} \left(\frac{f'(t_s)}{f(t_s)} - \frac{S'''(t_s)}{2S_p''(t_s)}\right) \\ a_1 &= \frac{f(t_s)}{S_p''(t_s)} \left(\frac{f''(t_s)}{2f(t_s)} - \frac{f'(t_s)S'''(t_s)}{2f(t_s)S_p''(t_s)} - \frac{S''''(t_s)}{6S_p''(t_s)}\right). \end{aligned} \tag{3.20}$$

The second order expansion of the mapping of eq.(3.11) can be re-written as

$$t - t_s = \beta\sqrt{\tau} - \alpha\beta^2\tau, \tag{3.21}$$

where

$$\beta = \left[\frac{2}{iS_p''(t_s)}\right]^{\frac{1}{2}}, \quad \alpha = \frac{S'''(t_s)}{6S_{t_s}''} \tag{3.22}$$

Combining eq.(3.19) with eq.(3.21) and substituting into eq.(3.18), we obtain

$$I^{SAD} = -ie^{iS_p(t_s)} \int_L d\tau \left[\frac{a_{-1}}{\beta}\frac{1}{\sqrt{\tau}} + (a_{-1}\alpha + a_0) + (a_{-1}\alpha^2\beta + a_1\beta)\sqrt{\tau}\right] e^{-\tau} \tag{3.23}$$

Recall the integral representation of the Gamma function

$$\int_L e^{-\tau}\tau^{\nu} d\tau = (e^{2\pi i\nu} - 1)\Gamma(\nu + 1), \tag{3.24}$$

which can be applied to eq.(3.23) to obtain

$$I^{SAD} = 2i\sqrt{\pi}\frac{a_{-1}}{\beta}e^{iS_p(t_s)} + i\sqrt{\pi}(a_{-1}\alpha^2\beta + a_1\beta)e^{iS_p(t_s)}. \tag{3.25}$$

The first order term in eq.(3.25) is the same as eq.(3.1) in the introduction. The next leading order correction is given by the third order term because

$$\int_L d\tau(a_{-1}\alpha + a_0)e^{-\tau} = 0. \tag{3.26}$$

Chapter 4

Testing the strong field approximation and other approximations

In this chapter we will apply the asymptotic expansions derived in Chapter 3 to the transition amplitudes derived in Chapter 2 for three well studied models: the zero range potential, the hydrogen atom and the hydrogen molecular ion. The critical approximations will be tested by comparing the results with the exact numerical integrations.

4.1 The zero-range potential

In this section, we present results of numerical calculations of the differential and total ionization rates under the SFA and various additional approximations, for the case of an atom with zero-range potential. The zero-range potential model has been extensively used for the study of strong field ionization [26, 70] and high harmonic generation [71, 33]. The three dimensional delta function potential

$$V_a(\mathbf{r}) = \frac{2\pi}{\kappa}\delta(\mathbf{r})\frac{\partial}{\partial r} \tag{4.1}$$

supports a single bound state

$$\psi_i(\mathbf{r}) = \sqrt{\frac{\kappa}{2\pi}}\frac{e^{-\kappa r}}{r} \tag{4.2}$$

with ionization potential $I_p = \dfrac{\kappa^2}{2}$. The momentum representation of this wave function can readily be evaluated:

$$\langle \mathbf{k} + \mathbf{A}(t) | \, \psi_i \rangle = \int d^3\mathbf{r} \; e^{-i[\mathbf{k}+\mathbf{A}(t)]\cdot\mathbf{r}} \; \psi_i(\mathbf{r}) = \frac{\sqrt{2\pi\kappa}}{\frac{1}{2}[\mathbf{k}+\mathbf{A}(t)]^2 + \frac{1}{2}\kappa^2} = \frac{\sqrt{2\pi\kappa}}{\dot{S}_p(t)}. \tag{4.3}$$

Eq.(2.32) becomes simply

$$L_n(\mathbf{k}) = -\sqrt{\frac{\kappa}{2\pi}} \int_0^{2\pi} d\tau \; e^{iS_p(\tau)} \tag{4.4}$$

so that in eq.(3.25) is applicable, yielding asymptotically

$$L_n(\mathbf{k}) = -\sqrt{\kappa} \left[\frac{e^{iS_p(\tau_+)}}{[S_p''(\tau_+)]^{1/2}} + \frac{e^{iS_p(\tau_-)}}{[S_p''(\tau_-)]^{1/2}} \right] \; e^{i\pi/4}. \tag{4.5}$$

Here we only adopt the leading order term in eq.(3.25) which will be sufficient in the case of zero-range potential. The *tunneling limit* of the ionization rate when $\gamma \ll 1$ can now be obtained from eq.(4.16)-(4.19) as

$$\Gamma_{ad} = \frac{\kappa}{8z\gamma^3} \sqrt{\frac{3\omega}{\pi\gamma}} e^{-\frac{8z}{3}\gamma^3 \left(1 - \frac{\gamma^2}{10}\right)}. \tag{4.6}$$

(See AppendixD for more details)

Substituting the static result eq.(C.17) into eq.(2.37), we obtain the quasi-static ionization rate

$$\Gamma_{qs} \simeq \frac{E_0}{2\kappa} \sqrt{\frac{3E_0}{\pi\kappa^3}} \; e^{-\frac{2\kappa^3}{3E_0}}, \tag{4.7}$$

which is identical to the lowest order adiabatic SFA rate of eq.(4.6) if we ignore the $\mathcal{O}(\gamma^2)$ term in the exponent. Such agreement has not been obtained for the case of the hydrogen atom where the electron interacts with the nucleus by the long-range Coulomb potential. This result proved SFA to be quantitatively accurate for the ionization of a zero-range potential atom.

In the next step we choose the parameter $\kappa = 1$ so that $I_p = \frac{1}{2}$ and use this model to examine the validity of the crucial approximations in the theory. We first discuss the calculations of the "exact" SFA rates of eqs.(2.34) and (2.35), which require the numerical evaluation of the amplitude eq.(4.4). The integral in eq.(4.4) can be calculated either

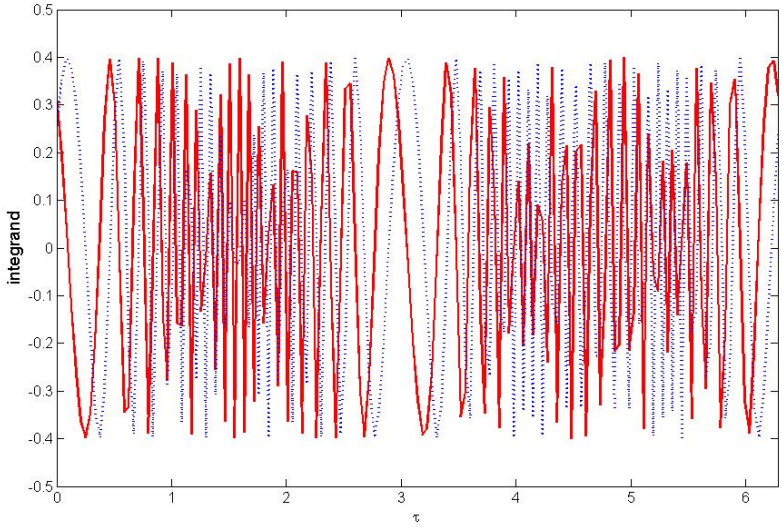

Figure 4.1: Integrand of eq.(4.4) along real path τ.

for real $0 \leq \tau \leq 2\pi$, or along a suitable path in the complex τ-plane. To illustrate the numerical procedure, we choose an exciting laser with $\lambda = 800$ nm and intensity $I = 10^{15}$ W/cm^2, giving a Keldysh parameter $\gamma = 0.338$. The threshold photon number for excitation is $n_{th} = 48$ where n_{th} is the smallest integer $n_{th} \geq n_0$. In Fig. 4.1 we plot the real and imaginary parts of the integrand of eq.(4.4) for $n - n_{th} = 1$ and $\theta = \frac{\pi}{4}$. Clearly, the integrand is a rapidly varying function of τ. Since the integrand is an analytic function of τ, by Cauchy Theorem, the path of integration can be deformed to the complex path $z = \tau + i$ arcsinh γ, $0 \leq \tau \leq 2\pi$, as the integrals along $z = iy$ arcsinh γ and $z = 2\pi + i(1 - y)$ arcsinh γ, $0 \leq y \leq 1$, cancel each other due to the periodicity of the integrand. In Fig. 4.2 we consider the behavior of the integrand along this complex path, and we observe that the integrand is a smooth function of τ. Thus we expect numerical integration along the complex path to be more efficient than along the real path. Indeed, we found the integral along the complex path converges to 6 significant figures using a simple trapezoidal method with 51 points, while to achieve the same accuracy along the real path, more than 200 points are required. Similar efficiency of the complex integration is found for other laser parameters. Hence in our calculation of the "exact" SFA rates, we employ the complex integration method.

The approximations crucial to the understanding of the strong-field dynamics were

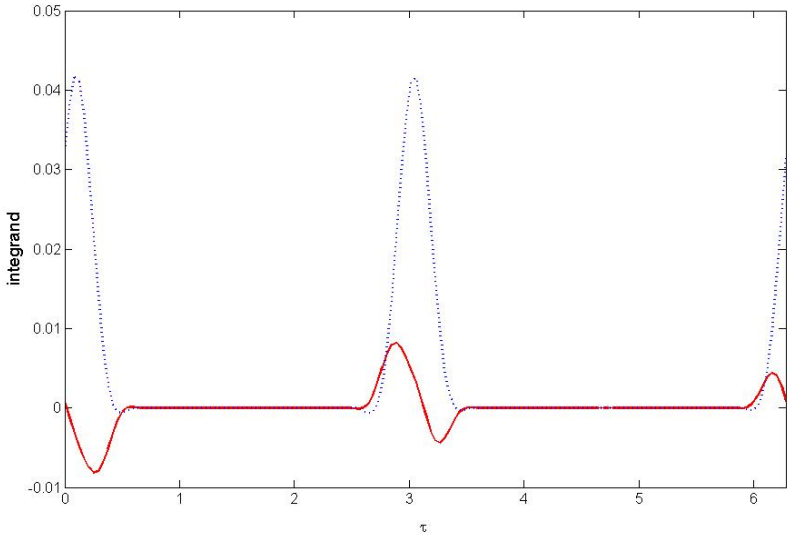

Figure 4.2: Integrand of eq.(4.4) along complex path $z = \tau + i \text{ arcsinh } \gamma$.

Table 4.1: Keldysh parameters for laser parameters used in present study.

I_0 (W/cm^2)	$\lambda = 400$ nm	$\lambda = 532$ nm	$\lambda = 800$ nm	$\lambda = 1064$ nm
1×10^{14}	2.135	1.605	1.068	0.803
5×10^{14}	0.955	0.718	0.478	0.359
1×10^{15}	0.675	0.508	0.338	0.254
5×10^{15}	0.302	0.227	0.151	0.114

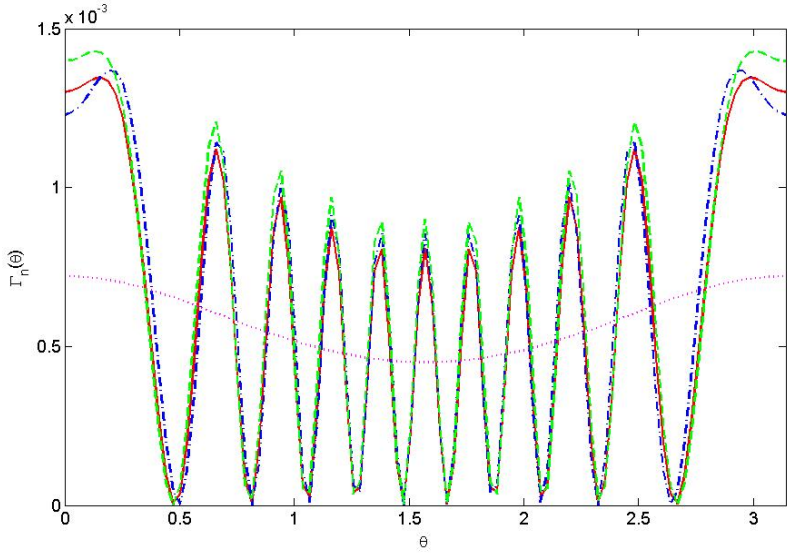

Figure 4.3: $\Gamma_n(\theta)$ for $n - n_{th} = 0$. $\lambda = 800$ nm and $I = 10^{15}$ W/cm^2. Solid line: exact SFA; dot-dash line: SPA; dash line: LPEA; dotted line: LPEANI, interference ignored.

- The method of steepest descent (also refereed as saddle-point approximation),
- The low photoelectron energy approximation (LPEA),
- The low photoelectron approximation neglecting interference (LPEANI).

The saddle-point approximation (SPA) is used to evaluate the integral over τ for the transition amplitude $L_n(\mathbf{k})$, resulting in eq.(D.5) for the ionization rate. Secondly, the low photoelectron energy approximation (LPEA) is employed to give the simple expression for the probability density of eq.(D.16), with which the differential ionization rate $\Gamma_n(\theta)$ of eq.(2.35) can be evaluated. Furthermore, when the interference term in eq.(D.16) is neglected (low photoelectron energy approximation neglecting interference, LPEANI), the sum over the number of photons absorbed and the integral over θ can be evaluated analytically, in the limit where the Keldysh parameter γ is small, to give the adiabatic ionization rate Γ_{ad} of eq.(4.6), which can be compared with the quasi-static rate Γ_{qs} of eq.(4.7). It is important to determine the validity these approximations as the laser parameters change. Here we calculate the differential and total ionization rates for the laser parameters shown in Table 4.1, in which we list the corresponding values of the Keldysh parameter γ.

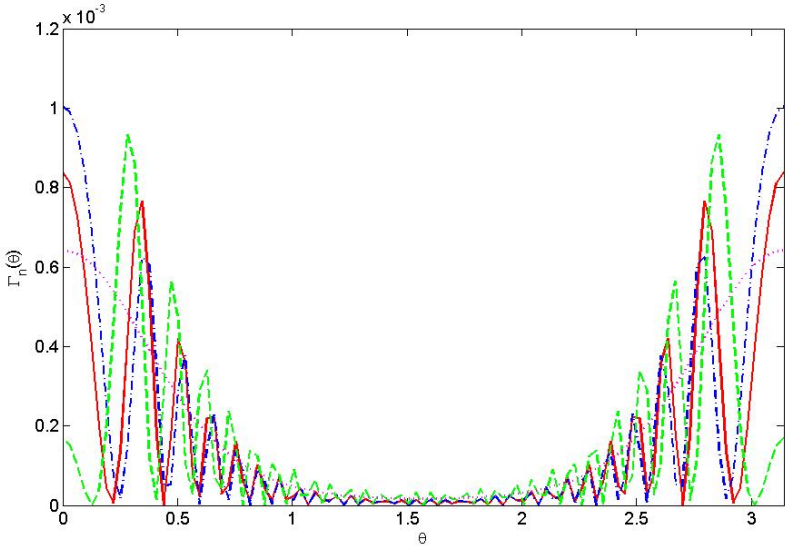

Figure 4.4: $\Gamma_n(\theta)$ for $n - n_{th} = 5$. See caption for Fig.4.3.

In Fig. 4.3, the differential ionization rates $\Gamma_n(\theta)$ for $n - n_{th} = 0$ are presented for the exact SFA as well as various approximate calculations for $\lambda = 800$ nm and $I = 10^{15}$ W/cm^2. In this case, both the SPA and the LPEA results agree very well with the exact SFA results, reproducing the oscillations of $\Gamma_n(\theta)$ as a function of θ. As expected, when the interference term of the LPEA is neglected, these oscillations disappear, replaced by an average smooth spectrum. Similar comparison is made in Fig. 4.4 for the differential ionization rates for $n - n_{th} = 5$. The SPA still gives reasonable results, reproducing again the oscillations of the differential ionization rate, although deviation from the exact SFA results is discernable near $\theta = 0$ and $\theta = \pi$. In general the SPA gives reasonable results for all the laser parameters used in this study. The LPEA tends to over-estimate the differential ionization rate, and the oscillations suffer a phase shift when compared with the exact result. This is not surprising since photoelectrons with larger $n - n_{th}$ will have higher kinetic energy, making the LPEA less accurate.

Fig. 4.5 shows the results for the integral ionization rate $\Gamma_T^{(n)} = \int d\theta\, \Gamma_n(\theta)$ as a function of $n - n_{th}$ for $\lambda = 800$ nm and $I = 10^{15}$ W/cm^2. The SPA results agree very well with the exact SFA results, reproducing the oscillations of $\Gamma_T^{(n)}$ as a function of n. The LPEA results also show oscillations as a function of n, although the LPEA oscillations get out of phase from the exact SFA, and the LPEA tends to over-estimate the integral rate. Again,

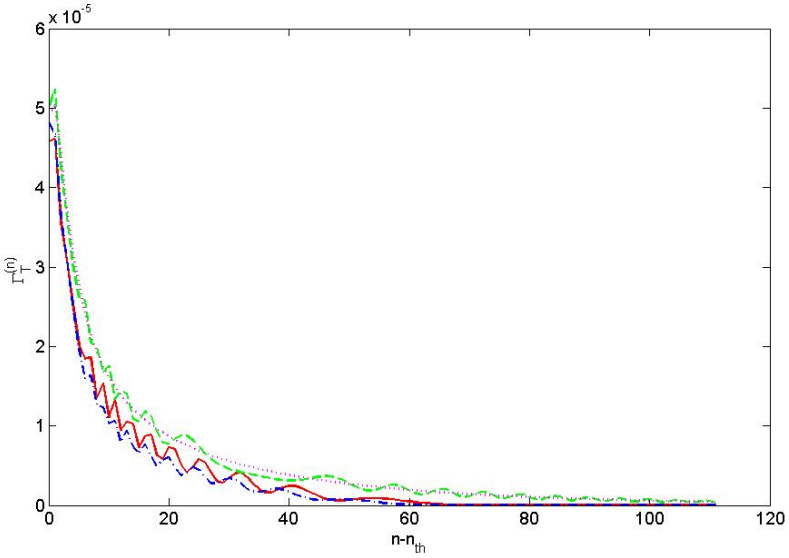

Figure 4.5: $\Gamma_T^{(n)}$ as a function of $n - n_{th}$. See caption for Fig.4.3.

neglecting the interference term of the LPEA produces a smooth average spectrum.

We present the results for the total ionization rate Γ_T in Fig. 4.6 for the laser parameters given in Table 4.1. Naturally, the ionization rate increases rapidly as the laser intensity increases, and decreases as the laser wavelength increases although in the log scale, the variation with wavelength becomes less pronounced with increasing laser intensities. In the log scale, the differences between the various approximations are difficult to be distinguished. In Fig. 4.7, we plot the absolute relative errors for the SPA, the LPEA, and the LPEANI. In these calculations, the sum over n and the integral over θ in eq.(2.34) are performed numerically. Overall the SPA gives the best results, with average relative errors about 10%. As the laser wavelength increases, both the LPEA and the LPEANI generally become more accurate. This trend indicates that at low laser frequencies, the electrons can be viewed as tunneling out the potential barrier with small momentum.

In the study of strong field ionization, it is customary [15, 72, 73] to describe the dynamics as "multiphoton" or "tunneling" according to the Keldysh parameter $\gamma > 1$ or $\gamma < 1$, respectively, although it has been argued that strong field phenomena may require additional parameters for a complete description [20, 74]. Thus it is interesting to plot the relative errors as a function of the Keldysh parameter in Fig. 4.8 using the same data

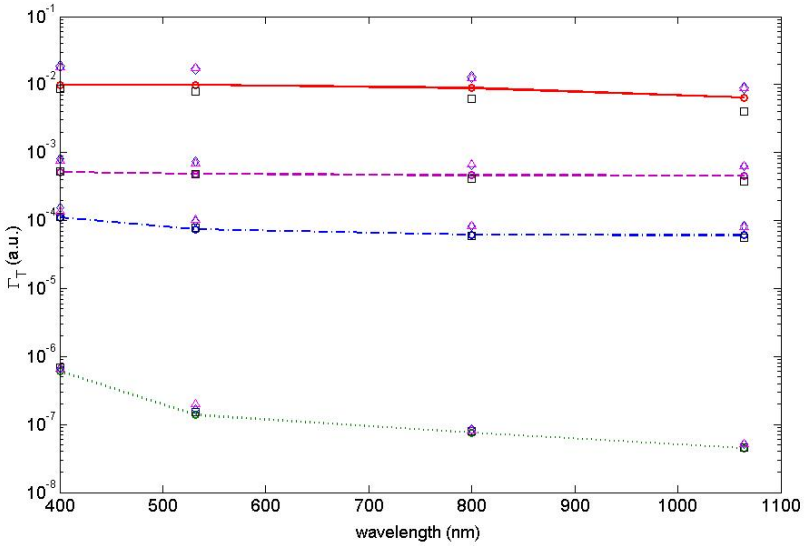

Figure 4.6: Γ_T as a function of laser parameters. Squares: SPA; diamonds: LPEA; triangles: LPEANI. Dotted line: $I = 1 \times 10^{14}$ W/cm^2; dot-dash line: $I = 5 \times 10^{14}$ W/cm^2; dash line: $I = 1 \times 10^{15}$ W/cm^2; solid line: $I = 5 \times 10^{15}$ W/cm^2.

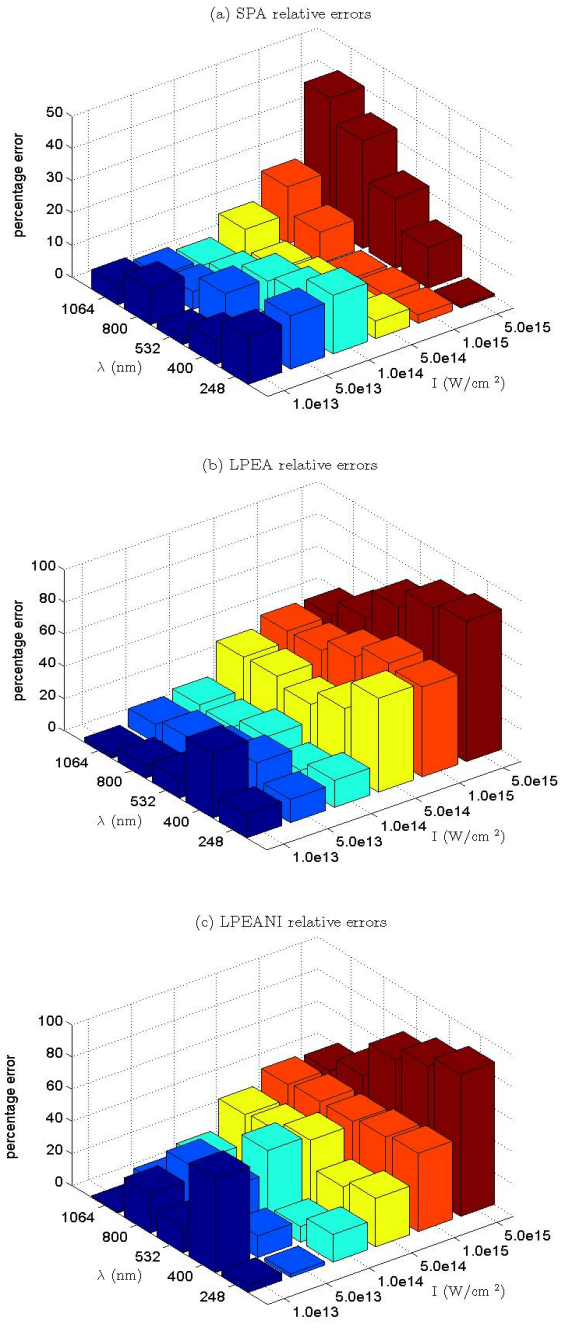

Figure 4.7: Relative errors in Γ_T as a function of laser parameters for (a) SPA, (b) LPEA, and (c) LPEANI. See caption for Fig.4.6

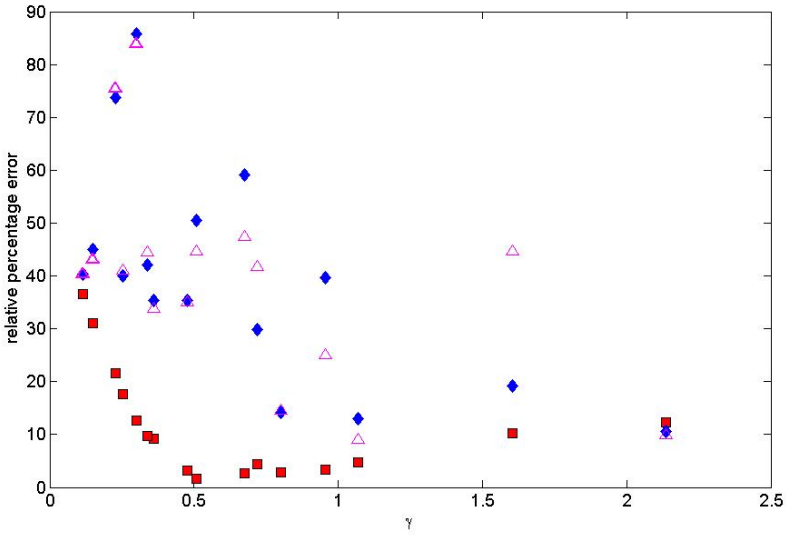

Figure 4.8: Relative errors in Γ_T as a function of γ. Squares: SPA; diamonds: LPEA; triangles: LPEANI.

from Fig. 4.7. As we have already seen, the saddle-point approximation works reasonably well for both the multiphoton ionization region and the tunneling ionization region. Error introduced by the SPA is less than 40% in the worst case studied here. The SPA errors appear to be mainly a function of γ only, for the various laser intensities and wavelengths studied. However, the saddle-point approximation result is not a monotonic function of the Keldysh parameter. From the multiphoton region the SPA relative error first decreases as γ decreases until it reaches the tunneling region with $\gamma \simeq 0.5$, then it increases as γ further decreases. The lowest errors occurs around $0.5 < \gamma < 1$ with the laser intensity between 10^{14} W/cm^2 and 10^{15} W/cm^2. The region $\gamma < 0.5$ corresponds to high laser intensities and low wavelengths, and the SPA errors become larger again even though the Keldysh parameter is small. The relative errors from the LPEA, and the LPEANI are more scattered and consistently worse that the SPA results. The relative errors from the LPEA and LPEANI are comparable with each other for $\gamma < 0.5$ although they are rather larger ($\sim 40\%$) and peak around $\gamma \simeq 0.3$ at about $\sim 80\%$. The relative errors generally decrease as γ increases.

Finally, we summarize the results for the total ionization rates under different approximations along with the exact SFA results for various laser parameters in Table 4.2. As mentioned earlier, the saddle-point approximation gives rather accurate results for all laser

Table 4.2: Total ionization rate Γ_T in a.u.

I_0 (W/cm^2)		$\lambda = 400$ nm	$\lambda = 532$ nm	$\lambda = 800$ nm	$\lambda = 1064$ nm
1×10^{14}	exact SFA	6.03×10^{-7}	1.39×10^{-7}	7.51×10^{-9}	4.49×10^{-9}
	SPA	6.77×10^{-7}	1.53×10^{-7}	7.87×10^{-8}	4.61×10^{-8}
	LPEA	6.67×10^{-7}	1.65×10^{-7}	8.49×10^{-8}	5.13×10^{-8}
	LPEANI	6.62×10^{-7}	2.00×10^{-7}	8.20×10^{-8}	5.14×10^{-8}
	Γ_{ad}	–	–	–	5.07×10^{-8}
	Γ_{qs}	–	–	–	2.27×10^{-8}
5×10^{14}	exact SFA	1.10×10^{-4}	7.39×10^{-5}	6.13×10^{-5}	6.07×10^{-5}
	SPA	1.14×10^{-4}	7.72×10^{-5}	5.94×10^{-5}	5.51×10^{-5}
	LPEA	1.54×10^{-4}	9.61×10^{-5}	8.29×10^{-5}	8.21×10^{-5}
	LPEANI	1.38×10^{-4}	1.05×10^{-4}	8.27×10^{-5}	8.12×10^{-5}
	Γ_{ad}	1.26×10^{-4}	1.01×10^{-4}	8.58×10^{-5}	8.12×10^{-5}
	Γ_{qs}	7.56×10^{-5}	7.56×10^{-5}	7.56×10^{-5}	7.56×10^{-5}
1×10^{15}	exact SFA	5.16×10^{-4}	4.87×10^{-4}	4.64×10^{-4}	4.54×10^{-4}
	SPA	5.30×10^{-4}	4.79×10^{-4}	4.19×10^{-4}	3.74×10^{-4}
	LPEA	8.20×10^{-4}	7.32×10^{-4}	6.59×10^{-4}	6.36×10^{-4}
	LPEANI	7.60×10^{-4}	7.04×10^{-4}	6.70×10^{-4}	6.41×10^{-4}
	Γ_{ad}	7.81×10^{-4}	7.23×10^{-4}	6.83×10^{-4}	6.69×10^{-4}
	Γ_{qs}	6.53×10^{-4}	6.53×10^{-4}	6.53×10^{-4}	6.53×10^{-4}
5×10^{15}	exact SFA	0.0099	0.0099	0.0089	0.0064
	SPA	0.0087	0.0078	0.0061	0.0040
	LPEA	0.0184	0.0173	0.0129	0.0090
	LPEANI	0.0182	0.0174	0.0127	0.0090
	Γ_{ad}	0.0197	0.0195	0.0194	0.0194
	Γ_{qs}	0.0194	0.0194	0.0194	0.0194

parameters while the low photoelectron energy approximations LPEA and LPEANI tend to overestimate the total ionization rates. The adiabatic rate Γ_{ad} and the quasi-static rate Γ_{qs} are meaningful only in the tunneling region where $\gamma < 1$. Eq.(2.36) shows that Γ_{qs} is independent of the laser frequency, while Γ_{ad} of eq.(D.23) has only a weak dependence in laser frequency via the correction term in the exponent. For the moderately high intensities of 5×10^{14} and 1×10^{15} W/cm^2, they provide semi-quantitative results, although the correction term in Γ_{ad} seems to make the results *worse* than Γ_{qs} for most of the laser parameters studied here. At the laser intensity of 10^{14} W/cm^2, Γ_{ad} and Γ_{qs} give the worst results as expected, since the Keldysh parameter γ is large at low intensities. However, at the high laser intensity of 5×10^{15} W/cm^2, both Γ_{ad} and Γ_{qs} over-estimate the total ionization rate Γ_T by about a factor of two, even though the Keldysh parameter is small. This suggests that the Keldysh parameter alone may not be enough to specify the adiabatic condition in strong fields [74].

4.2 The hydrogenic atom

The hydrogen atom has a long-range Coulomb potential:

$$V_b = -\frac{1}{r} \tag{4.8}$$

with ground state wavefunction

$$\phi_i(r) = \frac{1}{\sqrt{\pi}} e^{-r}. \tag{4.9}$$

We can apply the result of (3.16) to calculate the ionization amplitude (2.32). For the simple case of an hydrogenic atom in its $1s$ ground state,

$$\langle \mathbf{k} + \mathbf{A}(t) \mid \phi_i \rangle = \frac{2\sqrt{\pi}}{\left[\frac{1}{2}\left(\mathbf{k} + \mathbf{A}(t)\right)^2 + I_p\right]^2} = \frac{2\sqrt{\pi}}{S'_p(t)^2}, \tag{4.10}$$

where we use eq.(2.20) to evaluate $S'_p(t) = S'(t) + I_p$. Substituting eq.(4.10) into eq.(2.32), we obtain

$$L_n(\mathbf{k}) = -\frac{2\sqrt{\pi}}{T} \int_0^T dt \frac{e^{iS_p(t)}}{S'_p(t)}. \tag{4.11}$$

For low-frequency and high-intensity laser excitation, the integral is dominated by the local behavior of the integrand at the saddle points $\{t_s\}$ given by

$$S_p'(t_s) = \frac{1}{2}\left[\mathbf{k} + \mathbf{A}(t_s)\right]^2 + I_p = 0. \tag{4.12}$$

For plane-polarized monochromatic laser excitation (eq.(2.25)), the saddle point equation (4.12) gives rise to two complex saddle points t_+ and t_- which contribute to the integral dominantly. The ionization amplitude (4.11) is proportional to the integral of eq.(3.3) if we identify $\lambda w(z)$ with $iS(t)$, $g(z) = 1$ and $\nu = 1$. Using eq.(3.16) and recognizing the deformed paths to go around both $t_\pm$ correspond to Case B, we obtain the second order asymptotic result for the ionization amplitude

$$L_n(\mathbf{k}) \;=\; \omega i\sqrt{\pi}\left[\frac{e^{iS_+}}{S_+''}(1+\delta_+) + \frac{e^{iS_-}}{S_-''}(1+\delta_-)\right] \tag{4.13}$$

where

$$\delta_\pm = \frac{i\sqrt{2}S_\pm'''}{3\Gamma(\frac{1}{2})[S_\pm'']^2}\left(iS_\pm''\right)^{1/2}, \tag{4.14}$$

$S_\pm = S_p(t_\pm)$, $S_\pm'' = S_p''(t_\pm)$, and $S_\pm''' = S_p'''(t_\pm)$. Similar results were obtained in reference [75] which was derived from a different method. Our method has the advantage that the asymptotic nature of each term is rigorously given by Watson's lemma, and higher order terms, should they become necessary, can be systematically derived.

Next we will compare the results of first and second order expansion with those from exact calculation of the Keldysh integral of eq.(4.11). The laser parameters are chosen to be in the tunneling ionization region. Because of conservation of energy the momentum k can only take discrete values given by

$$k_n = \sqrt{2\left(n\omega - U_p - I_p\right)}, \tag{4.15}$$

where the photon order n can be any positive integer such that the momentum is real.

In Figs.4.9 and 4.10, we compare the ionization probability distributions of a hydrogen atom ($I_p = 0.5$) obtained from our asymptotic expansions with those from exact numerical evaluation of eq.(4.11) for different photon orders. We choose laser wavelength $\lambda \approx 900\,\mathrm{nm}$ and intensity $\mathrm{I}_0 \approx 2 \times 10^{14}\mathrm{W/cm}^2$, giving $n_0 = 19.8$ and it takes a minimum of $n = 20$ photons to ionize the atom. Our calculation shows that the low photon order electrons will have broader angular distribution than the high photon order electrons. The saddle

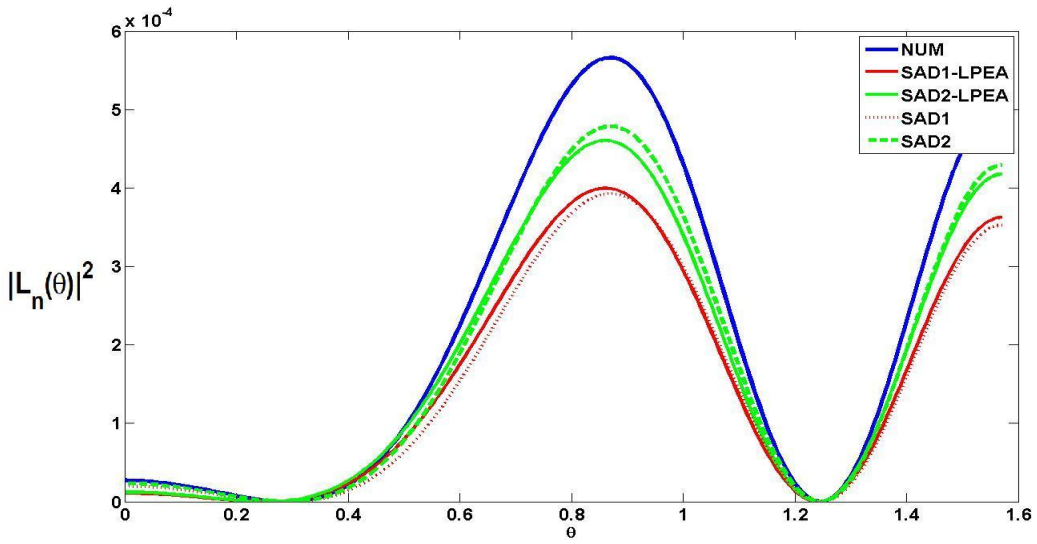

Figure 4.9: Ionization probability distribution $|L_n(\theta)|^2$ of hydrogen atom with $I_p = 0.5$ for $n = 20$, $E_0 = 0.07$ and $\omega_L = 0.05$. The blue continuous line is the exact numerical integration; the green dashed line, second-order saddle point result; the red dot line, the first-order saddle point result; the green continuous line, second-order saddle point result with LPEA; the red continuous line, first-order saddle point result with LPEA.

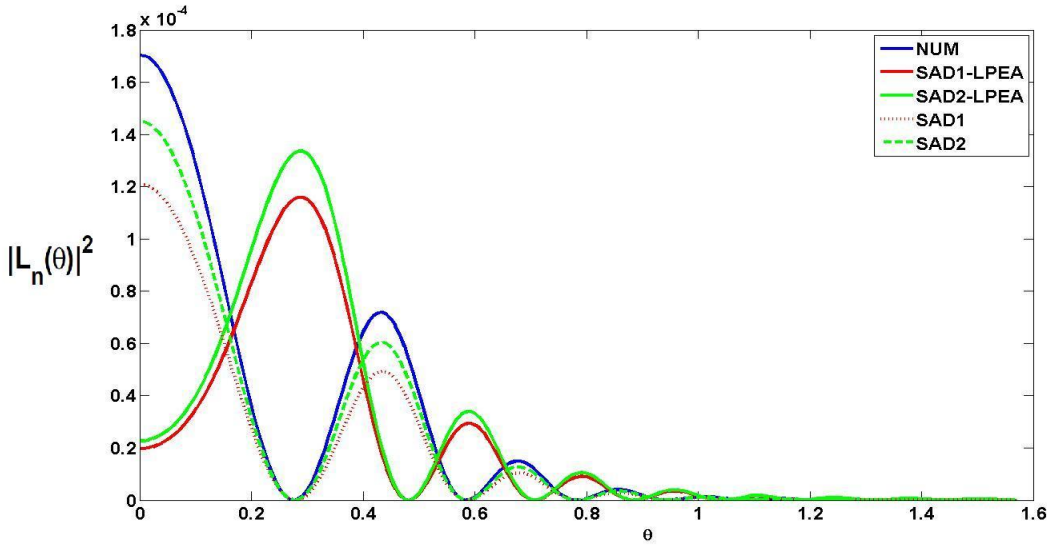

Figure 4.10: Same as Fig. 4.9 except that $n = 25$

point approximation tends to underestimate the total probability of ionization; however the shape of the angular distribution is maintained, and the second order results are in closer agreement with the exact calculations. Our systematic approach can be generalized to ionization from excited states for which the singularities at the saddle points will be of higher order, and higher order MSD will become necessary [56].

To facilitate the derivation of analytical formulas it is also worth examining the low photoelectron energy momentum approximation (LPEA) [26, 43]. Following our paper [43], we expand about $k = 0$ to obtain

$$\begin{aligned} S_+ &\approx i\left[n\,\mathrm{arcsinh}\gamma - \mathrm{z}\gamma\sqrt{1+\gamma^2}\right] \\ &\quad +2\sqrt{\frac{z(1+\gamma^2)}{\omega}}k\cos\theta - \frac{ik^2\gamma\cos^2\theta}{2\omega\sqrt{1+\gamma^2}} + O(k^3), \end{aligned} \tag{4.16}$$

$$\begin{aligned} S_- &\approx n\,\pi + i\left[n\,\mathrm{arcsinh}\gamma - \mathrm{z}\gamma\sqrt{1+\gamma^2}\right] \\ &\quad -2\sqrt{\frac{z(1+\gamma^2)}{\omega}}k\cos\theta - \frac{ik^2\gamma\cos^2\theta}{2\omega\sqrt{1+\gamma^2}} + O(k^3), \end{aligned} \tag{4.17}$$

$$S''_{\pm} \approx 4i\omega^2 z\gamma\sqrt{1+\gamma^2} + O(k), \tag{4.18}$$

and

$$S'''_{\pm} \approx 4\omega^3 z\left(1+2\gamma^2\right) + O(k). \tag{4.19}$$

Here, $\gamma = \sqrt{I_p/2U_p}$ is the Keldysh parameter, $z = U_p/\omega$ is the intensity parameter, and θ is the angle between the electric field of the laser and momentum $\mathbf{k}$.

Using the LPEA results of eqs.(4.16)-(4.19) and following the procedure of reference [43] to integrate over θ, sum over n, and take the limit that the Keldysh parameter γ is small (the tunneling limit), we obtain the total ionization rate

$$\Gamma_T = \frac{1}{2}\left(1+\frac{2}{3}\sqrt{\frac{2E_0}{\pi\kappa^3}}\right)\kappa^{1/2}\sqrt{3\pi E_0}\; e^{-\frac{2\kappa^3}{3E_0}}, \tag{4.20}$$

where $\kappa = \sqrt{2I_p}$. The second term in the bracket is the contribution from the second order asymptotic expansion. For a laser intensity of $\mathrm{I_0} \approx 2\times 10^{14}\mathrm{W/cm^2}$, eq.(4.20) indicates that the second order contribution is about 10%.

We also assess the validity of the LPEA in Figs. 4.9 and 4.10. For low photon orders i.e. $n = 20$ in Fig. 4.9, the LPEA results are in good agreement with the corresponding saddle point results. When we increase the photon order to $n = 25$ in Fig. 4.10, the LPEA introduces a "phase shift" to the angular distribution.

The ionization rate after absorption of n photons is obtained by integrating over the angles:

$$\Gamma_n = \int_0^{\pi} d\theta\ \sin\theta |L_n|^2. \tag{4.21}$$

In order to see how much error the LPEA introduces to the total ionization rate, we plot the partial ionization rate Γ_n as a function of the photon order in Fig. 4.11. We observe that the LPEA results follow the exact calculations closely, implying that the LPEA is reliable for the laser parameters chosen. This suggests that the LPEA mainly distorts the angular distribution of the photoelectrons for higher photon orders, but may not significantly affects the total ionization rate.

The *tunneling limit* of the ionization rate for the hydrogen atom (eq.(4.20)) is different from the quasi-static result

$$\Gamma_{qs} = 4\sqrt{\frac{3}{\pi E_0}}\; e^{-\frac{2}{3E_0}}. \tag{4.22}$$

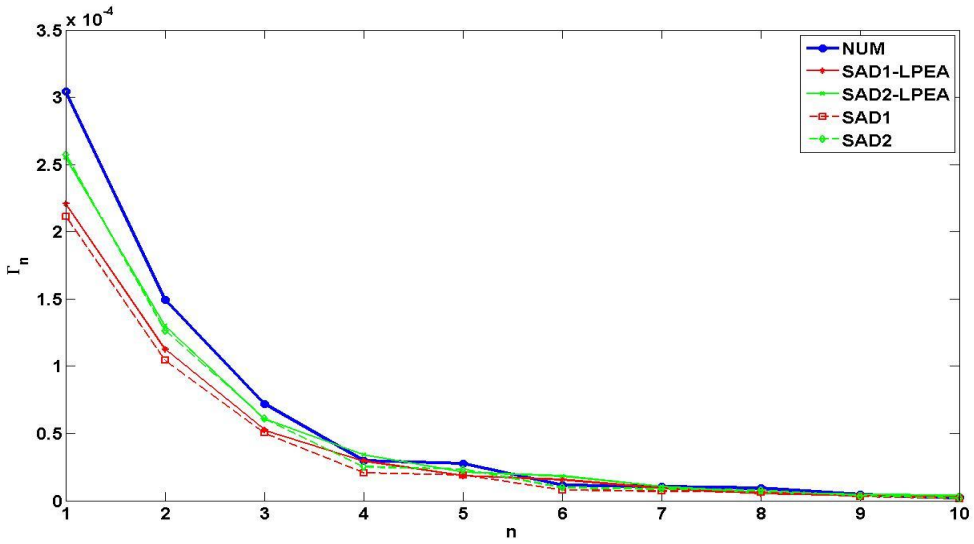

Figure 4.11: Plot Γ_n versus n for hydrogen atom with $I_p = 0.5$. $E_0 = 0.073$ and $\omega_L = 0.05$. The blue continuous line (circle) is the exact numerical integration; the green dashed line (diamond), second-order saddle point result; the red dashed line (square), the first-order saddle point result; the green continuous line (cross), second-order saddle point result with LPEA; the red continuous line (star), first-order saddle point result with LPEA.

Such disagreement has already been noted by Keldysh, who attributed it to the neglect of the Coulomb interaction in the final state by the SFA. He then suggested that a "crude quasiclassical analysis" including this interaction would result in a correction factor $I_p\gamma/\hbar\omega(1+\gamma^2)^{1/2}$ to the ionization rate. However, no detail was given, and we are not aware of any derivation of this factor in the literature. Quasiclassical analysis of strong field ionization has subsequently been studied by Perelomov and co-workers [27, 24, 25] (see Popov [30] for a recent review), and recently by Popruzhenko and co-workers [76, 77, 28]. For a linearly polarized laser field eq.(2.25), a Coulomb correction factor

$$Q = \frac{4}{E_0^2} \tag{4.23}$$

was obtained for the hydrogen atom [24, 30, 77, 28] (see also eq.(2.95)). Similar correction factor was found by Bauer using the WKB Coulomb correction for the final state of the ionizing electron [55], and by Vanne and Saenz who studied the adiabatic limit of the velocity-gauge SFA [78]. However, multiplying the result of eq.(4.20) by Q still would not yield the quasi-static rate eq.(4.22). Hence the adiabatic limit of the SFA ionization rate for systems with Coulomb interactions and its relation to the quasi-static rate deserve further investigation.

4.3 The H_2^+ molecular ion

In this section we extend the Keldysh formalism to the ionization of the H_2^+ molecular ion. This model is the simplest example of a two-center binding potential which is given by

$$V_b(\mathbf{r}) = -\frac{1}{|\mathbf{r}-\frac{\mathbf{R}_0}{2}|} - \frac{1}{|\mathbf{r}+\frac{\mathbf{R}_0}{2}|}. \tag{4.24}$$

The ion is assumed to be oriented along the z-axis with its center at the origin. The internuclear separation is denoted by R_0. The initial electronic wave function is approximated by the LCAO-MO [50]

$$\phi_i = \sqrt{\frac{N\kappa^3}{2\pi}}\left(e^{-\kappa r_A} + e^{-\kappa r_B}\right), \tag{4.25}$$

where r_A, r_B are the distances of the electron from the nuclei. In this section we shall only consider H_2^+ in its equilibrium configuration with $R_0 = 2$ a.u., $I_p = 1.065$ a.u., and $\kappa = 1$. The normalization factor is

$$N = \frac{1}{1+\left(1+\kappa R_0+\frac{1}{3}\kappa^2 R_0^2\right)e^{-\kappa R_0}}. \tag{4.26}$$

It has long been recognized by Keldysh [15] that since the scattering amplitude has poles at the momentum corresponding to the bound state energies, the integrand for the ionization amplitude of eq.(2.31) or eq.(2.32) has poles at the saddle points, *provided that the exact wave function is used*, as illustrated by eq.(4.11) for the hydrogen atom. However, when an approximate wave function such as the LCAO-MO eq.(4.25) is used, the poles of the momentum wave function will be shifted from the saddle points, and eq.(2.32) will not be suitable for the saddle-point calculation of the ionization amplitude. Instead, eq.(2.31) should be used, and using eq.(4.25) and the Fourier transform eq.(4.10), we obtain (see eq.(7) of reference [79])

$$L_n(\mathbf{k}) = \int_0^T dt \ [f_1(t) + f_2(t)] \ e^{iS_p(t)} \tag{4.27}$$

where

$$\begin{aligned} f_1(t) &= -\frac{i\sqrt{N}}{\pi T}\frac{R_0 E(t)}{2}\sin\left(\frac{\nu_z(t)R_0}{2}\right)\frac{1}{\left[\frac{(\mathbf{k}+\mathbf{A})^2}{2}+I_p^H\right]^2}\ , \\ f_2(t) &= -\frac{i\sqrt{N}}{\pi T}\cos\left(\frac{\nu_z(t)R_0}{2}\right)\frac{\nu_z(t)}{\left[\frac{(\mathbf{k}+\mathbf{A})^2}{2}+I_p^H\right]^3}\ , \end{aligned} \tag{4.28}$$

$\nu_z(t)$ is the z-component of $\mathbf{k}+\mathbf{A}(t)$ and $I_p^H = 0.5$ a.u. is the ionization potential for the hydrogen atom. This expression differs from the atomic case in that the singularities do not coincide with the saddle points as noted above. To calculate the integral in eq.(4.27) by the saddle-point method, we distort the path of integration from the real t-axis to the path of steepest descent. Since the ionization potential of hydrogen is less then the ionization potential of the H_2^+ molecular ion, the distorted path encloses the poles of $f_1(t)$ and $f_2(t)$ which can be taken into account by the residue theorem. Hence

$$L_n(k_n) = L_n^{(SAD)} - 2\pi i \sum \mathrm{Res}\left[f_1(t) + f_2(t)\right] \tag{4.29}$$

where $L_n^{(SAD)}$ is the saddle-point contribution to the integral. In eq.(3.25), we obtain up to the third order asymptotic terms for $L_n^{(SAD)}$, where we note that the second order term vanishes for this integral. Numerical comparison with numerical integration of eq.(4.27) indicates that the first order term is adequate for the LCAO orbital. The first order

contribution is given by the first term of eq.(3.25)

$$L_n^{(SAD)} = \frac{\sqrt{2\pi N}}{\pi T}\frac{R_0}{2}\sum_{t_s} E(t_s)\sin\left(\frac{\nu_z(t_s)R_0}{2}\right)\left[\frac{1}{i\ddot{S}_p(t_s)}\right]^{\frac{1}{2}}\frac{e^{iS_p(t_s)}}{\left[\frac{(\mathbf{k}+\mathbf{A}(\mathbf{t_s}))^2}{2}+I_p^H\right]^2}$$
$$+ \frac{2\sqrt{2\pi N}}{\pi T}\sum_{t_s} E(t_s)\cos\left(\frac{\nu_z(t_s)R_0}{2}\right)\left[\frac{1}{i\ddot{S}_p(t_s)}\right]^{\frac{1}{2}}\frac{\nu_z(t_s)e^{iS_p(t_s)}}{\left[\frac{(\mathbf{k}+\mathbf{A}(t_s))^2}{2}+I_p^H\right]^3}, \quad (4.30)$$

where the saddle points t_s again are given by eq.(4.12). Since we consider only the equilibrium configuration, the sinusoidal factors in $f_1(t)$ and $f_2(t)$ can be considered to be slowly varying and are included only in the pre-exponential factors in $L_n^{(SAD)}$. For large internuclear separations these terms should be included in determining the saddle points [79]

$$\frac{1}{2}\left[\mathbf{k}+\mathbf{A}(t_s)\right]^2 + I_p \pm \mathbf{E}(t_s)\cdot\frac{\mathbf{R}}{2} = 0, \quad (4.31)$$

and oscillations in the ionization rate as a function of the internuclear separation will occur. For large internuclear separations the initial state should be dressed and low lying excited states should be included [45]. In this chapter we restrict our discussion at the equilibrium configuration. The contribution from the residue of the poles can be obtained from standard procedures. In Fig. 4.12, we plot the results for the total ionization rate of eq.(2.34) from exact numerical integration of eq.(4.27) and the saddle point calculation with residue correction (SAD-RC) of eq.(4.29). We also present the ionization rate from using only L_n^{SAD} of eq.(4.30) for $L_n(k_n)$. Clearly the contribution from the singularities is significant. As the intensity increases the error decreases as expected according to the theory of asymptotic analysis. We also plot the total ionization rate on the same graph calculated from a numerical solution of the time-dependent Schrödinger equation (TDSE) where we fix the nuclei at the equilibrium separation. The ground state energy as well as the electronic wave function is first obtained by the imaginary time method. We choose for calculation a rectangular box with $-30a.u. < x < 30a.u.$, $-30a.u. < y < 30a.u.$, and $-50a.u. < z < 50a.u.$ The second-order split operator method is used for time propagation and the FFT algorithm is employed. For real time propagation we use a 4-cycle laser pulse with sine-squared envelope. The laser parameters are chosen so that the depletion of ground state is not significant. Due to the use of absorbtion boundary conditions, the ionization rate is calculated from the depletion of the probability of the electron remaining in the box. A weak static electric field $E_{\text{drift}} = 0.001$ a.u. is applied in the x direction to

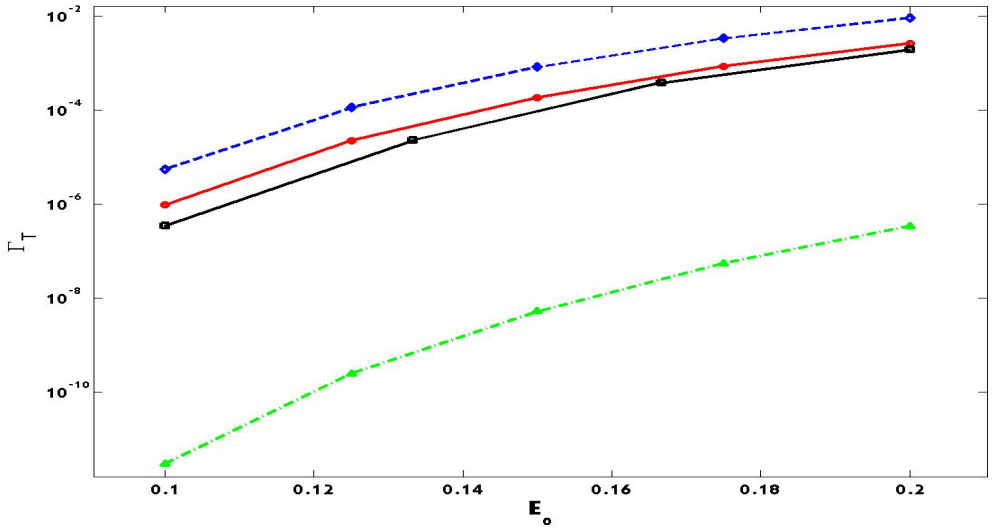

Figure 4.12: Total ionization rate versus electric field E_0 for model hydrogen molecular ion: $I_p = 1.065$. Laser frequency $\omega_L = 0.05$. The red continuous line (circle), exact numerical integration; the blue dashed line (diamond), saddle point calculation with the residue correction; the green dash-dot line (triangle), saddle point calculation without the residue correction; the black solid line (circle), TDSE calculation.

help the ionized electron to reach the boundary. This electric field is weak so that it will not affect the ionization rate. We check our program by comparing the results with reference [41] and found the qualitative trend is reproduced. This is sufficient for our purpose since SFA calculations are expected to be qualitatively accurate. Indeed we find in Fig. 4.12 that the Keldysh ionization rates agree well with the TDSE calculations. We also notice the error decreases as the intensity increases. This demonstrates the validity of SFA at large laser intensity.

Chapter 5

The strong field ionization calculator

5.1 Introduction

The computational method of solving time-dependent Schrödinger equation is developing rapidly during the past several decades. The method has been shown to be very accurate such that in most of the situations, it can predict the experimental results within quantitative accuracy; however, a serious draw back to the TDSE method is that it requires significant memory storage and takes considerable length of computation time. In some cases it is either implausible or unnecessary to use the TDSE method. An alternative way to interpret the experimental results is to combine the SFA-based theories with quantum chemistry softwares [22, 38, 80, 36, 37, 40]. A central problem of combining quantum chemistry software with the SFA-based theories is to justify the single active electron approximation (SAEA) and to obtain the one-electron wave function that will be used as the initial state in the SFA-based theories. Depending on the calculation, different initial wavefunctions may be obtained. Kjeldsen and Madsen [22, 38] used Hartree-Fock approximation to calculate the initial wavefunction, taking the highest occupied atomic/molecular orbital (HOMO) as the initial single active electron orbital. Since the electron correlation energy is completely absent in the Hartree-Fock calculation, the authors suggested that this method can only be meaningfully applied on molecular systems where effects of electron-electron correlation are small. Similar approach is taking by Becker *et al.* to study the polyatomic molecules and the saturated ionization of fullerenes [80, 36]. Reasonable agreement to experiments were found. Mishima and Lin improved the Hartree-Fock approximation by applying the modified GUASSIAN-2 model (G2M) to include the correlation energy at the initial state for large polyatomic molecules [37]. More recently, Vladimir studied the

strong field ionization of fluorine molecule using the molecular SFA in the velocity gauge based on the density-functional-theory (DFT) [40]. Accurate initial electronic orbital and binding energies were obtained so that the calculations were able to predict the correct trend of the ionization rate with respect to its companion atom.

In this chapter we present a graphic user interface (GUI) MATLAB program that combines the quantum chemistry software (GAMESS or GAUSSIAN) with the SFA-based theories. As the first step we implement the Hartree-Fock-SFA based laser-atom interaction. For the Hartree-Fock type calculations the simplest way to incorporate the single active electron approximation is to introduce the frozen orbital approximation under which the initial state is taken to be the highest occupied atomic orbital (HOAO) and all the low-lying orbitals are kept frozen. The HOAO can be expressed in terms of linear combination of Cartesian Gaussians. Since the analytic form of the Fourier transform of the Cartesian Guassian basis set can be found, we can represent the transition amplitude from the HOAO to the Volkov state as a linear combination of these analytic forms. The temporal integral is implemented numerically and the momentum integral in HHG calculation is evaluated using the saddle point method.

Since the physical interpretation of SFA-based theories is well understood, we expect this GUI program to be helpful to the interpretation of the experimental data. This program can be modified to adapt to any quantum chemistry calculations using Cartesian Guassian basis set. We expect our program to work adequately for the light atoms in which the correlation energy is small. A generalization to the heavy atoms and molecules will be considered in the future. Including the correlation energy will be our next task.

5.2 Single-active electron approximation

We briefly review the formal derivation in Chapter 2 under the context of Hartree-Fock approximation so that the single active electron approximation can be more rigorously formulated. The total Hamiltonian for a system interacting with laser field can be partitioned as $\hat{H}(t) = \hat{H}_0 + \hat{V}_L(t)$ where $\hat{H}_0$ is the Hamiltonian of the system unperturbed by the laser, and $\hat{V}_L(t)$ represents the interaction of the system with the laser. In the Keldysh formalism, the length gauge is used and

$$\hat{V}_L(t) = \sum_{i=1}^{N} \mathbf{r}_i \cdot \mathbf{E}(t) \tag{5.1}$$

is the interaction of the electrons with the electric field $\mathbf{E}(t)$ of the laser under the dipole approximation. The transition amplitude for the ionization is given by eq.(2.14). We ap-

proximate the initial electron wavefunction by the single-determinant Hartree-Fock wavefunction, written

$$\Phi_i(\tau) \approx \frac{1}{\sqrt{N!}} \det |\phi_1 \phi_2 ... \phi_N| \, e^{-iE_i t}. \tag{5.2}$$

In addition, we assume that the final electronic state of the ion is unrelaxed so that it can be written as

$$\begin{aligned} \Psi_f(\tau) &= \hat{U}(\tau, t) \, |\Phi_f(t)\rangle \\ &\approx \frac{1}{\sqrt{N!}} \det |\phi_V \phi_2 ... \phi_N| \, e^{-iE_f t}, \end{aligned} \tag{5.3}$$

where ϕ_V is a Volkov wavefunction given by eq.(2.19). Substitute eq.(5.2), (5.3) into eq.(2.14) we can obtain

$$M_{fi} \simeq -i \int_{-\infty}^{t} d\tau \; e^{iS_p(\tau)} \, \langle \mathbf{k} + \mathbf{A}(\tau) \, | \mathbf{r} \cdot \mathbf{E}(\tau) | \, \phi_1 \rangle \; , \tag{5.4}$$

which is similar to the one-electron transition amplitude of eq.(2.23). Consequently the amplitude $L_n(\mathbf{k})$ of eq.(2.31) is the central quantity of interest in the SFA calculation of strong field ionization [15, 26, 54, 44, 16, 17, 55, 56].

We employ the Lewenstein theory to calculate HHG spectrum of atoms [32] (see Chapter (2)). Based on the recent study we assume the major contribution to the HHG spectrum is coming from the HOAO [81]. Since the HHG spectrum is proportional to the Fourier transformation of the dipole moment we numerically integrate eq.(2.129) and use fast Fourier transform to obtain the spectrum.

5.3 Fourier representations of a general Gaussian

To calculate the photoelectron spectrum from eq.(2.31) and HHG spectrum from eq.(2.129) for a specific atom we need to know the electron orbital ϕ_1 as well as the ionization potential I_p. They can be obtained through a Hartree-Fock-type calculations (restricted close shell Hartree-Fock calculation (RHF) or restricted open shell Hartree-Fock calculation (ROHF)) with the Pople's N21 split valence basis sets (3-21G). In this basis set the electron orbital is represented by a linear combination of the Cartesian Gaussians:

$$\phi_1 = A_1 c_1 G(n, m, l, a_1) + A_1 c_2 G(n, m, l, a_2) + A_2 c_3 G(n, m, l, a_3), \tag{5.5}$$

where A_i, c_i are the coefficients and a_i are the exponents.

$$G(n,m,l,a) = \aleph x^n y^m z^l e^{-a\,r^2}. \tag{5.6}$$

The three integers n, m, l are determined by the orbital symmetry and $\aleph$ is the normalization constant. To calculate eq.(2.31) using eq.(5.5), we calculate the Fourier transformation of a general Gaussian from

$$\begin{aligned}
\tilde{G}(\mathbf{k},n,m,l,a) &= \int d^3\mathbf{r} e^{-i\mathbf{k}\cdot\mathbf{r}} G(n,m,l,a) = \left(i\frac{\partial}{\partial k_x}\right)^n \left(i\frac{\partial}{\partial k_y}\right)^m \left(i\frac{\partial}{\partial k_z}\right)^l \int d^3\mathbf{r}\; e^{-i\mathbf{k}\cdot\mathbf{r}} e^{-ar^2} \\
&= \left(i\frac{\partial}{\partial k_x}\right)^n \left(i\frac{\partial}{\partial k_y}\right)^m \left(i\frac{\partial}{\partial k_z}\right)^l \frac{\aleph\,(\pi)^{3/2}}{(a)^{3/2}} e^{-\frac{1}{4a}\left(k_x^2+k_y^2+k_z^2\right)}.
\end{aligned} \tag{5.7}$$

Recall the definition of Hermite polynomial

$$H_n(x)e^{-x^2} = (-1)^n \frac{d^n}{dx^n} e^{-x^2}, \tag{5.8}$$

we can rewrite eq.(5.7) as

$$\begin{aligned}
\tilde{G}(\mathbf{k},n,m,l,a) &= \frac{\aleph\,(\pi)^{3/2}}{(a)^{3/2}} \left(-\frac{i}{2\sqrt{a}}\right)^{n+m+l} \\
&\quad H_n\left(\frac{k_x}{2\sqrt{a}}\right) H_m\left(\frac{k_y}{2\sqrt{a}}\right) H_l\left(\frac{k_z}{2\sqrt{a}}\right) e^{-\frac{1}{4a}\left(k_x^2+k_y^2+k_z^2\right)},
\end{aligned} \tag{5.9}$$

where the Hermite polynomials are conveniently generated by the recurrence relation

$$\begin{aligned}
H_0(x) &= 1 \\
H_1(x) &= 2x \\
H_{n+1}(x) &= 2xH_n(x) - 2nH_{n-1}(x).
\end{aligned} \tag{5.10}$$

Substitute eq.(5.9) into eq.(2.32) and numerically implement the temporal integration we can obtain the transition amplitude

$$L_n(\mathbf{k}) = -\frac{1}{T}\int_0^T dt\; S_p'(t)\; e^{iS_p(t)} \sum_{i=1}^{3} A_i c_i \tilde{G}\left(\mathbf{k}+\mathbf{A}(t),n,m,l,a\right). \tag{5.11}$$

To calculate the HHG spectrum, the dipole matrix element can be obtained by using

$$\int d^3\mathbf{r}\; e^{-i\mathbf{k}\cdot\mathbf{r}} \mathbf{r} G(n,m,l,a) = -i\nabla_{\mathbf{k}} \tilde{G}\left(\mathbf{k},n,m,l,a\right) \tag{5.12}$$

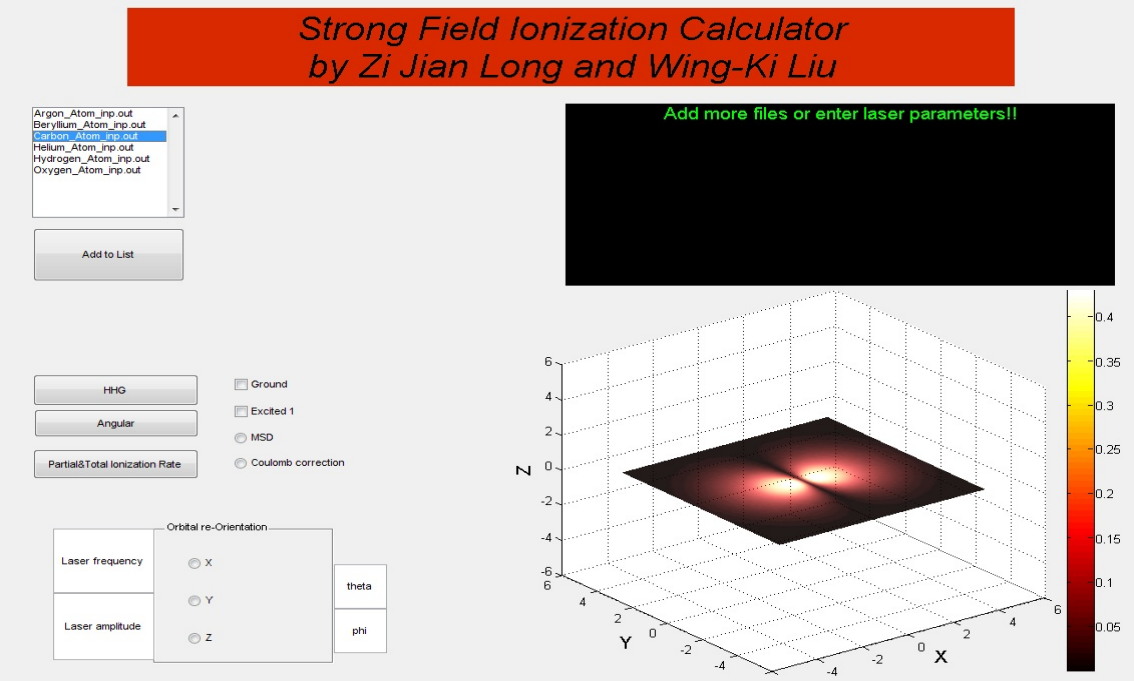

Figure 5.1: The interface of the program

so that

$$\mathbf{d}(\mathbf{k}) = -i\nabla_{\mathbf{k}} \sum_{i=1}^{3} A_i c_i \tilde{G}\left(\mathbf{k}, n, m, l, a\right). \tag{5.13}$$

5.4 Test calculations

5.4.1 Photoelectron angular distribution

The interface of our program is shown in Fig. 5.1. To use the calculator the user must manually create an input file and save it in the same folder as the program. A program that can automatically generate the input file is under development. Using the "Add file to List" button the user may add as many input files as demanded. The added files will appear in the list box as individual entries. When the user selecting the entry in the list box the program will plot the electron density distribution in the plot region and corresponding

data will be displayed in the message box. Laser parameters can be entered to the text boxes in atomic unit.

To obtain the photoelectron angular distribution the user can simply click the "Angular" button. As an example the photoelectron angular distributions of hydrogen atom are plotted in Figs. 5.2-5.4 for varies laser parameters and photon orders. The laser is linearly polarized alone the z-axis. The photoelectron waves form concentric rings on a spherical surface. It is interesting to notice the rings first become thinner and then denser as the Keldysh parameter decreases. The threshold photoelectrons have broad angular distribution and can be emitted both near the poles and the equator (i.e. along and perpendicular to the laser polarization). As the photon order increases the photoelectrons tend to be ejected only near the poles. This observation suggest that in the deep tunneling ionization region when large number of photons are required to ionize the system we would expect the photoelectrons to be ionized along the direction of the laser electric field only. This prediction is consistent with the quasi-static tunneling ionization picture [31].

In addition we compare our Fig. 5.2 with Fig.1 obtained in reference [82]. Both calculations predict a side-lobe emitted at 45^o and 135^o from the laser polarization direction (the main lobe) for the 10th order ATI photoelectrons. Despite the fact that results in reference [82] are obtained from a quantum electrodynamics calculation we still found reasonable agreement.

The photoelectron angular distributions of carbon atom are plotted in Fig. 5.5 for various laser parameters and photon orders. In this case the HOAO is chosen to be a p_x-type orbital and the laser polarization direction is along the z-axis. Similar as before we found the threshold photoelectrons are emitted closer to the equator and higher order photoelectrons are emitted closer to the poles. Comparing to the hydrogen atom case we notice the photoelectrons tend to be emitted from the direction of the lobes of that p-orbital. No photoelectron is emitted exactly at the poles for all photon order. This is because the initial wavefunction carries nonzero angular momentum along the laser polarization which will be conserved during the ionization process. Hence the azimuthal angular distribution of the initial state is preserved in the photoelectron emission.

5.4.2 Photoelectron energy distribution and total ionization rate

In addition we study the photoelectron energy distribution of an argon atom ionized by a laser field linearly polarized along the z-axis. The HOAO of argon atom consist of three degenerate p-type orbitals each is occupied by an anti-spin electron pair. Because the system

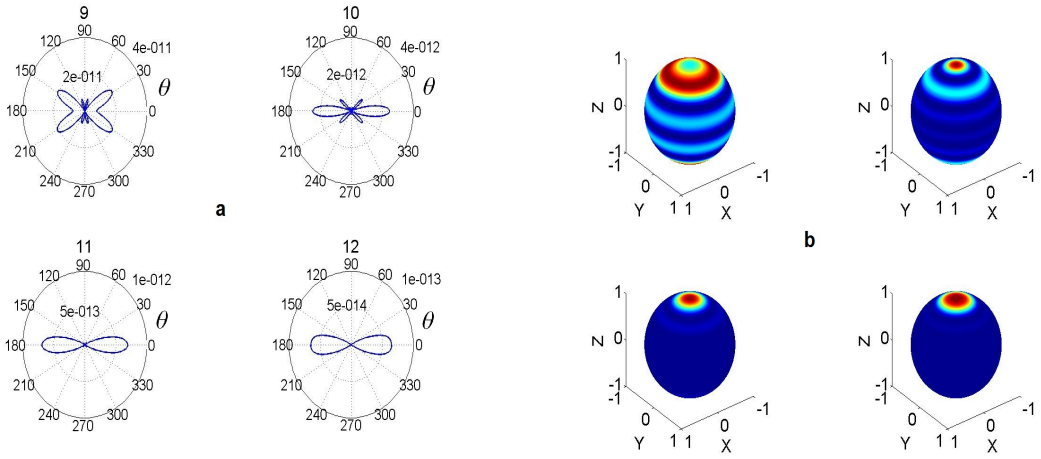

Figure 5.2: Photoelectron angular-distribution of hydrogen atom. In the multi-photon region where the Keldysh parameter $\gamma = 3.2$, $E_0 = 0.0206$, $\omega_L = 0.0652$. Panel (a): The polar plot with $\phi = 0$, photon order is indicated by the number above each plot; Panel (b): The 3D plot for the corresponding photon order.

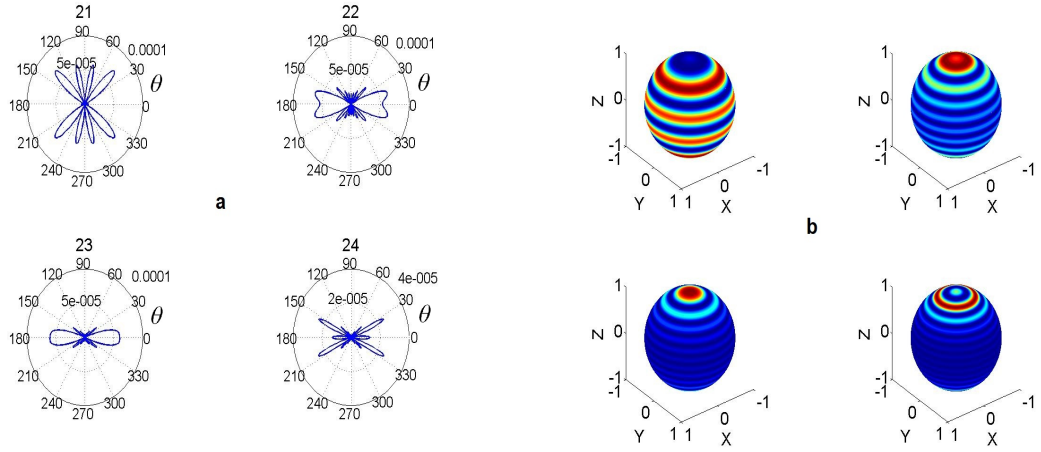

Figure 5.3: Photoelectron angular-distribution of hydrogen atom. In the transition region where the Keldysh parameter $\gamma = 0.68$, $E_0 = 0.073$, $\omega_L = 0.05$. Panel (a): The polar plot with $\phi = 0$, photon order is indicated by the number above each plot; Panel (b): The 3D plot for the corresponding photon order.

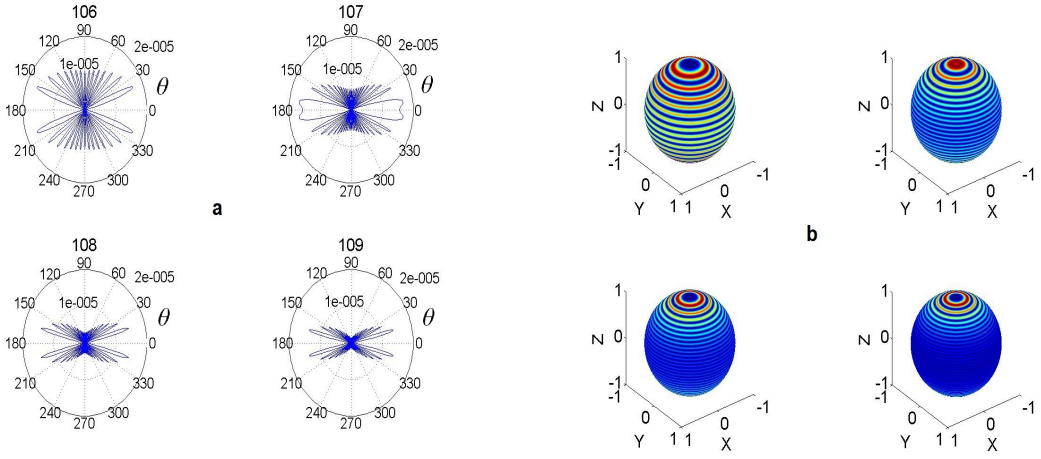

Figure 5.4: Photoelectron angular-distribution of hydrogen atom. In the tunneling region where the Keldysh parameter $\gamma = 0.34$ $E_0 = 0.073$, $\omega_L = 0.025$. Panel (a): The polar plot with $\phi = 0$, photon order is indicated by the number above each plot; Panel (b): The 3D plot for the corresponding photon order.

has azimuthal symmetry we consider p_x and p_y orbitals separately. The photoelectron energy distributions from the p_z-orbital as well as the p_x-orbital are plotted in Fig. 5.6. Both calculations show suppression in the lowest order ATI peaks. This phenomenon is known as the peak switching which is attributed to the upshifting of the ionization threshold by the pondermotive energy of the laser field (see [83] and the references therein). The intensities of the ATI peaks decay exponentially as the photon order increase. Small wiggles can be observed for the p_z-orbital photoelectron energy distribution. This is due to the two-center nature of the p-type orbitals from which the photoelectrons emitted interfere with each other. As discussed in reference [84] the interference will give rise to an additional sine factor in the transition amplitude. The phase of the sine function is proportional to the dot product of the photoelectron momentum with the relative position vector of the two centers. Since the photoelectron tends to be emitted parallel to the laser polarization direction, when the two-center is aligned with the laser polarization the interference pattern becomes more pronounced. This effect can be clearly seen in the Fig. 5.6 by comparing the p_z-orbital to the p_x-orbital. The total ionization rates for the two orbitals are plotted in Fig. 5.7. It shows that the ionization is more probable for the p_z-orbital than the p_x-orbital. Since the ionization rates are differed by two orders of magnitude it is reasonable to take into account only the p_z-orbital for the total ionization rate calculation.

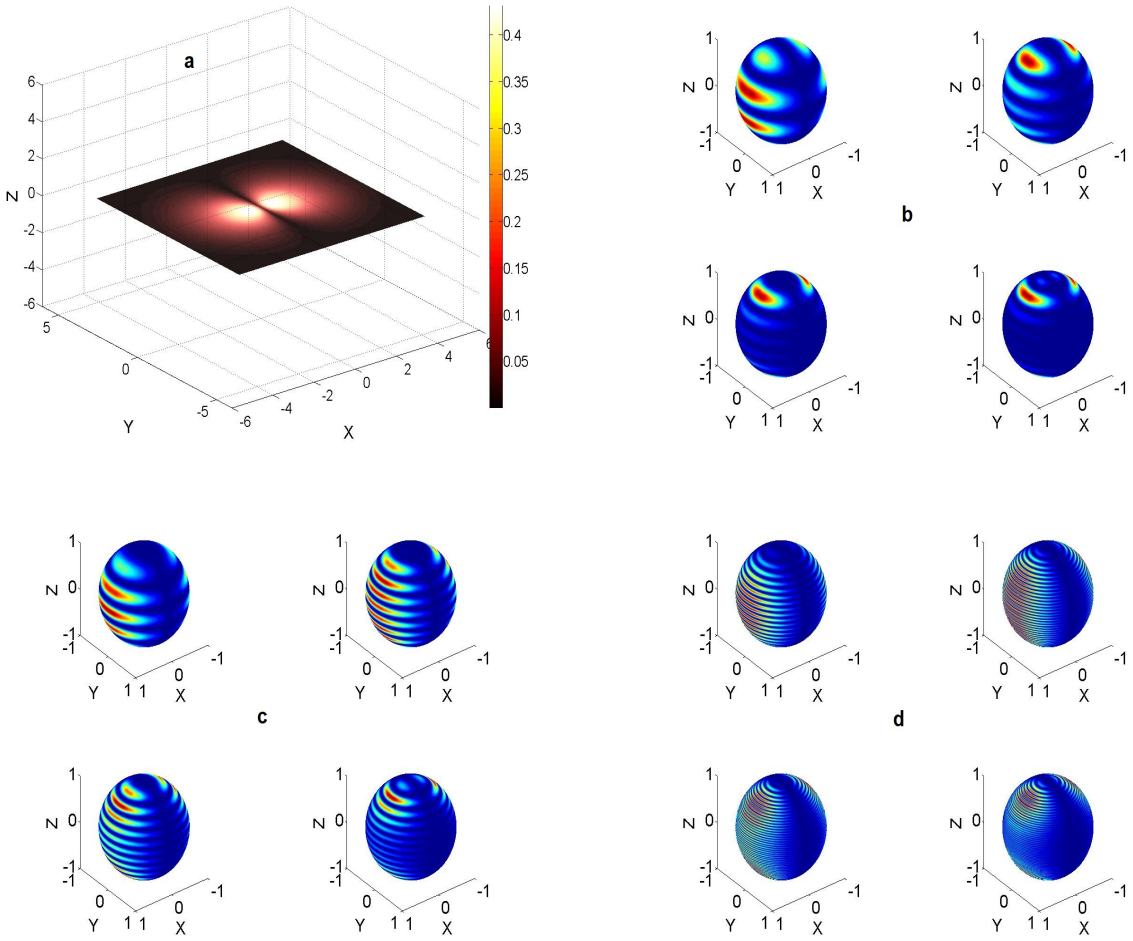

Figure 5.5: The valence electron p_x orbital (Panel a) and the photoelectron angular distribution of carbon atom (Panel $b-d$). The laser parameters are given by (b) $E_0 = 0.02$, $\omega_L = 0.06$; (c) $E_0 = 0.073$, $\omega_L = 0.05$; (d) $E_0 = 0.09$, $\omega_L = 0.025$.

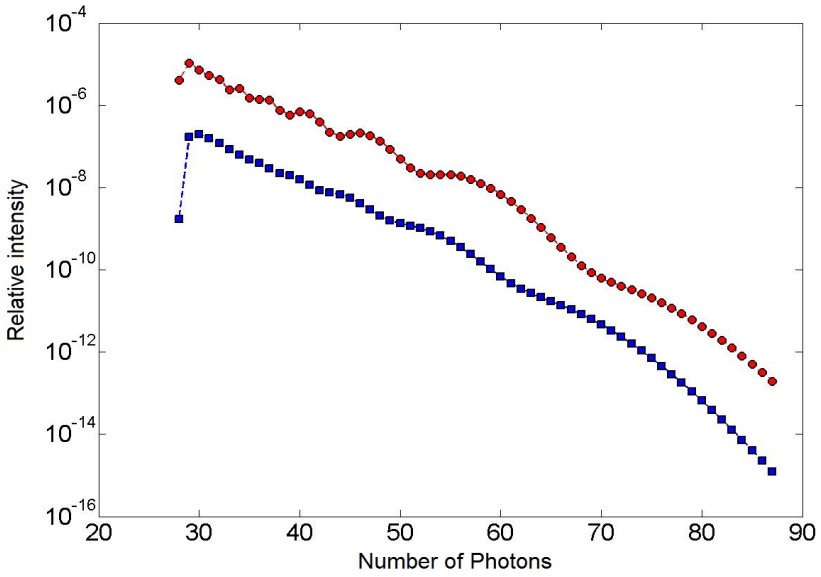

Figure 5.6: The photoelectron spectrum for Ar in the tunneling region where the Keldysh parameter $\gamma = 0.6$ $E_0 = 0.09$, $\omega_L = 0.05$. p_x orbital, the blue squares; p_z orbital, the red circles. Laser polarization is along the z-axis.

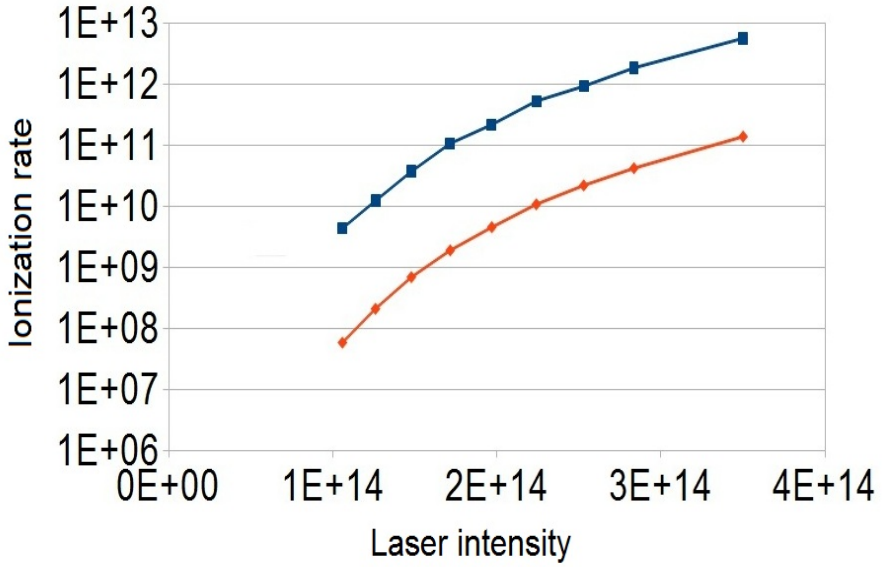

Figure 5.7: The total ionization rate (in sec^{-1}) of Ar atom versus the laser intensity (in W/cm^2). The laser frequency is $\omega_L = 0.05$. The blue curve (p_z-orbital); The red curve (p_x-orbital) .

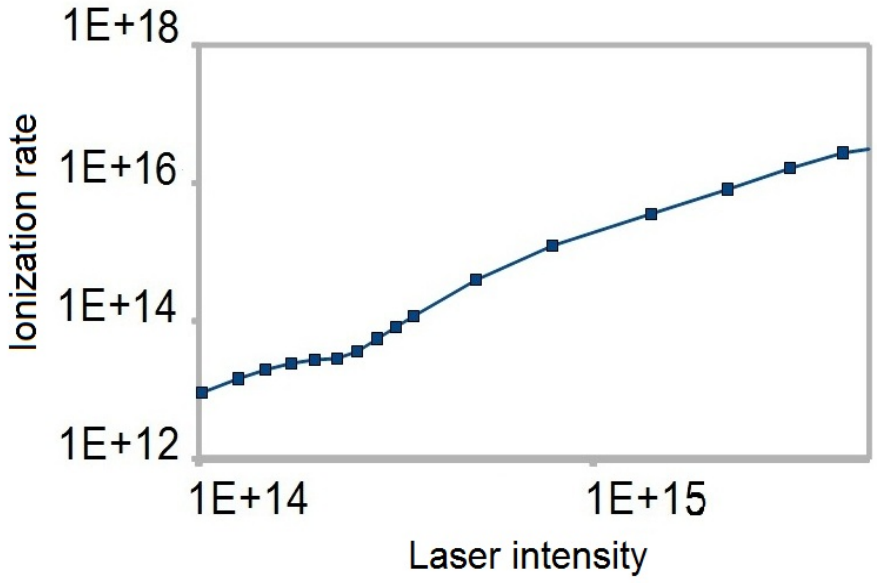

Figure 5.8: The total ionization rate (in sec^{-1}) of hydrogen atom versus laser intensity (in W/cm^2). Laser frequency is $\omega_L = 0.1838$ which corresponds to the laser wavelength of 248nm.

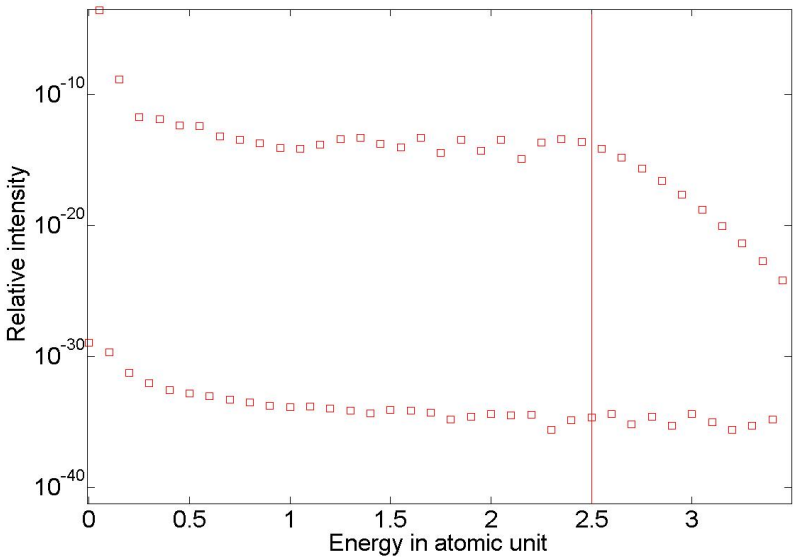

Figure 5.9: The HHG spectrum of Ar atom (p_z-orbital). The laser parameters are given by $E_0 = 0.074$, $\omega_L = 0.05$, $\theta_L = 0$ and $\phi_L = 0$. The vertical line indicates the location of the classical cutoff energy E_c.

Furthermore, we use our program to do the same calculation as in the reference [85] for the purpose of testing our program. As shown in Fig .5.8, our result agrees to the dotted line in Fig.1(a) of reference [85]. In this particular calculation, we obtain the ionization energy ($I_p = 0.496$) which is slightly higher than the exact value: 0.5 by 1%. This is caused by the basis truncation error when a finite-size Gaussian basis set is used.

5.4.3 HHG spectra

The HHG spectra can be obtained by numerically integrating eq.(2.129) and calculating the FFT of the dipole moment. In this section we study the HHG spectrum of argon atom in the presence of a linearly polarized laser field, where the polarization direction is given by $\hat{e} = \sin\theta_L \cos\phi_L \hat{x} + \sin\theta_L \sin\phi_L \hat{y} + \cos\theta_L \hat{z}$. First of all we select the p_z-orbital to be the active orbital for the HHG and plot the spectrum in Fig. 5.9. We found the odd harmonics have intensities that are 20 orders of magnitude larger than the even harmonics. This is a well-known effect which can be explained using the symmetry of the transition dipole

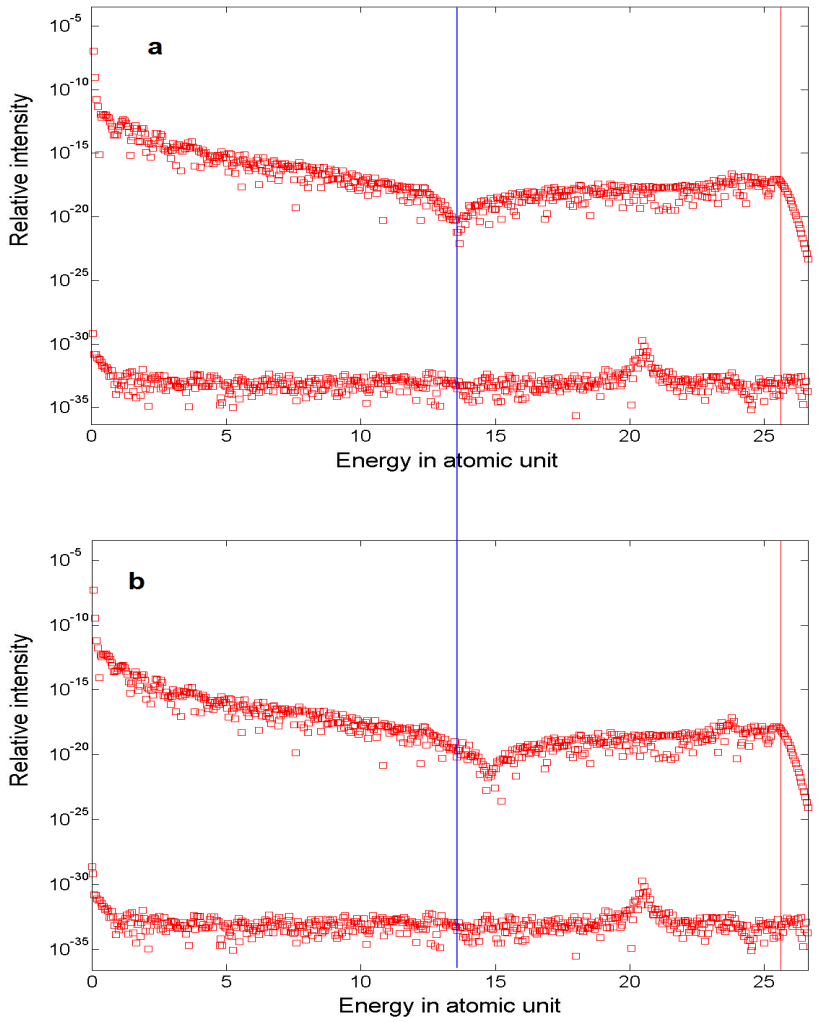

Figure 5.10: The HHG spectrum of Ar atom (p_z-orbital). The laser parameters are given by (a) $E_0 = 0.14$, $\omega_L = 0.025$, $\theta_L = 0$ and $\phi_L = 0$; (b) $E_0 = 0.14$, $\omega_L = 0.025$, $\theta_L = \frac{\pi}{4}$ and $\phi_L = 0$. The red thin vertical line indicates the location of the classical cutoff energy. The blue thick vertical line is for comparison of the locations of the two minima.

matrix elements (see Section 2.6). In addition, a relatively flat plateau can be seen followed by a sharp cutoff. The cutoff energy is in good agreement with the prediction given by the three step model [34]. The model predicts a cutoff energy at $E_c = I_p + 3.17U_p$. As we can see the program is capable of reproducing some of the important features of the HHG processes.

Using a low-frequency high-intensity laser field we can extend the cutoff energy to the soft X-ray region. A minimum is observed at 13.7 $a.u.$ as shown in Fig. 5.10a. To understand the origin of this minimum we make small variations to the laser parameters and found that the position of the minimum is unchanged with respect to the laser intensity and frequency provide the cutoff energy is high enough to reveal the minimum. In reference [86] a minimum is also observed experimentally in the HHG spectrum of argon which is located at $51eV$ ($\approx 2a.u.$). This minimum is closely related to the Cooper minimum [1] in the single-photon-ionization efficiency. The question is what causes the large difference in location between the Cooper minimum and our calculation. In reference [88] Lein proposed the two-center scattering model that explained the constructive or destructive interference in the HHG spectrum of diatomic molecules. We try to apply this model to explain the minimum in our calculation even though there is no actual two-Coulomb center in our problem. The double lobe of the p_z-orbital form a two-center emitter from which the high harmonic emissions interfere with each other. When the laser polarization is changed to $\theta = \frac{\pi}{4}$,$\phi = 0$ we found the minimum is shifted towards the higher energy region (see Fig. 5.10b); however, this shift is too small comparing with the prediction by the two-center scattering model. We found the model is inappropriate in this case. Furthermore, in references [89] the authors already point out that in general the two-center model is inaccurate in reproducing some of the interference features. They suggested an alternative time-dependent dipole model which is essentially the SFA in the velocity gauge with a semiclassical Coulomb correction. Since our program is based on SFA in the length gauge we speculate that it is because of the neglecting of the Coulomb potential that causes the large difference in location between the Cooper minimum and our calculation. To have a Cooper minimum at least one node should be present both in the initial and final wavefunctions of the transition dipole matrix. Therefore it is essential to include the Coulomb correction in order to reproduce the correct location of the minimum in the HHG spectrum.

[1] The existence of zeros in dipole matrix elements and the associated minimum (called Cooper minimum) in photoionization cross sections has been known for ground states of alkali atoms for long time [87]

Chapter 6

Numerical method in strong field physics

6.1 Introduction

The SFA-based theory must be compared with the exact numerical solution to the time-dependent Schrödinger equation (TDSE) in order to justify the approximations used in the theory. In this chapter we will introduce a numerical method that can be used to test our theory for the atomic case. The method was first introduced by Muller [90] and later developed to a density-functional-theory-based TDSE solver by Bauer [91]. It takes advantage of the symmetry of the ionization process and transforms the three-dimensional TDSE into a system of coupled one-dimensional TDSEs. The maximum angular momentum of the electron determines the truncation of the coupled system TDSEs. We will derive the formalisms in both the length gauge and the velocity gauge. The calculation is implemented in MATLAB.

6.2 The velocity gauge calculation

The time-dependent Schrödinger equation describing the electron-laser interaction in the velocity gauge reads

$$\left\{-\frac{\nabla^2}{2}+V(r)-iA(t)\partial_z\right\}\Psi(\mathbf{r},t)=i\partial_t\Psi(\mathbf{r},t), \tag{6.1}$$

where under the dipole approximation the interaction Hamiltonian in the spherical coordinates is given by

$$-iA(t)\partial_z = -iA(t)\left(\cos\theta\partial_r - \frac{\sin\theta}{r}\partial_\theta\right). \tag{6.2}$$

The electronic wavefunction expanded in a linear combination of the spherical harmonics as

$$\Psi(r,\theta,\phi) = \sum_{l'} \mathcal{R}_{l'm}(r,t)Y_{l'm}(\theta,\phi). \tag{6.3}$$

The Laplacian in spherical coordinate has the following form

$$\nabla^2 = \frac{1}{r^2}\frac{\partial}{\partial r}\left(r^2\frac{\partial}{\partial r}\right) + \frac{1}{r^2\sin\theta}\frac{\partial}{\partial\theta}\left(\sin\theta\frac{\partial}{\partial\theta}\right) + \frac{1}{r^2\sin^2\theta}\left(\frac{\partial^2}{\partial\phi^2}\right). \tag{6.4}$$

We recall the relation

$$\left\{\frac{1}{r^2\sin\theta}\frac{\partial}{\partial\theta}\left(\sin\theta\frac{\partial}{\partial\theta}\right) + \frac{1}{r^2\sin^2\theta}\left(\frac{\partial^2}{\partial\phi^2}\right)\right\}Y_{lm}(\theta,\phi) = -\frac{l(l+1)}{r^2}Y_{lm}(\theta,\phi) \tag{6.5}$$

such that when substituting eqs.(6.2)-(6.5) into eq.(6.1) and using the orthogonality relations of the spherical harmonics we obtain a set of coupled differential equations for the coefficients $\mathcal{R}_{lm}(r,t)$

$$\begin{aligned} i\partial_t\mathcal{R}_{lm}(r,t) = &\left\{-\frac{1}{2}\frac{1}{r^2}\frac{\partial}{\partial r}\left(r^2\frac{\partial}{\partial r}\right) + \frac{l(l+1)}{2r^2} + V(r)\right\}\mathcal{R}_{lm}(r,t) + \\ &+\sum_{l'}\left\langle lm\left|-iA(t)\left(\cos\theta\partial_r - \frac{\sin\theta}{r}\partial_\theta\right)\right|l'm\right\rangle\mathcal{R}_{l'm}(r,t), \end{aligned} \tag{6.6}$$

where

$$\left\langle lm\left|\hat{O}\right|l'm'\right\rangle = \int d\Omega Y^*_{lm}(\theta,\phi)\hat{O}Y_{l'm'}(\theta,\phi) \tag{6.7}$$

for any operator $\hat{O}$. Next we can define the new function $\phi_{lm}(r,t)$ by

$$\mathcal{R}_{lm}(r,t) = \frac{\phi_{lm}(r,t)}{r} \tag{6.8}$$

such that when substituting into eq.(6.6) we obtain

$$i\partial_t\phi_{lm}(r,t) = \left\{-\frac{1}{2}\frac{\partial^2}{\partial r^2} + \frac{l(l+1)}{2r^2} + V(r)\right\}\phi_{lm}(r,t) +$$
$$-iA(t)\sum_{l'}\left\langle lm\left|\left(\cos\theta r\partial_r r^{-1} - \frac{\sin\theta}{r}\partial_\theta\right)\right|l'm\right\rangle\phi_{l'm}(r,t), \tag{6.9}$$

where the operator $r\partial_r r^{-1}$ is due to the fact that $[r,\partial_r]\neq 0$. In order to evaluate the inner product in the second term of eq.(6.9) we use the recurrence relations [92]

$$\cos\theta Y_{l'm}(\theta,\phi) = \sqrt{\frac{(l'+m)(l'-m)}{(2l'+1)(2l'-1)}}Y_{l'-1m}(\theta,\phi)$$
$$+\sqrt{\frac{(l'+m+1)(l'-m+1)}{(2l'+1)(2l'+3)}}Y_{l'+1m}(\theta,\phi) \tag{6.10}$$

and

$$-\sin\theta\partial_\theta Y_{l'm}(\theta,\phi) = (l'+1)\sqrt{\frac{(l'+m)(l'-m)}{(2l'+1)(2l'-1)}}Y_{l'-1m}(\theta,\phi)$$
$$-l'\sqrt{\frac{(l'+m+1)(l'-m+1)}{(2l'+1)(2l'+3)}}Y_{l'+1m}(\theta,\phi). \tag{6.11}$$

When substituting the recurrence relations into eq.(6.9) we obtain

$$\begin{aligned}
i\partial_t\phi_{lm}(r,t) &= \left\{-\frac{1}{2}\frac{\partial^2}{\partial r^2} + \frac{l(l+1)}{2r^2} + V(r)\right\}\phi_{lm}(r,t) + \\
&- iA(t)\sqrt{\frac{(l+m+1)(l-m+1)}{(2l+1)(2l+3)}}r\partial_r r^{-1}\phi_{l+1m}(r,t) \\
&- iA(t)\sqrt{\frac{(l+m)(l-m)}{(2l+1)(2l-1)}}r\partial_r r^{-1}\phi_{l-1m}(r,t) \\
&- \frac{iA(t)}{r}(l+2)\sqrt{\frac{(l+m+1)(l-m+1)}{(2l+1)(2l+3)}}\phi_{l+1m}(r,t) \\
&+ \frac{iA(t)}{r}(l-1)\sqrt{\frac{(l+m)(l-m)}{(2l+1)(2l-1)}}\phi_{l-1m}(r,t).
\end{aligned} \tag{6.12}$$

Further substituting relation $r\partial_r r^{-1} = -r^{-1} + \partial_r$ into eq.(6.12), we obtain

$$\begin{aligned} i\partial_t \phi_{lm}(r,t) &= \left\{ -\frac{1}{2}\frac{\partial^2}{\partial r^2} + \frac{l(l+1)}{2r^2} + V(r) \right\} \phi_{lm}(r,t) + \\ &- iA(t)\sqrt{\frac{(l+m+1)(l-m+1)}{(2l+1)(2l+3)}}\partial_r \phi_{l+1m}(r,t) \\ &- iA(t)\sqrt{\frac{(l+m)(l-m)}{(2l+1)(2l-1)}}\partial_r \phi_{l-1m}(r,t) \\ &- \frac{iA(t)}{r}(l+1)\sqrt{\frac{(l+m+1)(l-m+1)}{(2l+1)(2l+3)}}\phi_{l+1m}(r,t) \\ &+ \frac{iA(t)}{r} l \sqrt{\frac{(l+m)(l-m)}{(2l+1)(2l-1)}}\phi_{l-1m}(r,t). \end{aligned} \tag{6.13}$$

The 3D TDSE is now reduced to a system of coupled 1D TDSEs. In practice one has to truncate the expansion in the eq.(6.3) at a maximum l value denoted as $Lmax$. Note there is no coupling between different values of m; hence it is set to be the same value as the initial state. This cylindrical symmetry is crucial for the current method to be applicable. The Crank-Nicholson method is then used to propagate the wavefunction in time. We approximate the radial Hamiltonian by first order finite-difference which reads

$$\begin{aligned} \frac{\partial^2}{\partial r^2}\phi_{lm}(r,t) &= \frac{\phi_{lm}(r+h,t) - 2\phi_{lm}(r,t) + \phi_{lm}(r-h,t)}{h^2} \\ \partial_r \phi_{lm}(r,t) &= \frac{\phi_{lm}(r+h,t) - \phi_{lm}(r-h,t)}{2h}. \end{aligned} \tag{6.14}$$

The method is accurate to $O(h^2)$. Higher order finite-difference is also available [90].

6.3 The length gauge calculation

In the length gauge calculation we start from the time-dependent Schrödinger equation

$$\left\{ -\frac{\nabla^2}{2} + V(r) + V_L(t) \right\} \Psi(\mathbf{r},t) = i\partial_t \Psi(\mathbf{r},t), \tag{6.15}$$

where in the dipole approximation the interaction Hamiltonian is given by

$$V_L(t) = r\cos\theta E(t). \tag{6.16}$$

The wavefunction can be written as a linear combination of the spherical harmonics as given by eq.(6.3). Substituting eq.(6.3)-(6.5) into eq.(6.15), we obtain a set of coupled differential equations for the coefficients $\mathcal{R}_{lm}(r,t)$

$$i\partial_t \mathcal{R}_{lm}(r,t) = \left\{ -\frac{1}{2}\frac{1}{r^2}\frac{\partial}{\partial r}\left(r^2\frac{\partial}{\partial r}\right) + \frac{l(l+1)}{2r^2} + V(r) \right\} \mathcal{R}_{lm}(r,t) + \\ + \sum_{l'} \langle lm \left| r\cos\theta E(t) \right| l'm \rangle \, \mathcal{R}_{l'm}(r,t). \tag{6.17}$$

We define again

$$\mathcal{R}_{lm}(r,t) = \frac{\phi_{lm}(r,t)}{r} \tag{6.18}$$

and substitute into eq.(6.17) to obtain

$$i\partial_t \phi_{lm}(r,t) = \left\{ -\frac{1}{2}\frac{\partial^2}{\partial r^2} + \frac{l(l+1)}{2r^2} + V(r) \right\} \phi_{lm}(r,t) + \\ + \sum_{l'} \langle lm \left| r\cos\theta E(t) \right| l'm \rangle \, \phi_{l'm}(r,t). \tag{6.19}$$

Using the recurrence relation eq.(6.10) and the orthogonality condition for spherical harmonics, we can write the above equation as

$$\begin{aligned} i\partial_t \phi_{lm}(r,t) &= \left\{ -\frac{1}{2}\frac{\partial^2}{\partial r^2} + \frac{l(l+1)}{2r^2} + V(r) \right\} \phi_{lm}(r,t) + \\ &+ rE(t)\sqrt{\frac{(l+m+1)(l-m+1)}{(2l+1)(2l+3)}}\phi_{l+1m}(r,t) \\ &+ rE(t)\sqrt{\frac{(l+m)(l-m)}{(2l+1)(2l-1)}}\phi_{l-1m}(r,t). \end{aligned} \tag{6.20}$$

Again the 3D TDSE now reduces to a system of coupled 1D TDSEs. The Crank-Nicholson method can be used to propagate the wavefunction. The equation is simpler in the length gauge than in the velocity gauge. In fact the Hamiltonian matrix in length gauge can be written as a sparse matrix with only 5 non-zero diagonals as compared to the velocity gauge Hamiltonian matrix which has 9 non-zero diagonals. Hence for a total ionization rate calculation when the grid size is not very large, the length gauge is a better choice. For the photoelectron spectrum calculation the grid size must be large enough to include all the outgoing electron waves it turns out the velocity gauge calculation gives better convergence.

6.4 The photoelectron spectrum

The photoelectron spectrum is given by

$$I(\epsilon) = |\langle \Phi_\epsilon | \Psi \rangle|^2 , \tag{6.21}$$

where $|\Psi\rangle$ is the wavefunction after time propagation and $|\Phi_\epsilon\rangle$ is the field-free eigenstates. Unfortunately, it is difficult to list all the eigenstates, therefore, calculation based on the definition is not practical. One practical way to obtain the photoelectron spectrum is the window operator first proposed by Schafer and Kulander [93]. The operator is defined as the following

$$\mathcal{W}(\epsilon, \gamma, n) = \frac{\gamma^{2^n}}{\left(\hat{H}_0 - \epsilon\right)^{2^n} + \gamma^{2^n}}, \tag{6.22}$$

where H_0 is the field-free Hamiltonian, ϵ is the energy coordinate; γ and n are parameters related to the window shape and width. Take the window operator and operate on the final wavefunction we obtain

$$\begin{aligned} \frac{\gamma^{2^n}}{\left(\hat{H}_0 - \epsilon\right)^{2^n} + \gamma^{2^n}} |\Psi\rangle &= \frac{\gamma^{2^n}}{\left(\hat{H}_0 - \epsilon\right)^{2^n} + \gamma^{2^n}} \sum_{\epsilon'} c_{\epsilon'} |\Phi_{\epsilon'}\rangle \\ &= \sum_{\epsilon'} \frac{\gamma^{2^n}}{\left(\epsilon' - \epsilon\right)^{2^n} + \gamma^{2^n}} c_{\epsilon'} |\Phi_{\epsilon'}\rangle, \end{aligned} \tag{6.23}$$

where $c_{\epsilon'}$ are the expansion coefficients of the wavefunction in the field-free basis. The photoelectron spectrum is given by

$$\begin{aligned} I(\epsilon) &= \lim_{\gamma \to 0} \left\langle \Psi \left| \frac{\gamma^{2^n}}{\left(\hat{H}_0 - \epsilon\right)^{2^n} + \gamma^{2^n}} \cdot \frac{\gamma^{2^n}}{\left(\hat{H}_0 - \epsilon\right)^{2^n} + \gamma^{2^n}} \right| \Psi \right\rangle \\ &= \lim_{\gamma \to 0} \sum_{\epsilon'} |c_{\epsilon'}|^2 \left(\frac{\gamma^{2^n}}{\left(\epsilon' - \epsilon\right)^{2^n} + \gamma^{2^n}} \right)^2 \end{aligned} \tag{6.24}$$

Since the function in the bracket of eq.(6.24) reduces to a delta function at the limit $\gamma \to 0$, the photoelectron spectrum can be obtained by scanning through a demand range of ϵ. In practice there is a fundamental difficulty in calculating eq.(6.24) directly. Since the

operator $\hat{H}_0$ is in the denominator it is computationally very expansive to directly compute the operation

$$|\chi\rangle = \frac{\gamma^{2^n}}{\left(\hat{H}_0 - \epsilon\right)^{2^n} + \gamma^{2^n}}|\Psi\rangle. \tag{6.25}$$

Instead one should be solving the linear system of equations

$$\mathcal{W}(\epsilon, \gamma, n)^{-1}|\chi\rangle = |\Psi\rangle \tag{6.26}$$

for $|\chi\rangle$, where the inverse operator $\mathcal{W}(\epsilon, \gamma, n)^{-1}$ can be written as a product form

$$\gamma^{2^n}\mathcal{W}(\epsilon, \gamma, n)^{-1} = \prod_{k=1}^{2^{n-1}} \left\{\hat{H}_0 - \epsilon + \gamma e^{i\nu_{nk}}\right\}\left\{\hat{H}_0 - \epsilon - \gamma e^{i\nu_{nk}}\right\} \tag{6.27}$$

and the constant phase is given by $\nu_{nk} = \frac{(2k-1)}{2^n}\pi$.

In our program, we implement the window operator with $n = 3$, $(k = 1, 2, 3, 4)$ so that the inverse window operator can be written as

$$\begin{aligned}\gamma^{2^n}\mathcal{W}(\epsilon, \gamma, n)^{-1} = &\left\{\hat{H}_0 - \epsilon + \gamma e^{i\nu_{nk=1}}\right\}\left\{\hat{H}_0 - \epsilon - \gamma e^{i\nu_{nk=1}}\right\} \\ &\left\{\hat{H}_0 - \epsilon + \gamma e^{i\nu_{nk=2}}\right\}\left\{\hat{H}_0 - \epsilon - \gamma e^{i\nu_{nk=2}}\right\} \\ &\left\{\hat{H}_0 - \epsilon + \gamma e^{i\nu_{nk=3}}\right\}\left\{\hat{H}_0 - \epsilon - \gamma e^{i\nu_{nk=3}}\right\} \\ &\left\{\hat{H}_0 - \epsilon + \gamma e^{i\nu_{nk=4}}\right\}\left\{\hat{H}_0 - \epsilon - \gamma e^{i\nu_{nk=4}}\right\}.\end{aligned} \tag{6.28}$$

By solving the linear system of equations (6.26) iteratively we can obtain the vector $|\chi\rangle$. From eq.(6.25) and eq.(6.24) we can see that the photoelectron spectrum is approximately given by

$$I(\epsilon) \approx \langle\chi|\chi\rangle, \tag{6.29}$$

provided γ is chosen to be small.

Chapter 7

Influence of ultra-short pulse on resonantly driving system

7.1 Introduction

One important class of laser-matter interaction, two-color ionization, has been studied for over a decade and covering a wide range of physical parameters [94, 95, 96, 97, 98, 95, 99, 100, 101]. The early studies use two commensurate laser fields to ionize the atoms so that the relative phase between the laser pulses becomes an important parameter. The phase-dependent effect has been discussed both theoretically [102, 101, 98] and experimentally [94, 103, 104]. Watanabe and Schumacher showed that both the total ionization rate and the above-threshold ionization (ATI) peaks vary periodically with the relative phase [104]. Schafer, *et al.* [102] suggested that the angular distribution for the lowest ATI peak can be controlled by the phase angle. In addition, Protopapas *et al.* [97, 98] studied the high harmonic generation spectrum in the two-color laser field and found that the plateau region can be extended, and the cutoff is sensitive to the relative phase between the two lasers. Furthermore, it has been found that the ATI spectrum generated by a fundamental field together with its 13th harmonics produced pronounced side-bands beside the main photoionization peak [105, 106]. The side-bands can be interpreted as the emission/absorption of additional photons to/from the intense fundamental field by the electron after ionization by the harmonic field. This observation supports the idea that the two-color ionization dynamics is more controllable than the one color ionization dynamics because the bound-free and free-free transitions are separable in the former case and entangled in a complex way in the latter [105]. More recently experiments have confirmed the possibility of gen-

erating attosecond pulses [107]. This result directly leads to another important category of the two-color experiments. When combining an attosecond x-ray pulse with a strong low frequency laser field [108, 109, 110, 111, 112] the attosecond streaking camera is born. This idea has been used to probe the electron and molecular dynamics and to characterize a laser pulse. Recent progress in the high harmonic generation technique also allows higher order harmonics to be used in the two-color experiment. One interesting aspects discussed by Ishikawa [113] is that the high frequency laser field (harmonic pulse) can drive transition between two bound states or between a bound state and a nearby virtual state, and a subsequent few cycle laser pulse can ionize the system. An enhancement of the conversion efficiency by 17 orders of magnitude in the high harmonic generation spectrum is discovered. Apparently the resonance effect plays a significant role in the ionization and high harmonic generation processes.

In this chapter a sufficiently strong high frequency laser is tuned on resonance with the ground state and the first excited state such that Rabi oscillation occurs between the two levels. In addition we observed the resonance two-photon ionization peak (TIP) in the photoelectron spectrum which is a result of simultaneous absorption of two high energy photons. Subsequently, depending on its intensity, an intense few-cycle laser pulse can either ionize the system or produce side-bands beside the TIP. We anticipate the appearance time of the few-cycle pulse relative to the Rabi oscillations can be used to control the ionization rate as well as the side-band intensities.

In section 7.2 we model the system using a one-dimensional hydrogen atom with soft-core potential first introduced by Eberly [114, 115]. We choose the intensity of the few-cycle pulse such that strong field ionization (SFI) from the excited state is possible. The SFI rate is in general much greater than the resonance two-photon ionization rate; hence it becomes dominant in this region. We show that the SFI probability depends on the appearance time of the few-cycle laser pulse periodically. By depleting the excited state, the intense short pulse not only resets the Rabi oscillation, but also introduces a time shift that is proportional to the pulse length. We then lower the intensity of the few-cycle pulse such that SFI is suppressed. Resonant two-photon ionization becomes dominant in this region. A subsequent few-cycle laser pulse generates side-bands near the resonance two-photon ionization peak. We show that the side-bands intensity can be controlled by adjusting the appearance time.

In section 7.3 we developed a general theory that can be used to describe the electron dynamics under few cycle laser pulse in the presence of resonant driving frequency. The theory is based on Dyson expansions of the time propagation operator which correspond to different partitions of the total Hamiltonian. We will show that the choice of the partition can be guided by the dominant physical process at varies laser intensities. Our theory is

capable of explaining most of the observations in the section 7.2 except the AC-stark shift out of resonance by the few-cycle laser pulse. In the end of this section a numerical solution to the 3D time-dependent Schrödinger equation for Hydrogen atom in the presence of both laser fields is given. The results support the qualitative prediction by our theory and agree with the one dimensional model in section 7.2.

7.2 One dimensional model study

The Hamiltonian of the system is given by

$$\hat{H} = \hat{H}_0 + xE(t), \quad \hat{H}_0 = -\frac{1}{2}\frac{\partial^2}{\partial x^2} - \frac{1}{\sqrt{1+x^2}}, \tag{7.1}$$

where $\hat{H}_0$ is Hamiltonian of an isolated atom, and we use the length gauge and the dipole approximation to describe the interaction of the atom with the lasers. By diagonalizing $\hat{H}_0$ in the spatial-grid representation, a set of energy eigenstates is obtained. The ground state ϕ_g has binding energy of $I_g = 0.67$ and is used as the initial state for the time propagation. The first excited state ϕ_e has binding energy $I_e = 0.2752$. The electric field due to the two lasers can be written as a sum of the high frequency continuous wave (HFCW) laser field and the low frequency few-cycle (LFFC) laser pulse:

$$E(t) = E_1 \ \sin(\omega_H t) + E_2 \ e^{-\alpha\tau^2} \sin\left(\omega_L \tau\right), \tag{7.2}$$

where $\tau = t - T_a$ and T_a is the appearance time of the LFFC laser pulse. We assume that the HFCW laser field is resonantly coupling the ground state to the first excited state so that $\omega_H = I_e - I_g = 0.3948$, and set the field amplitude $E_1 = 0.003$ in all our calculations. The central frequency of the LFFC pulse is $\omega_L = 0.05$ and the field amplitude varies from $E_2 = 0.05$ to $E_2 = 0.008$ in our studies. We choose $\alpha = 3 \times 10^{-5}$ in our calculations and propagate the system for a time interval of $T_I = 5026.5$ (315 cycles of the HFCW laser) using the split operator technique and the FFT algorithm [116]. During the time propagation we project the wave function onto the positive energy eigenstates to obtain the photoelectron spectrum (PES) in real time. Two virtual detectors are set up at the boundaries before the absorption region. These detectors will record the electron probability flux in real time. The sum of the electron flux over all interaction time can be interpreted as the total ionization probability.

We first consider the case of a high intensity LFFC pulse in the presence of a HFCW laser. As shown in Fig. 7.1(a) the total ionization rate has an oscillatory behavior as a

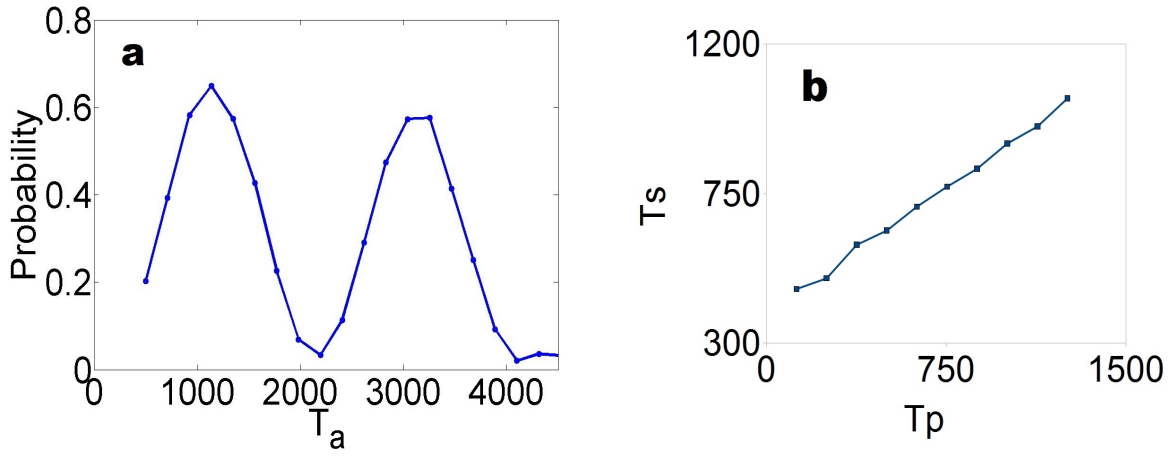

Figure 7.1: (a): Ionization probability versus T_a with $E_2 = 0.05$. (b): Time shift T_s (see Fig. 7.2) versus the trapezoidal pulse length T_p. Here $T_a = 2412$ and $E_2 = 0.04$.

function of T_a. Now the high intensity LFFC pulse will rapidly deplete the excited state population by over-the-barrier ionization. On the other hand the ground state is far below the potential barrier and it will survive the pulse. Before the appearance of the LFFC, the system undergoes Rabi oscillation in the presence of the HFCW laser (see Fig. 7.2). Consequently when the LFFC pulse is turned on near the maxima of the excited state population, the ionization rate reaches maxima, but when the LFFC pulse appears at the maxima of the ground state population, the ionization rate will be a minimum. Hence the ionization probability oscillates with the Rabi frequency, as observed in Fig. 7.1(a). In Fig. 7.2 we plot the populations of the ground state and the first excited state in the presence of a 5-cycle laser pulse. When the LFFC pulse arrives, the population in the excited state drops rapidly while the population in the ground states remains approximately constant. The observation suggests that the HFCW laser cannot efficiently couple the ground state and the first excited state in the presence of the LFFC pulse because of the AC Stark shift out of resonance. This phenomenon resembles the quantum Zeno effect [117]. It is clear that most ionization is from the excited states and not from the ground state because of the exponential dependence of the ionization rates on the ionization potential. After the pulse the system returns to the Rabi oscillations with a constant time shift T_s with respect to the unperturbed Rabi oscillation. The time shift is approximately equal to the LFFC pulse length, but it also depends on the rising and falling edges of the pulse. In order to eliminate the latter factor we introduced a trapezoidal pulse envelope with rising and falling times of one optical cycle, and we plot the time shift T_s versus the pulse length T_p

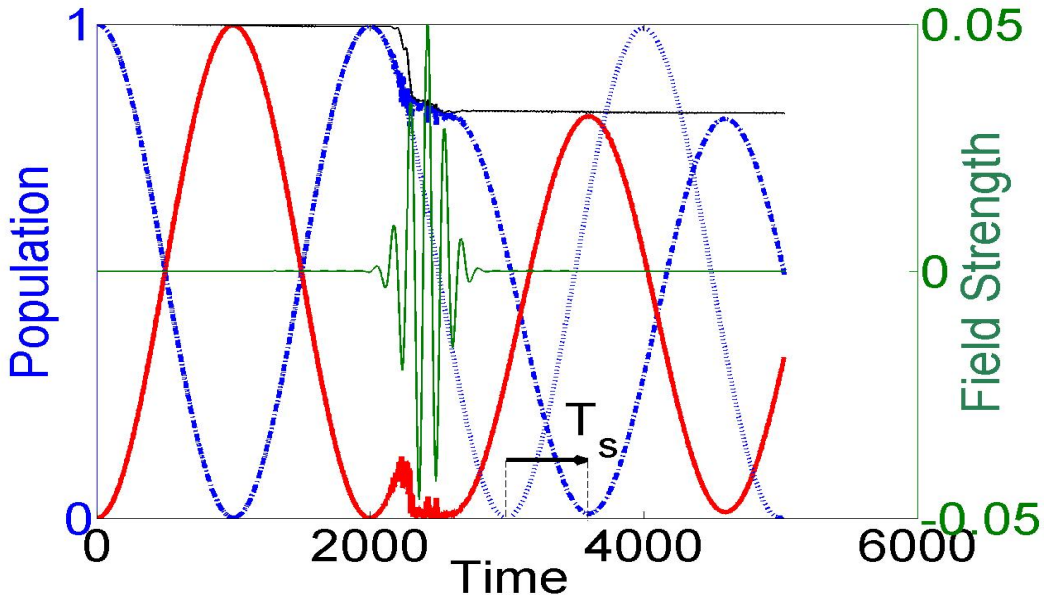

Figure 7.2: Ground state (dash-dotted) and first excited state (thick solid) populations versus time; Unperturbed Rabi oscillation (dotted); The LFFC pulse (thin solid); The total population in both states(dark thin solid); The dark arrow defines the time shift T_s. $T_a = 2412$. $E_1 = 0.003$ and $E_2 = 0.05$.

of the flat top region in Fig. 7.1(b). A linear relationship is obtained which suggests that one can use T_s to characterize the LFFC pulse.

Next we study in Fig. 7.3 the effect of a lower intensity LFFC pulse on the bound state dynamics of the two-level system. In this case, the population of the ground state does not remain constant in the presence of the LFFC pulse, indicating that the AC shift of the two levels is not sufficient to switch them totally out of resonance with the HFCW laser. The electron in the excited state is tunneling ionized by the LFFC pulse while the ground state population is pumped to replenish it. After the pulse, the system undergoes Rabi oscillations again with both states ϕ_g and ϕ_e populated. This behavior can be explained using the Feyman-Vernon-Hellwarth (FVH) representation [118] in which the system is described by a state vector in a Bloch sphere, while the *resonant* CW laser field is represented by a constant field vector along the x-axis. Initially the system is in its ground state and the state vector lies along the negative z-axis and hence will precess in the yz-plane about this field vector, giving rise to the Rabi oscillation. The appearance of a LFFC pulse of moderate intensity introduces an additional field vector along the negative z-axis

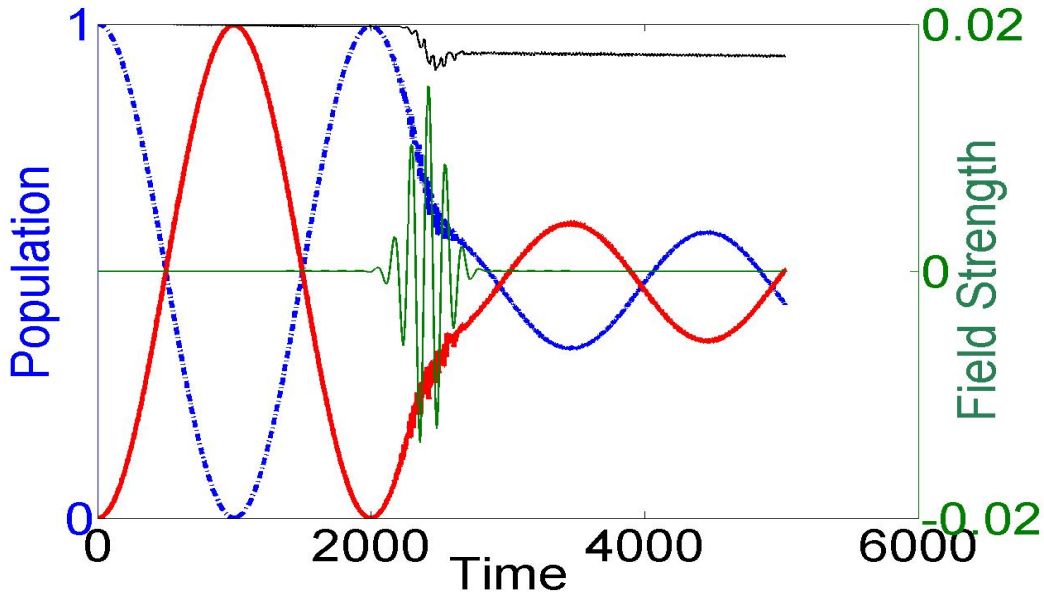

Figure 7.3: Ground state (dash-dotted) and first excited state (thick solid) populations versus time; The LFFC pulse (thin solid); The total population in both states(dark thin solid). $T_a = 2412$. $E_1 = 0.003$ and $E_2 = 0.015$.

so that the state vector no longer precesses in the yz-plane. After the passing of the LFFC pulse, the state vector will precess on a cone about the x-axis so that its z-component, which represents the population difference, will oscillate about 0 with an absolute value less than 1. We can characterize the electron dynamics by assuming that immediately after the LFFC pulse the bound state component of the wave function of the system can be approximated by

$$\psi_b = \sqrt{1 - P_I}\,[\cos\vartheta\ \phi_g + \sin\vartheta e^{i\varphi}\phi_e], \tag{7.3}$$

where ϑ, φ are real angles and P_I is the ionization probability. In the FHV representation, the length of the state vector represents the total population in the two states and the orientation is given by the angles 2ϑ and φ, respectively. We plot the angles as functions of the pulse amplitude E_2 in Fig. 7.4. Two regions can be recognized: a rapidly changing region followed by a plateau region. Such clear transition is an indication of the rapid depletion of the excited states. It is interesting to note that the onset of the plateau region occurs at an intensity just above the classical over-the-barrier value of $I_e^2/4$.

When the LFFC pulse intensity is further decreased, the tunneling ionization from the excited state is completely suppressed. Even in the absence of the LFFC pulse, the HFCW

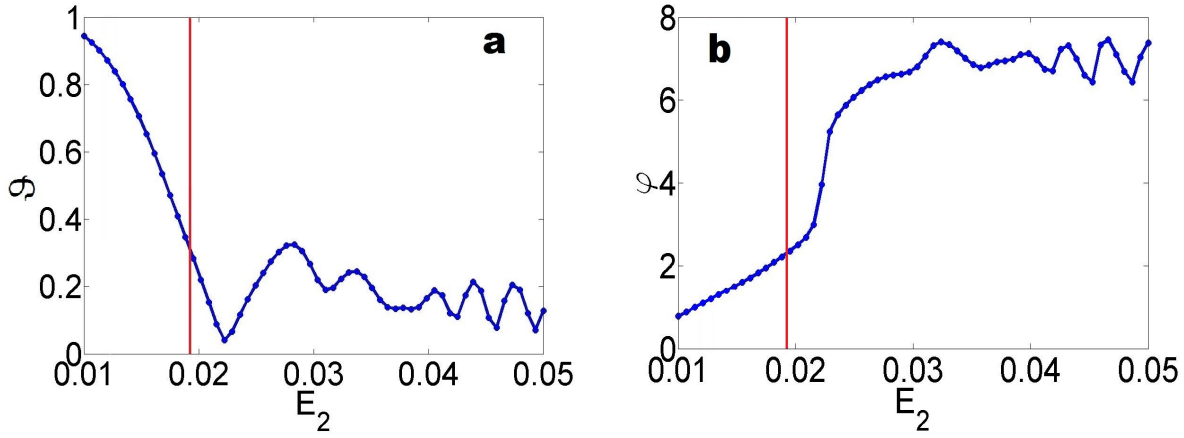

Figure 7.4: (a): ϑ versus E_2. (b): φ versus E_2, $T_a = 2412$. The vertical line (red) indicates the classical over the barrier field strength.

laser field is strong enough to cause resonance two-photon ionization, indicated by the peak at $2\omega_H - I_g = 0.12$ in the PES in Fig. 7.5(a). The ionization is multiphoton in nature, and it will generate symmetric electron flows to the left and to the right as shown in Fig. 7.5(b). We find the flux intensity oscillating with the Rabi frequency, and (not shown) the electron outgoing wave forms a train of wave packets. Each successive packet is separated by a distance $L = T_R v$, where T_R is the period of Rabi oscillation and v is the photoelectron velocity. Taking into account the traveling time from the atom to the detector, we find that the variation of the electron flux follows that of the excited state population. In the presence of the LFFC laser pulse, side-bands emerge near the TIP whose relative intensities oscillate with T_a as shown in Fig. 7.6. Since the side-bands can be interpreted as the absorption (appearing to the right of TIP) or emission (appearing to the left of TIP) of additional photons from/to the LFFC laser field in addition to the two high energy photons [106], one can effectively control the absorption/emission of additional photons by varying the time of appearance of the intense few-cycle pulse. The physical reason of this control relies on the fact that free electron does not absorb photons. When the electron wave packets created by the HFCW laser are far away from the parent atom at the time the LFFC pulse is applied, it will not absorb/emit additional photons from/to the intense laser pulse, and the side-band is suppressed. If the LFFC pulse is switched on when the electron wave packet is near the parent atom, the electron can efficiently absorb/emit additional photons from/to the intense laser pulse. We have developed an S-matrix formalism in three dimensions to address the physics behind the side-band control

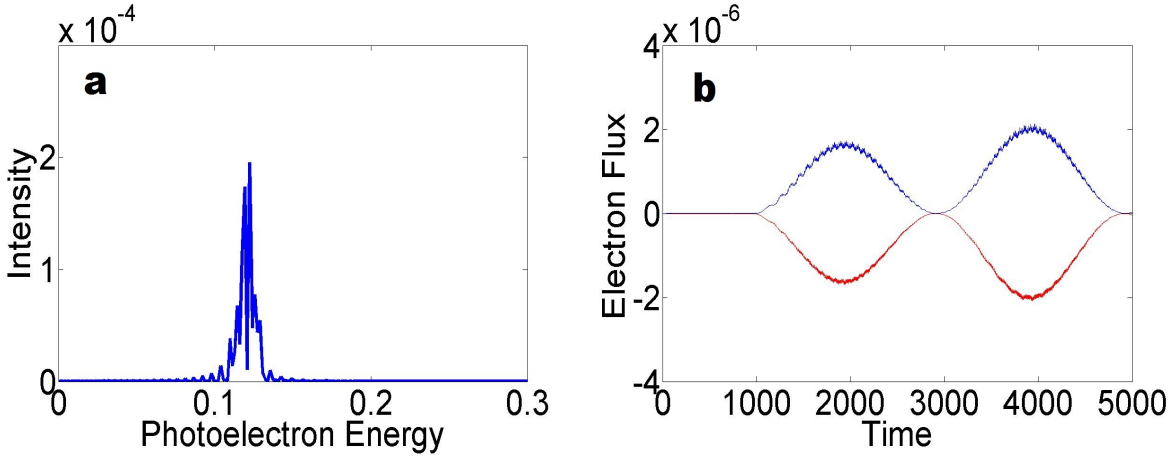

Figure 7.5: (a): photoelectron spectrum from the HFCW laser alone. (b): Total electron outgoing flux versus time. Positive flux indicates electron flow to the right while negative flux represents electron flow to the left. $E_1 = 0.003$.

scheme (see section 7.3 for detail). Using the velocity gauge, we found that the total transition amplitude M_{fi} can be written as a sum over the partial transition amplitudes of distinct photon orders M_{fi}^n, where n represents the number of photons absorbed from or emitted to the few-cycle laser pulse during ionization. When the LFFC pulse length T_p is sufficiently large so that the interference between different photon orders becomes negligible, the side-band peak intensities are given by

$$|M_{fi}^n|^2 \;=\; 2\pi T_p^2 \left| J_n\left(\zeta, \frac{z}{2}\right)\right|^2 (\omega_L \zeta)^2 \sin^2\left(\frac{\Omega}{2} T_a\right) |\tilde{\phi}_e(k_n)|^2, \tag{7.4}$$

where $J_n(\zeta, \frac{z}{2})$ is the generalized Bessel function [20] with $z = U_{2p}/\omega_L$, $\zeta = E_2 k_n \cos\theta$, θ is the angle between the laser polarization and the outgoing momentum $\mathbf{k}_n$ of the ionized electron, $U_{2p} = E_2^2/4\omega_L$ is the ponderomotive potential of the low-frequency laser, $k_n \approx \sqrt{2(\omega_H - I_e - U_{2p} + n\omega_L)}$, $\tilde{\phi}_e(k_n)$ is the Fourier transform of the excited state wave function, and Ω is Rabi frequency. (See the next section for the derivation of eq.7.4.) It is clear from Eq.(7.4) the side-band intensities will oscillate in the Rabi frequency with respect to the appearance time of the few-cycle laser pulse T_a. Indeed this behavior is verified by the numerical simulation as shown in Fig. 7.6 (see inset window).

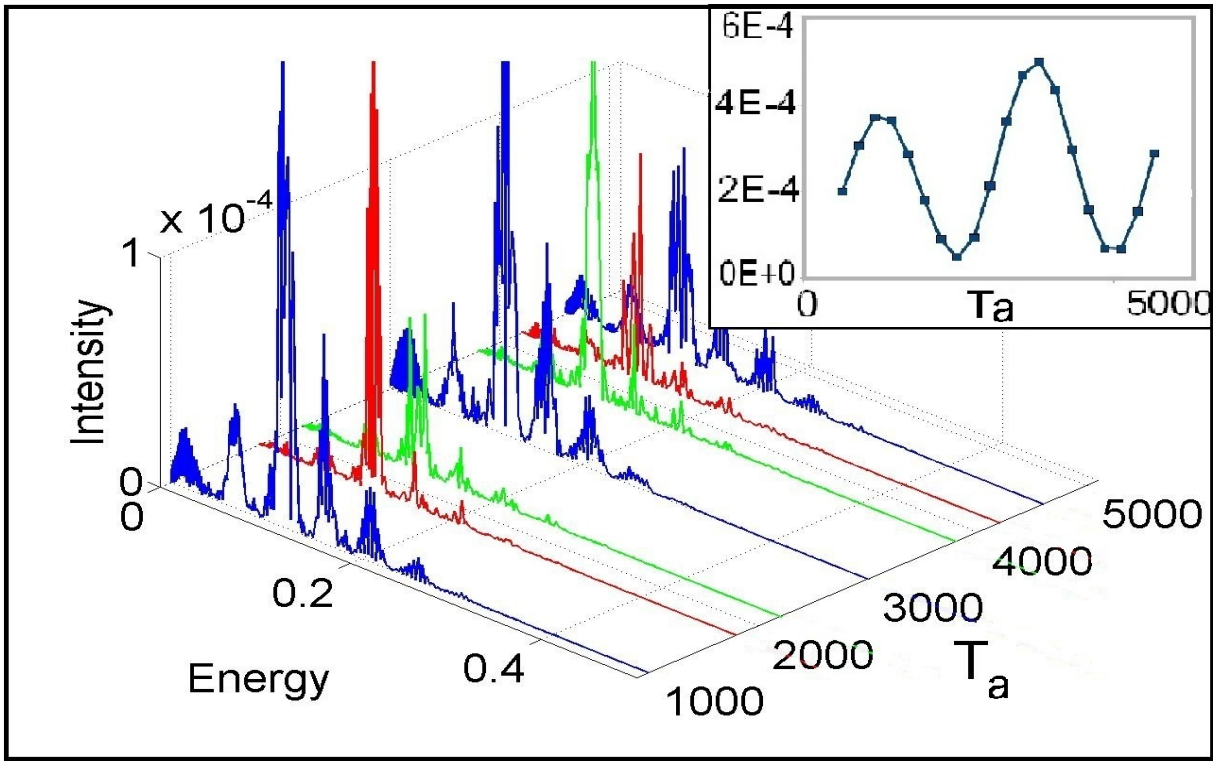

Figure 7.6: The PES at different appearance time T_a. Inset: Peak intensity of the first photon absorption side-band versus appearance time T_a. $E_2 = 0.008$.

7.3 The theory of electron dynamics under few cycle laser pulse in the presence of resonant driving frequency

In order to understand the observations in the previous section we study the system from a more general point of view. The total Hamiltonian of the system can be written as

$$\hat{H}(t) = \hat{H}_0 + V_L(t) + V_H(t), \tag{7.5}$$

where the field-free Hamiltonian contains the kinetic energy term and the binding potential term given by

$$\hat{H}_0 = \hat{T} + V_b(\mathbf{r}). \tag{7.6}$$

The interaction with laser fields are described in the velocity gauge under dipole approximation written

$$V_L(t) = -i\nabla \cdot \mathbf{A}_L(t) + \frac{1}{2}\mathbf{A}_L^2(t) \tag{7.7}$$

and

$$V_H(t) = -i\nabla \cdot \mathbf{A}_H(t), \tag{7.8}$$

where the the vector potentials are related to the laser electric fields by $\mathbf{E}_L(t) = -\partial_t \mathbf{A}_L(t)$ and $\mathbf{E}_H(t) = -\partial_t \mathbf{A}_H(t)$ respectively. In writing the interaction Hamiltonian eq.(7.7) and eq.(7.8), we have introduced additional time dependent factors in the gauge transformation so that the time dependent terms $\frac{1}{2}\mathbf{A}_H^2(t)$ and $\mathbf{A}_L(t) \cdot \mathbf{A}_H(t)$ were transformed away. Since we are interested in the influence of ultrashort pulse on resonantly driven systems, the high frequency laser field $\mathbf{E}_H(t)$ is chosen to be a CW laser that will resonantly couple two real orbitals of the system given by the field-free Hamiltonian in eq.(7.6). The low frequency laser is chosen to be a high intensity few-cycle laser pulse. More explicitly the electric fields are given by the equations

$$\mathbf{E}_H(t) = \mathbf{E}_1 \sin(\omega_H t) \tag{7.9}$$

and

$$\mathbf{E}_L(\mathfrak{t}) = \mathbf{E}_2 \mathfrak{f}(\mathfrak{t}) \sin(\omega_L \mathfrak{t} + \phi), \tag{7.10}$$

where $\mathfrak{f}(\mathfrak{t}) = \mathfrak{f}(t - T_a)$ is the envelope function of the laser pulse which is centered at T_a with the pulse length T_p. We refer the parameter T_a as the appearance time of the pulse.

The Schrödinger equation for the system reads

$$i\partial_t|\Psi(t)\rangle = \hat{H}(t)|\Psi(t)\rangle. \tag{7.11}$$

To reformulate the above equation in the S-matrix language we can introduce the partition to the total Hamiltonian

$$\hat{H}(t) = \hat{H}_H(t) + V_L(t) \tag{7.12}$$

such that the reference system,

$$i\partial_t|\Psi_H(t)\rangle = \hat{H}_H(t)|\Psi_H(t)\rangle, \tag{7.13}$$

is assumed to be soluble. In addition, we define the time evolution operators corresponding to the total and the reference Hamiltonian

$$\left\{i\partial_t - \hat{H}(t)\right\}\hat{U}(t,t') = 0,\ \hat{U}(t',t') = \hat{1}, \tag{7.14}$$

$$\left\{i\partial_t - \hat{H}_H(t)\right\}\hat{U}_H(t,t') = 0,\ \hat{U}_H(t',t') = \hat{1} \tag{7.15}$$

such that these time evolution operators are related by the Dyson equations

$$\hat{U}(t,t') = \hat{U}_H(t,t') - i\int_{t'}^{t} d\tau \hat{U}(t,\tau)V_L(\tau)\hat{U}_H(\tau,t'), \tag{7.16}$$

$$\hat{U}(t,t') = \hat{U}_H(t,t') - i\int_{t'}^{t} d\tau \hat{U}_H(t,\tau)V_L(\tau)\hat{U}(\tau,t'). \tag{7.17}$$

We emphasize on the fact that the partition in eq.(7.12) leads to the Dyson expansion given by eq.(7.16) ,(7.17); however, the partition is by no means unique. One can show that an alternative partition,

$$\hat{H}(t) = \hat{H}_L(t) + V_H(t), \tag{7.18}$$

will lead to another set of Dyson expansions given by

$$\hat{U}(t,t') = \hat{U}_L(t,t') - i\int_{t'}^{t} d\tau \hat{U}(t,\tau)V_H(\tau)\hat{U}_L(\tau,t'), \tag{7.19}$$

$$\hat{U}(t,t') = \hat{U}_L(t,t') - i\int_{t'}^{t} d\tau \hat{U}_L(t,\tau)V_H(\tau)\hat{U}(\tau,t'). \tag{7.20}$$

Furthermore, the reference Hamiltonian $H_L(t)$ can be partitioned according to $H_L(t) = H_0 + V_L(t)$. We can further write

$$\hat{U}_L(t,t') = \hat{U}_0(t,t') - i\int_{t'}^{t} d\tau \hat{U}_L(t,\tau)V_L(\tau)\hat{U}_0(\tau,t'), \tag{7.21}$$

where the $\hat{U}_0(\tau,t')$ is the field-free time evolution operator. The transition amplitude to the field-free final states $|\psi_f(t)\rangle$ is given by

$$M_{fi} \equiv \lim_{t\to\infty}\langle\psi_f(t)|\Psi(t)\rangle = \langle\psi_f(t)|\hat{U}(t,t')|\psi_i(t')\rangle, \tag{7.22}$$

where $|\psi_i(t')\rangle$ denotes the initial field-free state from which the system is evolved. For different laser intensities different Dyson expansion, eq.(7.16 - 7.21), may be used to expand the transition amplitude eq.(7.22). In the next subsections we will discuss these cases separately.

7.3.1 High intensity LFFC laser pulse

When the intensity of the LFFC laser pulse is high we substitute eq.(7.16) into eq.(7.22) and obtain

$$\begin{aligned}\langle\psi_f(t)|\hat{U}(t,t')|\psi_i(t')\rangle &= \langle\psi_f(t)|\hat{U}_H(t,t')|\psi_i(t')\rangle \\ -i\int_{t'}^{t} d\tau\langle\psi_f(t)|\hat{U}(t,\tau)V_L(\tau)\hat{U}_H(\tau,t')|\psi_i(t')\rangle.\end{aligned} \tag{7.23}$$

Based on the 1D model studied in the previous section we anticipate that the tunneling ionization rate by a high intensity LFFC pulse is much greater than the resonance two-photon ionization rate, hence the leading term on the RHS of eq.(7.23) is ignored for the moment. Using the SFA we can write the second term as [15, 43]

$$\langle\psi_f(t)|\hat{U}(t,t')|\psi_i(t')\rangle \approx -i\int_{t'}^{t} d\tau\langle\mathbf{k}|\hat{U}_V(t,\tau)V_L(\tau)\hat{U}_H(\tau,t')|\psi_i(t')\rangle, \tag{7.24}$$

where $\hat{U}_V(t,\tau)|\mathbf{k}\rangle$ is the Volkov solution to the TDSE for an electron in the presence of LFFC laser field only. Consider eq.(7.24) which describes an electron initially prepared in

a field-free state and then propagated by the HFCW laser field. At time τ the electron is perturbed by the LFFC laser pulse $V_L(\tau)$, ionized. After the ionization, the electron is only propagated by the LFFC laser pulse such that both the Coulomb potential and the HFCW laser field are neglected. The transition time τ has to be considered at all possible moments so that a coherent summation is carried out as an integral in eq.(7.24). Before the ionization the electron is bounded so that most of the electron wave packet is concentrated at the nuclear core region. Hence we can approximate the pre-ionization propagation by a two-level system in the presence of a resonant HFCW laser field. After the ionization, the strong field approximation can be applied because the free electron wave-packet spreads out in the space such that the effect by Coulomb potential is significantly reduced. We write the pre-ionization wavefunction as

$$\hat{U}_H(\tau, t')|\psi_i(t')\rangle \approx c_g(\tau)|\phi_g\rangle + c_u(\tau)|\phi_u\rangle, \tag{7.25}$$

where $|\phi_g\rangle$ and $|\phi_u\rangle$ are the eigenstates of the field-free Hamiltonian. The coefficients will satisfy the TDSE

$$\begin{pmatrix} -I_g & \mu(\tau) \\ \mu^*(\tau) & -I_u \end{pmatrix} \begin{pmatrix} c_g(\tau) \\ c_u(\tau) \end{pmatrix} = i\partial_\tau \begin{pmatrix} c_g(\tau) \\ c_u(\tau) \end{pmatrix}, \tag{7.26}$$

where $\mu(\tau)$ is the transition dipole moment given by

$$\mu(\tau) = -i\mathbf{A}_H(\tau) \cdot \langle\phi_g|\nabla|\phi_u\rangle. \tag{7.27}$$

I_g, I_u denote the corresponding ionization potentials. The time dependent coefficients c_g and c_u should contain both the information of the ionization potential as well as the population in each state. When substituting eq.(7.25) into equation 7.24 we obtain

$$\begin{aligned} M_{fi} \approx & -i \int_{t'}^{t} d\tau \langle \mathbf{k}|\hat{U}_V(t,\tau)V_L(\tau)c_g(\tau)|\psi_g\rangle \\ & -i \int_{t'}^{t} d\tau \langle \mathbf{k}|\hat{U}_V(t,\tau)V_L(\tau)c_u(\tau)|\psi_u\rangle. \end{aligned} \tag{7.28}$$

The first term on the RHS gives us the Keldysh transition amplitude from the ground state and the second term on the RHS gives us the Keldysh transition amplitude from the excited states. Use the coordinate representation of the Volkov solution we obtained

$$\begin{aligned} M_{fi} \approx & -i \int_{t'}^{t} d\tau \langle \mathbf{k}|\psi_g\rangle c_g(\tau) e^{iS(\tau)} V_L(\tau) \\ & -i \int_{t'}^{t} d\tau \langle \mathbf{k}|\psi_u\rangle c_u(\tau) e^{iS(\tau)} V_L(\tau), \end{aligned} \tag{7.29}$$

where

$$S(\tau) = \frac{1}{2}\int^{\tau} dt' \left[\mathbf{k} + \mathbf{A}_L(t')\right]^2 \tag{7.30}$$

and $\langle \mathbf{k}|\psi_g\rangle$, $\langle \mathbf{k}|\psi_u\rangle$ are the Fourier transform of the ground state and the excited state respectively. From the theory of two-level system, we assume the coefficients are given by

$$\begin{aligned} c_g(\tau) &= \cos(\frac{\Omega\tau}{2})e^{iI_g\tau} \\ c_u(\tau) &= i\sin(\frac{\Omega\tau}{2})e^{iI_u\tau}, \end{aligned} \tag{7.31}$$

where Ω is the Rabi frequency. Recall that the tunneling ionization rate depends exponentially on the laser intensity and the ionization potential. Considering the large ionization potential difference between the two levels, we assume that only the ionization from the excited state are possible. Hence we obtain

$$M_{fi} \approx \langle \mathbf{k}|\psi_u\rangle \int_{t'}^{t} d\tau \sin(\frac{\Omega\tau}{2}) V_L(\tau) \exp\left\{ iI_u\tau + \frac{1}{2}\int^{\tau} dt' \left[\mathbf{k} + \mathbf{A}_L(t')\right]^2 \right\}. \tag{7.32}$$

Note the integration is gated by the envelope function $\mathfrak{f}(\mathfrak{t})$ such that $\int_{t'}^{t} \rightarrow \int_{T_a - T_p/2}^{T_a + T_p/2}$. The LFFC laser pulse is relatively short comparing to the Rabi period so that the time dependent factor $\sin(\frac{\Omega\tau}{2})$ remains approximately constant during LFFC pulse interaction. We can replace it by a constant factor $\sin(\frac{\Omega T_a}{2})$ which then can be pulled out from the integration and written

$$M_{fi} \approx \langle \mathbf{k}|\psi_u\rangle \sin(\frac{\Omega T_a}{2}) \int_{T_a - T_p/2}^{T_a + T_p/2} d\tau V_L(\tau) \exp\left\{ iI_u\tau + \frac{1}{2}\int^{\tau} dt' \left[\mathbf{k} + \mathbf{A}_L(t')\right]^2 \right\}. \tag{7.33}$$

Since the ionization probability is proportional to the $|M_{fi}|^2$, we immediately see the periodical dependence of the ionization rate on the time of appearance T_a. It has the same period as the Rabi oscillation. For more accurate calculations, the integration in eq.(7.32) can be implemented numerically after the functional form of the LFFC laser pulse is given.

7.3.2 Low intensity LFFC laser pulse

When the intensity of the LFFC laser pulse is low we substitute eq.(7.20) into eq.(7.22) and obtain

$$\begin{aligned} \langle \psi_f(t)|\hat{U}(t,t')|\psi_i(t')\rangle &= \langle \psi_f(t)|\hat{U}_L(t,t')|\psi_i(t')\rangle \\ -i\int_{t'}^{t} d\tau \langle \psi_f(t)|\hat{U}_L(t,\tau)V_H(\tau)\hat{U}(\tau,t')|\psi_i(t')\rangle. \end{aligned} \tag{7.34}$$

The same expression is also obtained in reference [119]. The first term on the RHS is associated with the direct multi-photon ionization of the system by the LFFC laser pulse only, while the second term takes into account the simultaneous interaction with both laser fields. In the side-band study we only consider the second term because the intensity of the LFFC pulse is low enough such that the tunneling ionization probability from both of the real orbitals can be neglected. Using the SFA for the continuum and approximating the pre-ionization state by two-level system, we can write the transition amplitude as

$$\begin{aligned}\langle\psi_f(t)|\hat{U}(t,t')|\psi_i(t')\rangle \;\approx\; & \\ &- \; i\int_{t'}^{t} d\tau \langle \mathbf{k}|\hat{U}_V(t,\tau)V_H(\tau)c_g(\tau)|\psi_g\rangle \\ &- \; i\int_{t'}^{t} d\tau \langle \mathbf{k}|\hat{U}_V(t,\tau)V_H(\tau)c_u(\tau)|\psi_u\rangle. \end{aligned} \tag{7.35}$$

Since the direct ionization from the ground state is much less probable comparing to the ionization from the excited state, we neglect the first term on the RHS of eq.(7.35) and write

$$M_{fi} \approx -i\int_{t'}^{t} d\tau \langle \mathbf{k}|\hat{U}_V(t,\tau)V_H(\tau)c_u(\tau)|\psi_u\rangle. \tag{7.36}$$

Using the coordinate representation of the Volkov solution we obtain

$$M_{fi} \approx -i\langle \mathbf{k}|\psi_u\rangle \int_{t'}^{t} d\tau c_u(\tau)e^{iS(\tau)}V_H(\tau), \tag{7.37}$$

where $S(\tau)$ is the same as in eq.(7.29) and

$$V_H(\tau) = \mathbf{k}\cdot\mathbf{A}_H(\tau). \tag{7.38}$$

Substituting eq.(7.31) into eq.(7.37) we can partition the integral into three regions:

$$\begin{aligned} M_{fi} \approx\; & \langle \mathbf{k}|\psi_u\rangle \int_{t'}^{T_a-T_p/2} d\tau \sin(\frac{\Omega\tau}{2}) \exp\left\{ i\frac{1}{2}\int^{\tau} dt'' \left[\mathbf{k}+\cancel{\mathbf{A}_L(t'')}\right]^2 + iI_u\tau \right\} V_H(\tau) \\ &+\langle \mathbf{k}|\psi_u\rangle \int_{T_a-T_p/2}^{T_a+T_p/2} d\tau \sin(\frac{\Omega\tau}{2}) \exp\left\{ i\frac{1}{2}\int^{\tau} dt'' \left[\mathbf{k}+\mathbf{A}_L(t'')\right]^2 + iI_u\tau \right\} V_H(\tau) \\ &+\langle \mathbf{k}|\psi_u\rangle \int_{T_a+T_p/2}^{t} d\tau \sin(\frac{\Omega\tau}{2}) \exp\left\{ i\frac{1}{2}\int^{\tau} dt'' \left[\mathbf{k}+\cancel{\mathbf{A}_L(t'')}\right]^2 + iI_u\tau \right\} V_H(\tau). \end{aligned} \tag{7.39}$$

The first and the third terms on the RHS describe the ionization by HFCW laser field when the LFFC laser pulse is turned off. They will only give us a two-photon ionization peak in the photoelectron spectrum. We will discuss them in the next subsection. The second term describes the ionization by a HFCW laser field to the continuum which is also dressed by the LFFC laser pulse; therefore, it will give us both the two-photon ionization peak and the side-bands in the photoelectron spectrum. Hence we focus our study on the second term in eq.(7.39). Numerical integration of this equation is straight forward; however, we need to proceed further in order to extract a simple physical picture. Assume the envelope function of the vector potential is given by a square function so that $\mathbf{A}_L(\tau)$ is given by

$$\begin{cases} \mathbf{A}_{L0}\sin(\omega_L(\tau - T_a)), & \text{if } \tau \in \left[T_a - \frac{T_p}{2}, T_a + \frac{T_p}{2}\right] \\ 0, & \text{otherwise} \end{cases} \tag{7.40}$$

and the vector potential of the HFCW laser is given by

$$\mathbf{A}_H(\tau) = \mathbf{A}_{H0}e^{-i\omega_H\tau}. \tag{7.41}$$

When substituting eq.(7.40), (7.41) into eq.(7.39) and completing the integral in the exponent we obtain

$$M_{fi} \approx \langle \mathbf{k}|\psi_u\rangle \int_{T_a - T_p/2}^{T_a+T_p/2} d\tau \exp\left\{ i\left(\frac{\mathbf{k}\cdot\mathbf{A}_{L0}}{\omega_L}\cos(\omega_L\tau) - \frac{U_p}{2\omega_L} sin(2\omega_L\tau)\right)\right\} \times \sin(\frac{\Omega\tau}{2})\mathbf{k}\cdot\mathbf{A}_{H0}e^{i\left(I_u + U_p + \frac{k^2}{2} - \omega_H\right)\tau}, \tag{7.42}$$

where $U_p = \frac{A_{L0}^2}{2}$ is the pondermotive potential. Representing the periodic function as Fourier series we obtain

$$\exp\left\{ i\left(\frac{\mathbf{k}\cdot\mathbf{A}_{L0}}{\omega_L}\cos(\omega_L\tau) - \frac{U_p}{2\omega_L} sin(2\omega_L\tau)\right)\right\} = \sum_n J_n(\zeta, \frac{z}{2})\, e^{in\omega_L\tau}, \tag{7.43}$$

where $z = U_{2p}/\omega_L$, $\zeta = E_2 k_n \cos\theta$, θ is the angle between the laser polarization and the outgoing momentum $\mathbf{k}_n$ of the ionized electron. When substituting eq.(7.43) into eq.(7.42) and evaluating the integral by adding a Gaussian envelope we can obtain the eq.(7.4). The equation clearly shows an oscillation of the side-bands intensity as a function of the time of appearance.

7.3.3 The resonant two-photon ionization

The first and the third terms on the RHS of eq.(7.39) describe the ionization by HFCW laser field when the LFFC laser pulse is turned off. The electron is ionized through absorption of two photons from the HFCW laser field. In order to understand the periodic dependence of the side-bands it is worth to examine the resonant two photon ionization one step further. We start with eq.(7.36) and change the Volkov propagator to a free particle propagator.

$$M_{fi} \approx -i \int_{t'}^{t} d\tau \langle \mathbf{k}|\hat{U}_{free}(t,\tau)V_H(\tau)c_u(\tau)|\psi_u\rangle. \tag{7.44}$$

Use the coordinate representation of the free electron wave function and the time dependent coefficient in eq.(7.31) we can obtain

$$\begin{aligned} M_{fi} \approx & \langle \mathbf{k}|\psi_u\rangle \mathbf{k}\cdot\mathbf{A}_{H0}\left(\frac{1}{2i}\right)\int_{t'}^{t} d\tau e^{i\left[\frac{k^2}{2}+I_u-\omega_H+\frac{\Omega}{2}\right]} \\ & +\langle \mathbf{k}|\psi_u\rangle \mathbf{k}\cdot\mathbf{A}_{H0}\left(\frac{1}{2i}\right)\int_{t'}^{t} d\tau e^{i\left[\frac{k^2}{2}+I_u-\omega_H-\frac{\Omega}{2}\right]}, \end{aligned} \tag{7.45}$$

where the explicit form of the vector potential in eq.(7.41) is also assumed. The time integral in eq.(7.45) will give rise to two delta functions that enforce the conservation of energy.

$$\begin{aligned} M_{fi} \approx & \langle \mathbf{k}|\psi_u\rangle \mathbf{k}\cdot\mathbf{A}_{H0}\left(\frac{1}{2i}\right)\delta(\frac{k_+^2}{2}+I_u-\omega_H-\frac{\Omega}{2}) \\ & +\langle \mathbf{k}|\psi_u\rangle \mathbf{k}\cdot\mathbf{A}_{H0}\left(\frac{1}{2i}\right)\delta(\frac{k_-^2}{2}+I_u-\omega_H+\frac{\Omega}{2}). \end{aligned} \tag{7.46}$$

Assume the Rabi frequency Ω is much less than $\omega_H - I_u$ thus the two photoelectron momentum k_+ and k_- differ only by a small value given by

$$k_+ - k_- \approx \frac{\Omega}{\sqrt{2\Delta}}, \tag{7.47}$$

where $\Delta = \omega_H - I_u$. The result implies that the outgoing electron wavefunction can be described as a superposition of two momentum components with slightly different values. The interference pattern will give rise to beats in the photoelectron flux as shown in the panel (b) of Fig.7.5. This temporal modulation of the outgoing electron flux by Rabi frequency is confirmed by numerical simulation. It is not surprising to see the side-bands amplitude follows the same time variation as the outgoing photoelectron flux. This observation suggests that the continuum-continuum transition only occurs within a very short time window defined by the ionization process.

7.4 3D numerical studies

In this section we perform limited calculations using a 3D time-dependent Schrödinger equation (TDSE) solver for the hydrogen atom to compare with some of the 1D results. Due to the large computational demand of the 3D calculations, we are not able to explore all the parameter space used in the previous section, and we consider only the case of a low intensity LFFC laser pulse in the presence of a HFCW laser.

The total Hamiltonian is now given by

$$\hat{H} = -\frac{1}{2}\nabla^2 - \frac{1}{r} + r\cos\theta E(t), \tag{7.48}$$

where $E(t)$ is the electric field of the two lasers given by eq.(7.2). We assume that both lasers have linear polarization along the z-axis so that θ is the polar angle of the electron coordinate $\mathbf{r}$. The TDSE is solved in spherical coordinates where the angular part of the wavefunction is expanded in the spherical harmonics

$$\Psi(\mathbf{r}, t) = \sum_{l=0}^{L_{max}} R_{l,m}(r) Y_{l,m}(\theta, \phi). \tag{7.49}$$

Since the Hamiltonian commutes with the angular momentum operator $\hat{L}_z$, the quantum number m remains to be a good quantum number during the time propagation. We choose the initial state to be the ground state of a hydrogen atom. The wavefunctions of the hydrogen atom in the absence of the lasers are calculated using the imaginary time propagation method [120], giving ionization energies $I_g = 0.4988$ and $I_u = 0.1250$ for the ground and excited states, respectively. The HFCW laser is on resonance so that $\omega_H = I_g - I_u = 0.3737$. The field strength is $E_1 = 0.003$ which corresponds to the laser intensity 3.16×10^{11} W/cm^2. The central frequency of the LFFC pulse is chosen to be $\omega_L = 0.1$ so that the side-bands are well separated from each other. The LFFC field amplitude is $E_2 = 0.008$ and we use a Gaussian envelope function $\mathfrak{f}(\tau) = e^{-\alpha\tau^2}$ with $\alpha = 6 \times 10^{-5}$ so that the laser pulse contains approximately 5 cycles within the envelope as in the 1D model. The Crank-Nicholson method is used to propagate the wavefunction in time.

We show in Fig. 7.7 the populations for the ground state and the first excited state when only the HFCW laser field is present. The Rabi oscillations can be clearly observed with a period of $T_R = 2820$. When the LFFC laser pulse is applied, side-bands appear whose amplitudes vary as a periodic function of the appearance time T_a (see Fig. 7.8). This observation is consistent with Fig. 7.6 for the 1D case, providing support that the 1D calculations can be used to study at least qualitatively the two-color ionization phenomena.

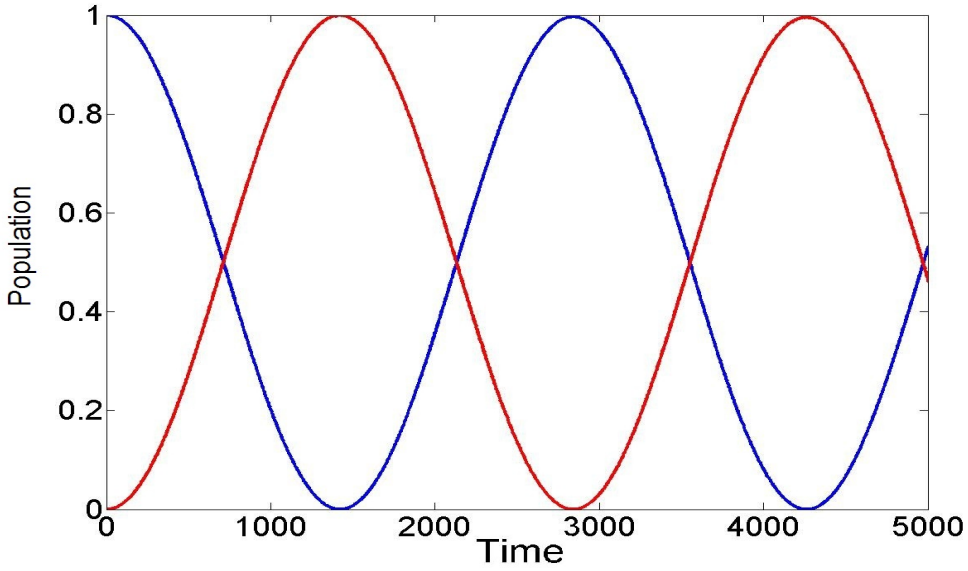

Figure 7.7: The ground state (blue) and the first excited state (red) populations as a function of time.

7.5 Conclusion

We have studied the electron dynamics under few-cycle laser pulse in the presence of a resonant driving frequency for different pulse intensities and appearance times. In this case the electron dynamics can be understood by dividing the time evolution into two regions temporarily. Before ionization the electron is evolved in a two level system coupled by the high frequency laser field. After the ionization the binding potential and the high frequency laser field are neglected so that the electron can be described by a Volkov state. Based on this two-stage model our conclusions can be summarized as the following. For the high laser intensity, the SFI rate is found to be a periodic function of the appearance time T_a. The pulse resets the bound portion of electronic wave function to the ground state and introduces a time shift T_s which is proportional to the pulse length. At low intensity where SFI is completely suppressed, side-bands appear near the TIP. We find that the side-band peak intensity also depends periodically on the pulse appearance time T_a. These findings can be used to characterize the few-cycle pulse as well as controlling the ionization processes.

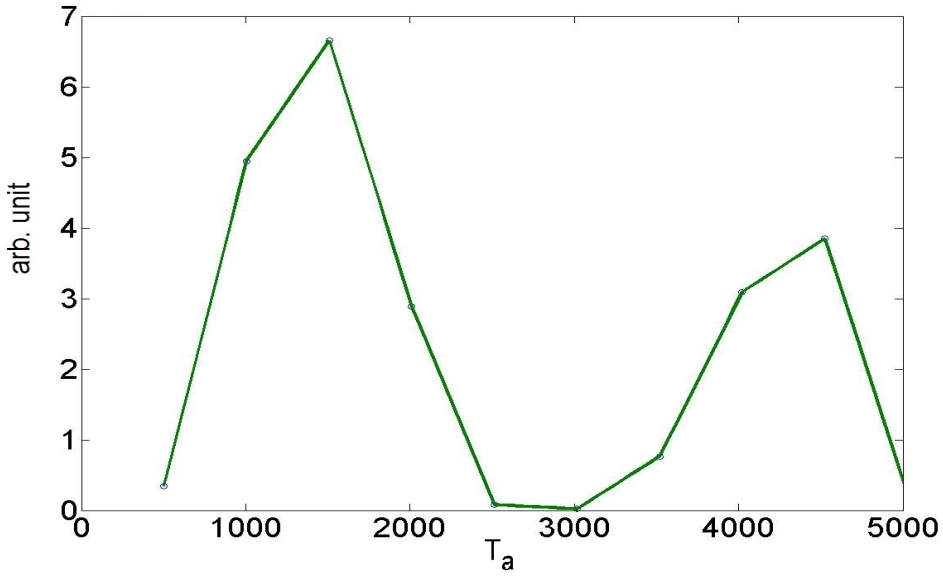

Figure 7.8: The one-photon side-band intensity as a function of appearance time T_a.

Chapter 8

Future works

One of the major role of theory is to interpret the experimental data such that hidden information can be extracted. Up until now the most reliable theoretical method is to start from the first principle, solve the time-dependent Schrödinger equation numerically and obtain the measurable quantities using the electronic wavefunction and quantum mechanical postulates. The drawback of the *ab initio* calculation is that it requires astronomical computational power even for a reasonable small system like water molecule; therefore, its application to larger molecules seems to be improbable.

On the other hand, by combining the quantum chemistry software with the SFA-based theory, ionization of large molecules can be calculated at the cost of a reasonable computational power. This approach will become very useful when the following problems can be solved. (i) The Coulomb-correction problem: It is known that the SFA completely neglected the Coulomb potential when the electron is excited to the continuum. A comparison between the long-range Coulomb interaction case (the hydrogen atom) and the zero-range potential case in Chapter 4 clearly illustrates the effect of long-range Coulomb tail during the ionization dynamics. In the atomic case, the effect of a long-rage Coulomb tail can be added to the theory by using a semi-classical method [27] as described in Chapter 2. The semiclassical Coulomb correction which is proven to be successful in the atomic case should be extended to the molecular case. A crucial step is to implement the matching procedure and obtain a second order classical trajectory for a molecular system that has complex geometry. (ii) Rescattering-related problems: During the ionization process, because of the oscillatory nature of laser fields, a significant fraction of the ionized electron will revisit the parent ion. The theory should include rescattering effects in the transition amplitude. Depending on the laser parameters, three physical processes may occur during the rescattering. First of all the electron may re-collide elastically with the residue ion and

then leave the core region, giving rise to HATI [121]. Secondly, the electron may re-collide inelastically with the residue ion such that excitation or ionization of the second electron can be caused, producing NSDI [122]. Thirdly, the electron may be recaptured by the residue ion through the emission of a high energy photon, generating high harmonic spectra, a topic we cover in this thesis. All of the aforementioned rescattering processes can be described using the SFA and a higher order expansion in the S-matrix formalism. (iii) The excited-state problem: A study of the H_2^+ molecular ion in Chapter 4 suggests that electronic excited states play significant roles in the strong field ionization of molecules especially when the molecule is in a high vibrational state. The theory must include contributions from excited states. This problem can be partially solved by partitioning the Hilbert space into a bound subspace and a continuum subspace as described in Chapter 2. A two-level system or a few-level system can be used to approximate the bound subspace dynamics while the Volkov wavefunction can be used to simulate the electron dynamics in the continuum. The transition amplitude from the bound state to the continuum becomes a superposition of the KFR-type transition amplitudes with time dependent coefficients.

In the near future we would like to tackle the aforementioned problems and generalize the SFI-calculator to molecular cases.

APPENDICES

Appendix A

Green's Functions and time evolution operators

We can express the total wave function $|\Psi(t)\rangle$ in terms of the unperturbed wave function $|\Phi(t)\rangle$ using the Green's function (GF) technique [16]. The full GF is defined by

$$\left[i\partial_t - \hat{H}(t)\right] \hat{G}(t,t') = \delta(t-t'). \tag{A.1}$$

Similarly, the GF for the unperturbed Hamiltonian is defined by

$$\left[i\partial_t - \hat{H}_0(t)\right] \hat{G}_0(t,t') = \delta(t-t'). \tag{A.2}$$

$|\Psi(t)\rangle$ can then be related to $|\Phi(t)\rangle$ by the Lippmann-Schwinger equations [16] by writing the Schrödinger equation (2.2) as

$$\left[i\partial_t - \hat{H}_0(t)\right] |\Psi(t)\rangle = \hat{V}(t)\, |\Psi(t)\rangle. \tag{A.3}$$

Using the unperturbed GF eq.(A.2) and treating the RHS of eq.(A.3) as an inhomogeneous term, a particular solution is given by

$$\int_{-\infty}^{\infty} d\tau\, \hat{G}_0(t,\tau)\hat{V}(\tau)|\Psi(\tau)\rangle. \tag{A.4}$$

We now impose the requirement of causality that

$$\hat{G}(t,t') = 0, \quad \hat{G}_0(t,t') = 0 \qquad \text{when } t < t'. \tag{A.5}$$

(such GFs are called retarded Green's functions [123]). Adding the homogeneous solution $\Phi(t)$ to the particular solution eq.(A.4), we obtain the general solution to eq.(A.3), which is the first Lippmann-Schwinger equation after imposing the causality requirement of eq.(A.5):

$$|\Psi(t)\rangle = |\Phi(t)\rangle + \int_{-\infty}^{t} d\tau\ \hat{G}_0(t,\tau)\hat{V}(\tau)|\Psi(\tau)\rangle, \tag{A.6}$$

The usual perturbation expansion of $|\Psi(t)\rangle$ is obtained by iterating eq.(A.6).

A second Lippmann-Schwinger equation for $|\Psi(t)\rangle$ can be obtained by writing eq.(2.4) as

$$\left[i\partial_t - \hat{H}(t)\right]|\Phi(t)\rangle = -\hat{V}(t)\ |\Phi(t)\rangle. \tag{A.7}$$

Again, treating the RHS of eq.(A.7) as an inhomogeneous term and using the full GF eq.(A.1) we find the general solution to eq.(A.7) to be

$$|\Phi(t)\rangle = |\Psi(t)\rangle - \int_{-\infty}^{\infty} d\tau\ \hat{G}(t,\tau)\hat{V}(\tau)|\Phi(\tau)\rangle, \tag{A.8}$$

where now $\Psi(t)$ is the homogeneous solution to eq.(A.7). Rearranging this equation and imposing the causality requirement of eq.(A.5), we obtain the second Lippmann-Schwinger equation:

$$|\Psi(t)\rangle = |\Phi(t)\rangle + \int_{-\infty}^{t} d\tau\ \hat{G}(t,\tau)\hat{V}(\tau)|\Phi(\tau)\rangle. \tag{A.9}$$

The GFs $\hat{G}(t,t')$ and $\hat{G}_0(t,t')$ are related by the Dyson equations [16]

$$\hat{G}(t,t') = \hat{G}_0(t,t') + \int_{t'}^{t} d\tau\ \hat{G}_0(t,\tau)\hat{V}(\tau)\hat{G}(\tau,t') \tag{A.10}$$

$$\hat{G}(t,t') = \hat{G}_0(t,t') + \int_{t'}^{t} d\tau\ \hat{G}(t,\tau)\hat{V}(\tau)\hat{G}_0(\tau,t'), \tag{A.11}$$

The first Dyson equation (A.10) can be obtained by letting

$$\hat{G}(t,t') = \hat{G}_0(t,t') + \delta\hat{G}(t,t') \tag{A.12}$$

and substituting $\hat{G}_0 = \hat{G} - \delta\hat{G}$ into eq.(A.2):

$$\left[i\partial_t - \hat{H}_0(t)\right] \delta\hat{G}(t,t') = \hat{V}(t)\ \hat{G}(t,t'), \tag{A.13}$$

Treating the RHS of eq.(A.13) as an inhomogeneous term and using the unperturbed GF eq.(A.2), we find

$$\delta\hat{G}(t,t') = \int_{-\infty}^{\infty} d\tau\ \hat{G}_0(t,\tau)\hat{V}(\tau)\hat{G}(t,t'). \tag{A.14}$$

Eq.(A.12) and the causality requirement eq.(A.5) give the first Dyson equation (A.10). The second Dyson equation (A.11) can be similarly obtained by substituting eq.(A.12) into eq.(A.1):

$$\left[i\partial_t - \hat{H}(t)\right] \delta\hat{G}(t,t') = \hat{V}(t)\ \hat{G}_0(t,t'). \tag{A.15}$$

whose solution is obtained using the full GF eq.(A.1)

$$\delta\hat{G}(t,t') = \int_{-\infty}^{\infty} d\tau\ \hat{G}(t,\tau)\hat{V}(\tau)\hat{G}_0(t,t'). \tag{A.16}$$

Applying the causality requirement eq.(A.5) then gives the second Dyson equation (A.11). Eq.(A.10) or (A.11) can be substituted into eq.(A.9) to develop appropriate expansion of the total wave function. This is the approach of Becker and Faisal [16].

The GFs defined above are closely related to the evolution operators used by Milosevic, et al. [17] We first obtain the initial conditions for the GFs by integrating eqs.(A.1) and (A.2) across the discontinuity:

$$i\hat{G}(t^+,t) = 1, \quad i\hat{G}_0(t^+,t) = 1. \tag{A.17}$$

Along with the causality requirement, we can define operators $\hat{U}(t,t')$ and $\hat{U}_0(t,t')$ by [123]

$$\hat{G}(t,t') = -i\theta(t-t')\hat{U}(t,t'), \quad \hat{G}_0(t,t') = -i\theta(t-t')\hat{U}_0(t,t'), \tag{A.18}$$

where $\theta(t-t')$ is the Heaviside step function, and $\hat{U}(t,t')$, $\hat{U}_0(t,t')$ are continuous at $t=t'$. Substituting eq.(A.18) into eqs.(A.1), (A.2) and (A.17) gives the equations of motion and initial conditions (2.5) and (2.6) for these operators. Using eq.(A.18), the Dyson equations for the evolution operators (2.9) and (2.10) can be obtained directly from those for the

GF, eqs.(A.10) and (A.11).

Note that while it is permissible from eq.(A.18) to use the retarded GF as propagator $|\Psi(t)\rangle = i\hat{G}(t,t')|\Psi(t')\rangle$, this is only valid for $t > t'$, while the evolution operator $\hat{U}(t,t')$ can propagate the wavefunction both forward and backward in time. (For $t < t'$, $\hat{U}(t,t')$ is related to the advanced Green's function [123]. We will not be concerned with the advanced Green's function here.)

Using the Lippmann-Schwinger equation (A.9) for the total wave function and the orthogonality of the initial and final states, the transition amplitude eq.(2.13) can also be written as

$$M_{fi} = \lim_{t\to\infty} \int_{-\infty}^{t} d\tau \ \langle \Phi_f(t)|\hat{G}(t,\tau)\hat{V}_L(\tau)|\Phi_i(\tau)\rangle, \tag{A.19}$$

which, of course, is the same as eq.(2.14) in light of eq.(A.18).

Appendix B

Transition Rate

We first give an heuristic derivation of the ionization rate eq.(2.33) from the transition amplitude eq.(2.30) [124, 125, 62]. The rate of ionization can be defined by

$$\Gamma_{fi} = \lim_{t\to\infty} \frac{1}{t} |M_{fi}|^2 = \lim_{t\to\infty} \frac{(2\pi)^2}{t} \sum_{n,n'} L_n(\mathbf{k})\, L_{n'}(\mathbf{k})\, \delta\left(E_{ATI} - n\omega\right) \delta\left(E_{ATI} - n'\omega\right) \quad \text{(B.1)}$$

where $E_{ATI} = \frac{k^2}{2} + U_p + I_p$. The first delta function allows one to replace E_{ATI} by $n\omega$, and using the Fourier representation of the second delta function

$$\delta\left(E_{ATI} - n'\omega\right) = \delta\left[(n-n')\omega\right] = \lim_{t\to\infty} \frac{1}{2\pi} \int_{-t/2}^{t/2} d\tau e^{i(n-n')\omega\tau} = \begin{cases} 0, & n \neq n' \\ \frac{t}{2\pi}, & n = n' \end{cases}, \quad \text{(B.2)}$$

we obtain

$$\Gamma_{fi} = 2\pi \sum_{n} \delta\left(E_{ATI} - n\omega\right) |L_n(\mathbf{k})|^2, \quad \text{(B.3)}$$

which is eq.(2.33).

A rigorous derivation of the transition rate of the form of eq.(B.3) in time-independent collision theory is given by Goldberger and Watson [126]. For our time-dependent case, we can similarly defining the transition rate at time t by

$$\Gamma_{fi}(t) = \frac{d}{dt}|m_{fi}(t)|^2 = m_{fi}(t)\frac{d}{dt}m^*_{fi}(t) + c.c., \quad \text{(B.4)}$$

where similar to the derivation of eq.(2.23), $m_{fi}(t)$ is the transition amplitude at time t:

$$m_{fi}(t) = -i \int_{-\infty}^{t} dt' \; e^{iS_p(t')} \; \langle \mathbf{k} + \mathbf{A}(t') \, | \mathbf{r} \cdot \mathbf{E}(t') | \, \psi_i \rangle \; . \tag{B.5}$$

Eq.(2.28) can be used to express the integrand of eq.(B.5) as

$$e^{iS_p(t')} \; \langle \mathbf{k} + \mathbf{A}(t') \, | \mathbf{r} \cdot \mathbf{E}(t') | \, \psi_i \rangle \; = e^{iE_{ATI}t'} \sum_n L_n(\mathbf{k}) \; e^{-in\omega t'}, \tag{B.6}$$

so that the transition rate eq.(B.4) becomes

$$\begin{aligned} \Gamma_{fi}(t) &= \int_{-\infty}^{t} dt' \; e^{iS_p(t')} \; \langle \mathbf{k} + \mathbf{A}(t') \, | \mathbf{r} \cdot \mathbf{E}(t') | \, \psi_i \rangle \; e^{-iS_p(t)} \; \langle \psi_i \, | \mathbf{r} \cdot \mathbf{E}(t) | \, \mathbf{k} + \mathbf{A}(t) \rangle + c.c. \\ &= \sum_{n,n'} L_n(\mathbf{k}) L^*_{n'}(\mathbf{k}) e^{i(n-n')\omega t} \int_0^{\infty} d\tau \; e^{-i(E_{ATI} - n\omega)\tau} + c.c. \end{aligned} \tag{B.7}$$

where $\tau = t - t'$ in the last step. As $t \to \infty$, terms with $n \neq n'$ oscillate rapidly and interfere destructively so that only the $n = n'$ terms survive. Evaluating the integral over τ and introducing the factor $\epsilon \to 0^+$ to ensure the convergence of the integral in eq.(B.7), we obtain the transition rate

$$\begin{aligned} \Gamma_{fi} &= \sum_n |L_n(\mathbf{k})|^2 \left[\frac{-i}{E_{ATI} - n\omega - i\epsilon} + \frac{i}{E_{ATI} - n\omega + i\epsilon} \right] \\ &= 2\pi \sum_n \delta \left(E_{ATI} - n\omega \right) |L_n(\mathbf{k})|^2 \end{aligned} \tag{B.8}$$

which is eq.(B.3).

Appendix C

Tunneling ionization picture

In this appendix, we consider the ionization rate for the bound state of an atom with zero-range potential of eq.(4.1) in the presence of a static electric field E_0. While the rate can be obtained as a special case of the general formula of eq.(4) of PPT [26], it is instructive to present a derivation following the exposition of Bisgaard and Madsen [127]. Assuming the external electric field is along the z-direction, the interaction energy eq.(7.7) is simply $V_L = E_0 z$, and the time-independent Schrödinger equation is

$$\left[-\frac{1}{2}\nabla^2 + V_a + V_L\right]\psi(\mathbf{r}) = -\frac{1}{2}\kappa^2\psi(\mathbf{r}), \tag{C.1}$$

where $-\frac{1}{2}\kappa^2$ is the energy eigenvalue of the bound state wave function eq.(4.2) in the *absence* of the external field. Eq.(C.1) is separable in the parabolic coordinates [57, 127]

$$\xi = r + z, \quad \eta = r - z, \quad \phi = \tan^{-1}\left(\frac{y}{x}\right). \tag{C.2}$$

Symmetry of the initial bound state wave function eq.(4.2) suggests that the wave function $\psi(\mathbf{r})$ should have cylindrical symmetry and independent of the azimuthal angle ϕ so that $\psi(\mathbf{r})$ is independent of ϕ. Thus we assume

$$\psi(\mathbf{r}) = \frac{1}{\sqrt{2\pi\xi\eta}} f_1(\xi) f_2(\eta). \tag{C.3}$$

For $r > 0$, $V_a = 0$ and $V_L = \frac{1}{2}E_0(\xi - \eta)$. Substituting eq.(C.3) into eq.(C.1) and expressing the Laplacian in terms of the parabolic coordinates yield [57, 127]

$$-\frac{1}{2}\chi_1'' + U_1(\xi)\chi_1(\xi) = -\frac{\kappa^2}{8}\chi_1(\xi), \tag{C.4}$$

$$-\frac{1}{2}\chi_2'' + U_2(\eta)\chi_2(\eta) = -\frac{\kappa^2}{8}\chi_2(\eta), \tag{C.5}$$

where $\chi_1(\xi) = \sqrt{\xi}f_1(\xi)$, $\chi_2(\eta) = \sqrt{\eta}f_2(\eta)$, β is the separation constant, and the effective potentials are given by

$$U_1(\xi) = -\frac{1}{8\xi^2} + \frac{E_0}{8}\xi - \frac{\beta}{2\xi}, \tag{C.6}$$

$$U_2(\eta) = -\frac{1}{8\eta^2} - \frac{E_0}{8}\eta + \frac{\beta}{2\eta}. \tag{C.7}$$

Tunneling occurs at large negative z close to the z-axis where $\xi \simeq 0$ and $\eta \simeq -2z \gg 1$. The ionization can be calculated from the flux of the probability current density through a surface S perpendicular to the negative z-direction [57, 127]:

$$w_{stat} = -\int_S j_z dS = \int_0^\infty d\xi \, \frac{|\chi_1(\xi)|^2}{\xi} \, \mathrm{Im}\, \chi_2^*(\eta)\chi_2'(\eta), \tag{C.8}$$

where the current density $j_z = \mathrm{Re}\,(\psi * \frac{1}{i}\frac{\partial\psi}{\partial z})$ and $dS = \rho d\rho d\phi \simeq \frac{1}{2}\eta d\xi d\phi$. For $\xi \simeq 0$, the term $E_0\xi$ in U_2 of eq.(C.7) can be neglected, and eq.(C.4) has the approximate solution

$$\chi_1(\xi) \simeq \xi^{\frac{1}{2}} \exp\left(-\frac{1}{2}\kappa\xi\right) \qquad \text{with} \qquad \beta = \frac{\kappa}{2}. \tag{C.9}$$

The ionization rate (C.8) then becomes

$$w_{stat} = \frac{1}{\kappa}\mathrm{Im}\, \chi_2^*(\eta)\chi_2'(\eta), \qquad \eta \gg 1. \tag{C.10}$$

To find $\chi_2(\eta)$ at large η, we find appropriate solutions to eq.(C.5) by the WKB method [57]. The classical turning points for U_2 are determined from solving $U_2(\eta) = -\kappa^2/8$, yielding the inner and outer turning points $\eta_1 = 2/\kappa$ and $\eta_0 = \kappa^2/E_0$, respectively. The JWKB wave function is then given by

$$\chi_2(\eta) = \begin{cases} \frac{C}{\sqrt{|p|}} \exp(-\int_{\eta_0}^{\eta} |p| d\eta), & \eta_1 < \eta < \eta_0 \\ \\ \frac{C}{\sqrt{p}} \exp(i\int_{\eta_0}^{\eta} p d\eta + i\frac{\pi}{4}), & \eta > \eta_0 \end{cases}, \tag{C.11}$$

where $\frac{p^2}{2} = -\frac{\kappa^2}{8} - U_2(\eta)$ and C is a normalization constant to be determined. Thus at large $\eta > \eta_0$, eq.(C.11) gives $\chi_2^*(\eta)\chi_2'(\eta) = i|C|^2$ so that

$$w_{stat} = \frac{|C|^2}{\kappa}. \tag{C.12}$$

To determine the normalization C, we shall compare the wave function eq.(C.3) in the tunneling region $\eta_1 < \eta < \eta_0$ where V_L becomes negligible with the bound state wave function eq.(4.2). In this region, $|p(\eta)|$ can be approximated by

$$|p(\eta)| = \left[2\left(\frac{\kappa^2}{8} - \frac{1}{8\eta^2} - \frac{E_0}{8}\eta + \frac{\kappa}{4\eta}\right)\right]^{\frac{1}{2}} \simeq \frac{\kappa}{2}\left(1 - \frac{E_0\eta}{\kappa^2}\right)^{\frac{1}{2}} + \frac{1}{2\eta}\left(1 - \frac{E_0\eta}{\kappa^2}\right)^{-\frac{1}{2}}, \tag{C.13}$$

and we obtain [127]

$$\int_{\eta_0}^{\eta} |p| d\eta \simeq -\frac{\kappa^3}{3E_0} + \frac{\kappa\eta}{2} - \ln\left(\frac{\eta E_0}{4\kappa^2}\right)^{-\frac{1}{2}}. \tag{C.14}$$

Thus

$$\chi_2(\eta) = C\sqrt{\frac{2}{\kappa}}\left(\frac{\eta E_0}{4\kappa^2}\right)^{-1/2} \exp\left(-\frac{\kappa\eta}{2}\right) \exp\left(\frac{\kappa^3}{3E_0}\right), \tag{C.15}$$

where it suffices to use $|p(\eta)| \simeq \kappa/2$ for the pre-exponential factor. Substituting eqs.(C.9) and (C.15) into eq.(C.3) gives the wave function

$$\psi(\mathbf{r}) = \frac{2C}{\eta}\sqrt{\frac{\kappa}{\pi E_0}} \exp\left(-\frac{\kappa}{2}(\eta + \xi)\right) \exp\left(\frac{\kappa^3}{3E_0}\right). \tag{C.16}$$

Comparing the WKB wave function (C.16) with the bound state wave function (4.2) and noting that $\eta + \xi = r$, and $\eta \simeq 2r$ at large r and close to the negative z-axis, we obtain $C = \sqrt{\frac{E_0}{2}}\, e^{-\kappa^3/3E_0}$. From eq.(C.12) we obtain finally

$$w_{stat} = \frac{E_0}{2\kappa}\, e^{-2\kappa^3/3E_0}. \tag{C.17}$$

Appendix D

Analytical expression of L_n

For low frequency and high intensity laser excitation, the integrand of the transition amplitude $L_n(\mathbf{k})$ eq.(2.31) or eq.(2.32) contains a rapidly oscillating function $e^{iS_p(t)}$ (see eq.(2.27)), and the integral can be evaluated by the saddle-point method [67]. The effect of the core potential $\hat{V}_a$ enters only through the momentum representation of the initial wave function in the SFA, and will be shown below to contribute only to the pre-exponential factor of the final result. It is convenient to define $\tau = \omega t$ so that in general $L_n(\mathbf{k})$ of eq.(2.31) or eq.(2.32) can be expressed as

$$L_n(\mathbf{k}) = \int_0^{2\pi} d\tau \, \frac{G(\tau) e^{iS_p(\tau)}}{[S_p'(\tau)]^\nu}, \tag{D.1}$$

where $S_p' = dS_p/d\tau$, G is a function analytic at the saddle points τ_i given by $S_p'(\tau_i) = 0$, and the parameter $\nu \geq 0$. The possible appearance of a pole at the zeros of S_p' of the integrand, as pointed out by Keldysh [15], is related to the scattering amplitude having poles at the bound state energies. For the zero-range potential considered in Chapter 4, $\langle \mathbf{k} + \mathbf{A}(t) | \phi_i \rangle \propto 1/S_p'$ in eq.(2.32) so that $\nu = 0$, while for the Coulomb potential $\langle \mathbf{k} + \mathbf{A}(t) | \phi_i \rangle \propto (1/S_p')^2$ for which $\nu = 1$.

From eq.(2.27) and taking advantage of the delta function in eq.(2.30),

$$S_p(\tau) = n\tau + \left(\frac{kE_0 \cos\theta}{\omega^2} \cos\tau - \frac{U_p}{\omega} \sin\tau \cos\tau \right) \tag{D.2}$$

which is a rapidly oscillating function of τ. Major contributions to the integral in eq.(D.1) come from the saddle points which are the roots of $S_p'(\tau_i) = 0$ where τ_i are complex in

general, and eq.(D.1) can be evaluated by the method of steepest descents. For the simple case $\nu = 0$, eq.(D.1) is given asymptotically by the well-known result [67]

$$L_n(\mathbf{k}) \sim \sum_i \left[\frac{2\pi}{iS_p''(\tau_i)}\right]^{\frac{1}{2}} iG(\tau_i)\, e^{iS_p(\tau_i)}, \tag{D.3}$$

where the integration path is deformed from the real τ-axis of eq.(D.1) to the path of steepest descent passing through τ_i in the direction $\theta_i = -\frac{\alpha_i}{2} + \frac{\pi}{2}$ in the complex τ-plane where $0 \leq \alpha < 2\pi$ is the argument of $[iS_p''(\tau_i)]$. For $\nu > 0$, the asymptotic evaluation of the integral is more complicated [67, 69, 54], and we have discussed this case in Chapter 3. In general, eq.(D.1) is given asymptotically by

$$L_n(\mathbf{k}) \sim \sum_i \mathfrak{P}_i\, e^{iS_p(\tau_i)}, \tag{D.4}$$

where the pre-exponential factor $\mathfrak{P}_i$ is proportional to $[S_p''(\tau_i)]^{-\frac{\nu+1}{2}}$. Hence we require the first and second derivative of $S(\tau)$ in the asymptotic evaluation of $L_n(\mathbf{k})$.

While the general case of a complex atom has been discussed by PPT [26] and others [54], to understand the procedure leading to the adiabatic limit of the ionization rate, it suffices to consider the simple case of an s-state initial wave function, where the pre-exponential factor of $L_n(\mathbf{k})$ is independent of θ. Substituting eq.(D.4) into eqs.(2.34) and (2.35) gives the asymptotic total ionization rate

$$\Gamma_T \simeq \sum_{n \geq n_0}^{\infty} \frac{k_n}{2\pi} \int_{-1}^{1} d\cos\theta \left| \sum_i \mathfrak{P}_i\, e^{iS_p(\tau_i)} \right|^2. \tag{D.5}$$

The derivative of $S(\tau)$ can be read off from the integrand of eq.(2.20), and from eq.(2.24) we obtain

$$S_p'(\tau) = \frac{1}{2\omega}\left(\mathbf{k} - \frac{\mathbf{E}_0}{\omega}\sin\tau\right)^2 + \frac{I_p}{\omega} = 2z\sin^2\tau - k\sqrt{\frac{4z}{\omega}}\cos\theta\sin\tau + \left(\frac{k^2}{2\omega} + 2z\gamma\right) \tag{D.6}$$

where $z = \dfrac{U_p}{\omega} = \dfrac{E_0^2}{4\omega^3}$ is the intensity parameter of Reiss [20], and γ is the Keldysh parameter of eq.(2.1) which can also expressed as $\gamma = \sqrt{\dfrac{I_p}{2U_p}}$. The second derivative of the combined action is

$$S_p''(\tau) = 4z\sin\tau\cos\tau - k\sqrt{\frac{4z}{\omega}}\cos\theta\sin\tau. \tag{D.7}$$

Setting $S_p'(\tau)$ in eq.(D.6) to zero yields the complex saddle points $\tau_\pm$

$$\sin\tau_\pm = \frac{k\cos\theta}{\sqrt{4\omega z}} \pm i\left(\gamma^2 + \frac{k^2\sin^2\theta}{4\omega z}\right)^{1/2},$$
$$\cos\tau_\pm = -i(\sin^2\tau_\pm - 1)^{1/2} \tag{D.8}$$

where $\cos\tau_\pm$ has a branch cut along $-1 \le \sin\tau_\pm \le 1$ on the real axis. Thus, $\sin\tau_- = [\sin\tau_+]^*$, $\cos\tau_- = -[\cos\tau_+]^*$, $\mathrm{Im}\tau_- = \mathrm{Im}\ \tau_+$ and $\mathrm{Re}\ \tau_- = \pi - \mathrm{Re}\ \tau_+$. Here we consider only the roots with $\mathrm{Im}\ \tau_i > 0$, as roots with $\mathrm{Im}\ \tau_i < 0$ will give unphysical solutions which become exponentially large [128].

Eq.(2.27) expressed as a function of τ indicates that for low frequency excitation, photoelectrons with large kinetic energy will appear in the spectrum with exponentially small probability so that it is reasonable [15, 26] to make the low photoelectron energy approximation (LPEA) and expand to second order in k

$$\sin\tau_\pm \simeq \pm i\gamma\left(1 + \frac{k^2\sin^2\theta}{8\omega z\gamma^2}\right) + \frac{k\cos\theta}{\sqrt{4\omega z}}. \tag{D.9}$$

This expansion for $\sin\tau_+$ has been given by Mishima, et al. [85] who attempted to evaluate the integral for $L_n(\mathbf{k})$ by the residue theorem. Unfortunately, their procedure was shown to be invalid [56]; nevertheless their papers [85, 129] provide many useful results in the study of the Keldysh theory. From eq.(D.9), we obtain

$$\begin{aligned}
\tau_+ &= i\ \mathrm{arcsinh}\ \gamma + \frac{k\cos\theta}{2\sqrt{\omega z\,(1+\gamma^2)}} + \frac{ik^2\left[\gamma + \frac{\sin^2\theta}{\gamma}\right]}{8\omega z\,(1+\gamma^2)^{3/2}},\\
\tau_- &= \pi + i\ \mathrm{arcsinh}\ \gamma - \frac{k\cos\theta}{2\sqrt{\omega z\,(1+\gamma^2)}} + \frac{ik^2\left[\gamma + \frac{\sin^2\theta}{\gamma}\right]}{8\omega z\,(1+\gamma^2)^{3/2}}.
\end{aligned} \tag{D.10}$$

Note that the inverse hyperbolic function can also be written as [29]

$$\mathrm{arcsinh}\ \gamma = \ln(\gamma + \sqrt{1+\gamma^2}). \tag{D.11}$$

From eq.(D.10), we obtain

$$\cos\tau_\pm \simeq \pm\sqrt{1+\gamma^2} - \frac{i\gamma k\cos\theta}{2\sqrt{\omega z(1+\gamma^2)}} \pm \frac{k^2[(1+\gamma^2)\sin^2\theta - \cos^2\theta]}{8\omega z\,(1+\gamma^2)^{3/2}}. \tag{D.12}$$

Substituting eq.(D.12) into eq.(D.2) results in

$$S_p(\tau_+) \simeq iR + 2\sqrt{\frac{z\,(1+\gamma^2)}{\omega}}k\cos\theta - \frac{ik^2\gamma\cos^2\theta}{2\omega\sqrt{1+\gamma^2}} \tag{D.13}$$

$$S_p(\tau_-) \simeq n\pi + iR - 2\sqrt{\frac{z\,(1+\gamma^2)}{\omega}}\,k\cos\theta - \frac{ik^2\gamma\cos^2\theta}{2\omega\sqrt{1+\gamma^2}}, \tag{D.14}$$

where $R = \Big[n\,\text{arcsinh}\,\gamma - z\gamma\sqrt{1+\gamma^2}\Big]$. Since $S_p''(\tau_i)$ appears only in the pre-exponential factor in eq.(D.4), it suffices to retain the lowest order $k=0$ terms in eqs.(D.9) and (D.12) so that

$$S_p''(\tau_\pm) \simeq 4iz\gamma\sqrt{1+\gamma^2}. \tag{D.15}$$

Thus $S_p''(\tau_+) = S_p''(\tau_-)$ and hence $\mathfrak{P}_+ = \mathfrak{P}_-$. Defining $\mathfrak{K} = |\mathfrak{P}_\pm|^2$, eq.(D.4) gives

$$\begin{aligned} |L_n(\mathbf{k})|^2 &\simeq \mathfrak{K}|e^{iS_p(\tau_+)} + e^{iS_p(\tau_-)}|^2 \\ &= 2\mathfrak{K}\left[1 + (-1)^n\cos\left(4k\cos\theta\sqrt{\frac{z(1+\gamma^2)}{\omega}}\,\right)\right] e^{-2R + \frac{k^2\gamma\cos^2\theta}{\omega\sqrt{1+\gamma^2}}}, \end{aligned} \tag{D.16}$$

which can be compared with eq.(53) of PPT [26] if we take advantage of the delta function in eq.(2.30) and replace n in the exponential factor by

$$n = \frac{1}{\omega}\left(U_p + I_p + \frac{k^2}{2}\right) = z + 2z\gamma^2 + \frac{k^2}{2\omega}. \tag{D.17}$$

Substituting eq.(D.16) into eq.(D.5) gives the total ionization rate

$$\Gamma_T \simeq \mathfrak{K}e^{-2\left[n_0\,\text{arcsinh}\,\gamma - z\gamma\sqrt{1+\gamma^2}\,\right]}\sum_{n\geq n_0}^{\infty} k_n\, e^{-2(n-n_0)\text{arcsinh}\,\gamma}\int_{-1}^{1}\frac{d\cos\theta}{\pi}\, e^{\frac{k_n^2\gamma\cos^2\theta}{\omega\sqrt{1+\gamma^2}}}, \tag{D.18}$$

where we neglect the cosine term in eq.(D.16) (the low photoelectron energy approximation neglecting interference LPEANI) since the sum over this term in the strong field limit is expected to average to zero [26], and we separate out the term $(2n_0\ \text{arcsinh}\ \gamma)$ in the exponent for convenience. Defining $\xi = 2(\text{arcsinh}\ \gamma - \frac{\gamma}{\sqrt{1+\gamma^2}})$, $\beta = \frac{2\gamma}{\sqrt{1+\gamma^2}}$, noting $k_n^2 = 2\omega(n-n_0)$, and making the substitution $y = \sqrt{\beta(n-n_0)}\cos\theta$, this expression is often written in term of the Dawson integral [130] as

$$\Gamma_T = \mathfrak{K}e^{-2\left[n_0\,\text{arcsinh}\,\gamma - z\gamma\sqrt{1+\gamma^2}\,\right]}\sqrt{\frac{2\omega}{\beta}}\,\frac{2}{\pi}\,S(\gamma, n_0), \tag{D.19}$$

where $S(\gamma, n_0) = \sum_{n \geq n_0}^{\infty} e^{-\xi(n-n_0)} w_0(\sqrt{\beta(n-n_0)}\ )$ is the function defined in eq.(18) of Keldysh [15], and $w_0(x) = e^{-x^2} \int_0^x e^{y^2}\, dy$ is a special case of eq.(56) of PPT [26] with $m = 0$.

We now study the *adiabatic limit* of the ionization rate when $\gamma \ll 1$. In this case, many terms contribute to the sum over n in eq.(D.18), and we may replace the sum by an integral over $x = n - n_0$ so that $k_n^2 = 2\omega x$. Interchanging the order of integration of x and $\cos\theta$, we find that

$$\begin{aligned} &\sum_{n \geq n_0}^{\infty} k_n e^{-2z(n-n_0)\mathrm{arcsinh}\gamma} \int_{-1}^{1} \frac{d\cos\theta}{\pi} e^{\frac{k_n^2 \gamma \cos^2\theta}{\omega\sqrt{1+\gamma^2}}} \\ &\simeq \int_{-1}^{1} \frac{d\cos\theta}{\pi} \int_0^{\infty} dx\ \sqrt{2\omega x}\ e^{-2x\left(\mathrm{arcsinh}\ \gamma - \frac{\gamma\cos^2\theta}{\sqrt{1+\gamma^2}}\right)} \\ &\simeq \frac{1}{2\gamma^2}\sqrt{\frac{3\omega}{\pi\gamma}}\,, \end{aligned} \tag{D.20}$$

where we have used the approximation [26]

$$\mathrm{arcsinh}\ \gamma - \frac{\gamma}{\sqrt{1+\gamma^2}} = \frac{1}{3}\gamma^3 + \mathcal{O}(\gamma^7). \tag{D.21}$$

Furthermore, setting $k = 0$ in eq.(D.17) gives $n_0 = z(1 + 2\gamma^2)$, and the first exponential factor in eq.(D.18) can be simplified by [26]

$$(1+2\gamma^2)\mathrm{arcsinh}\ \gamma - \gamma\sqrt{1+\gamma^2} \simeq \frac{4}{3}\gamma^3\left(1 - \frac{\gamma^2}{10}\right) + \mathcal{O}(\gamma^6). \tag{D.22}$$

Hence the total ionization rate eq.(D.18) reduces to $\Gamma_T \simeq \Gamma_{ad}$ where

$$\Gamma_{ad} = \mathfrak{K}\frac{1}{2\gamma^2}\sqrt{\frac{3\omega}{\pi\gamma}}\ \exp\left\{-\frac{8z}{3}\gamma^3\left(1 - \frac{\gamma^2}{10}\right)\right\}. \tag{D.23}$$

Identifying $8z\gamma^3 = \dfrac{2(2I_p)^{3/2}}{E_0}$, eq.(D.23) to lowest order in γ shows the well-known exponential dependence on the ionization potential and the electric field of the static field ionization rate [57] of eq.(2.36).

References

[1] Thomson, J. J. *Philosophical Magazine* **44**, 293 (1987). 1

[2] Maiman, T. H. *Nature* **187**, 4736 (1960). 1

[3] Franken, P. A., Hill, A. E., Peters, C. W., and Weinreich, G. *Phys. Rev. Lett.* **7**, 118 (1961). 2

[4] Harris, S. E., Oshman, M. K., and Byer, R. L. *Phys. Rev. Lett.* **18**, 732 (1967). 2

[5] Ou, Z. Y., Pereira, S. F., Polzik, E. S., and Kimble, H. J. *Opt. Lett.* **17**, 640 (1992). 2

[6] Kaiser, W. and Garrett, C. *Phys. Rev. Lett.* **7**, 229 (1961). 2

[7] Lallemand, P. and Bloembergen, N. *Phys. Rev. Lett.* **15**, 1010 (1965). 3

[8] Spence, D. E., Kean, P. N., and Sibbett, W. *Opt. Lett.* **16**, 42 (1991). 3

[9] Chin, S. L. *Femtosecond laser filamentation.* Spinger series on atomic, optical and plasma physics, USA, (2010). 3

[10] Gibbs, H. M., Hopf, F. A., Kaplan, D. L., and Shoemaker, R. L. *Phys. Rev. Lett.* **46**, 474 (1981). 3

[11] Armstrong, J. A., Bloembergen, N., Ducuing, J., and Pershan, P. S. *Phys. Rev.* **127**, 1918 (1962). 3

[12] Paulus, G. G., Nicklich, W., Xu, H., Lambropoulos, P., and Walther, H. *Phys. Rev. Lett.* **72**, 2851 (1994). 3

[13] Gordon, W. *Z. Phys.* **40**, 117 (1926). 3

[14] Volkov, D. M. *Z. Phys.* **94**, 250 (1935). 3

[15] Keldysh, L. V. *Sov. Phys. JETP* **20**, 1307 (1965). 4, 6, 7, 10, 14, 21, 45, 57, 63, 94, 115, 117, 119

[16] Becker, A. and Faisal, F. H. M. *J. Phys. B: At. Mol. Opt. Phys.* **38**, R1 (2005). 6, 8, 10, 13, 14, 63, 106, 107, 108

[17] Milosevic, D. B., Paulus, G. G., Bauer, D., and Becker, W. *J. Phys. B: At. Mol. Opt. Phys.* **39**, R203 (2006). 6, 8, 9, 14, 63, 108

[18] Faisal, F. H. M. *J. Phys. B* **6**, L89 (1973). 6, 14

[19] Reiss, H. R. *Phys. Rev. A* **22**, 1786 (1980). 6, 13, 14

[20] Reiss, H. R. *Prog. Quant. Electr.* **16**, 1 (1992). 6, 13, 16, 45, 90, 116

[21] Bauer, D., Milosevic, D. B., and Becker, W. *Phys. Rev. A* **72**, 023415 (2005). 6

[22] Kjeldsen, T. K. and Madsen, L. B. *J. Phys. B: At. Mol. Opt. Phys.* **37**, 2033 (2004). 6, 61

[23] Reiss, H. R. and Krainov, V. P. *Phys. Rev. A* **50**, R910 (1994). 7

[24] Perelomov, A. M. and Popov, V. S. *Sov. Phys. JETP* **25**, 336 (1967). 7, 56

[25] Popov, V. S., Kuznetsov, V. P., and Perelomov, A. M. *Sov. Phys. JETP* **26**, 222 (1968). 7, 56

[26] Perelomov, A. M., Popov, V. S., and Terentev, M. V. *Sov. Phys. JETP* **23**, 924 (1966). 7, 14, 17, 22, 39, 53, 63, 112, 116, 117, 118, 119

[27] Perelomov, A. M., Popov, V. S., and Terentev, M. V. *Sov. Phys. JETP* **24**, 207 (1967). 7, 16, 17, 21, 22, 56, 103

[28] Popruzhenko, S. V., Mur, V. D., Popov, V. S., and Bauer, D. *Phys. Rev. Lett.* **101**, 193003 (2008). 7, 56

[29] Popov, V. S. *Physics Uspekhi* **47**, 855 (2004). 7, 14, 117

[30] Popov, V. S. *Physics of Atomic Nuclei* **68**, 686 (2005). 7, 56

[31] Ammosov, V., Delone, N. B., and Krainov, V. P. *Soviet Phys. JETP* **64**, 1191 (1986). 7, 14, 16, 66

[32] Lewenstein, M., Balcou, P., Ivanov, M. Y., LHuillier, A., and Corkum, P. B. *Phys. Rev. A* **49**, 2117 (1994). 7, 11, 28, 63

[33] Becker, W., Lohr, A., Kleber, M., and Lewenstein, M. *Phys. Rev. A* **56**, 645 (1997). 7, 10, 39

[34] Corkum, P. B. *Phys. Rev. Lett.* **71**, 1994 (1993). 7, 75

[35] Sansone, G., Vozzi, C., Stagira, S., and Nisoli, M. *Phys. Rev. A* **70**, 013411 (2004). 7

[36] Muth-Bohm, J., Becker, A., Chin, S., and F.H.M.Faisal. *Chem. Phys. Lett.* **337**, 313 (2001). 7, 61

[37] Mishima, K., Hayashi, M., and Lin, S. H. *Phys. Rev. A* **71**, 053411 (2005). 7, 61

[38] Kjeldsen, T. K. and Madsen, L. B. *Phys. Rev. A* **71**, 023411 (2005). 7, 61

[39] Faisal, F. H. M., Becker, A., and Muth-Bohm, J. *Phys. Rev. Lett.* **85**, 2280 (2000). 7

[40] Usachenko, V. I., Pyak, P. E., and Kim, V. V. *Phys. Rev. A* **79**, 023415 (2009). 7, 61, 62

[41] Zuo, T. and Bandrauk, A. D. *Phys. Rev. A* **52**, R2511 (1995). 7, 60

[42] Bocharova, I., Karimi, R., Penka, E. F., Brichta, J.-P., Lassonde, P., Fu, X., Kieffer, J.-C., Bandrauk, A. D., Litvinyuk, I., Sanderson, J., and Légaré, F. m. c. *Phys. Rev. Lett.* **107**, 063201 (2011). 7

[43] Long, Z. J. and Liu, W. K. *Can. J. Phys.* **88**, 227 (2010). 8, 32, 33, 35, 36, 53, 54, 94

[44] Becker, W., Grasbon, F., Kopold, R., Milosevic, D. B., Paulus, G. G., and Walther, H. *Adv. At. Mol. Opt. Phys.* **48**, 35 (2002). 9, 14, 63

[45] Smirnova, O., Spanner, M., and Ivanov, M. *J. Mod. Opt.* **54**, 1019 (2007). 10, 58

[46] Kulander, K. C. *Phys. Rev. A* **38**, 778 (1988). 10

[47] Muller, H. G. *Phys. Rev. A* **60**, 1341 (1999). 10

[48] Nandor, M. J., Walker, M. A., , Woerkom, L. D. V., and Muller, H. G. *Phys. Rev. A* **60**, R1771 (1999). 10

[49] Awasthi, M., Vanne, Y. V., Saenz, A., and Castro, A. *Phys. Rev. A* **77**, 063403 (2008). 10

[50] Bransden, B. H. and Joachain, C. J. *Physics of atoms and molecules*. Prentice Hall, England, (2003). 11, 56

[51] Lohr, A., Kleber, M., Kopold, R., and Becker, W. *Phys. Rev. A* **55**, R4003 (1997). 11

[52] Figueira de Morisson Faria, C., Schomerus, H., and Becker, W. *Phys. Rev. A* **66**, 043413 (2002). 11

[53] Milosevic, D. B., Hasovic, E., Busuladzic, M., Gazibegovic-Busuladzic, A., and Becker, W. *Phys. Rev. A* **76**, 053410 (2007). 13

[54] Gribakin, G. F. and Kuchiev, M. Y. *Phys. Rev. A* **55**, 3760 (1997). 14, 63, 116

[55] Bauer, J. *Phys. Rev. A* **73**, 023421 (2006). 14, 56, 63

[56] Vanne, Y. V. and Saenz, A. *Phys. Rev. A* **75**, 033403 (2007). 14, 53, 63, 117

[57] Landau, L. D. and Lifshitz, E. M. *Quantum mechanics*. Pergamon press, London, 3 edition, (1977). 14, 112, 113, 119

[58] Smirnov, B. M. and Chibisov, M. I. *Soviet Phys. JETP* **22**, 585 (1966). 14

[59] Brichta, J. P., Liu, W.-K., Zaidi, A. A., Trottier, A., and Sanderson, J. H. *J. Phys. B: At. Mol. Opt. Phys.* **39**, 3769 (2006). 14

[60] Ilkov, F. A., Decker, J. E., and Chin, S. L. *J. Phys. B* **25**, 4005 (1992). 14, 16

[61] Walsh, T. D. G., Ilkov, F. A., and Chin, S. L. *J. Phys. B* **27**, 3767 (1994). 14

[62] Reiss, H. R. *Phys. Rev. A* **42**, 1476 (1990). 14, 110

[63] Krainov, V. P., Reiss, H. R., and Smirnov, B. M. *Radiative Processes in Atomic Physics*. John Wiley Publication, New York, New York, (1997). 15

[64] Reiss, H. R. and Krainov, V. P. *J. Phys. A: Math.* **36**, 5575 (2003). 15

[65] Bleistein, N. and Handelsman, R. A. *Asymptotic expansions of integrals*. Holt, Rinehart and Winston, New York, (1975). 17

[66] Smirnova, O., Spanner, M., and Ivanov, M. *Journal of Modern Optics* **54**(7), 1019 (2007). 24

[67] Bleistein, N. and Handelsman, R. A. *Asymptotic expansions of integrals*. Dover, New York, (1986). 31, 32, 33, 36, 115, 116

[68] Long, Z. J. and Liu, W. K. *J. Mod. Opt* **85**, 1141 (2011). 32

[69] Bleistein, N. *Mathematical Methods for Wave Phenomena*. Academic Press, Orlando, (1984). 33, 116

[70] Becker, W., Davidovich, L., and McIver, J. K. *Phys. Rev. A* **49**, 1131 (1994). 39

[71] Becker, W., Long, S., and McIver, J. K. *Phys. Rev. A* **50**, 1540 (1994). 39

[72] Colosimo, P., Doumy, G., Blaga, C. I., Wheeler, J., Hauri, C., Catoire, F., Tate, J., Chirla, R., March, A. M., Paulus, G. G., Muller, H. G., Agostini, P., and DiMauro, L. F. *Nature Phys.* **4**, 386 (2008). 45

[73] Blaga, C. I., Catoire, F., Colosimo, P., Paulus, G. G., Muller, H. G., Agostini, P., and DiMauro, L. F. *Nature Phys.* **5**, 335 (2009). 45

[74] Reiss, H. R. *Phys. Rev. Lett.* **101**, 043002 (2008). 45, 50

[75] Kjeldsen, T. K. and Madsen, L. B. *Phys. Rev. A* **74**, 023407 (2006). 51

[76] Popruzhenko, S. V., Paulus, G. G., and Bauer, D. *Phys. Rev. A* **77**, 053409 (2008). 56

[77] Popruzhenko, S. V. and Bauer, D. *J. Mod. Opt.* **55**, 2573 (2008). 56

[78] Vanne, Y. V. and Saenz, A. *Phys. Rev. A* **75**, 063403 (2007). 56

[79] Chirila, C. C. and Lein, M. *Phys. Rev. A* **73**, 023410 (2006). 57, 58

[80] Jaron-Becker, A., Becker, A., and Faisal, F. H. M. *Phys. Rev. Lett.* **96**, 143006 (2006). 61

[81] Etches, A. and Madsen, L. B. *J. Phys. B: At. Mol. Opt. Phys.* **43**, 155602 (2010). 63

[82] Bai, L., ZHang, J., Xu, Z., and Guo, D.-S. *Phys. Rev. Lett.* **97**, 193002 (2006). 66

[83] Yao, G. H., Xu, Z.-Z., and Wei, Y. *Phys. Rev. A* **40**, 5422 (1989). 68

[84] Muth-Bhm, J., Becker, A., and Faisal, F. H. M. *Phys. Rev. Lett.* **85**, 2280 (2000). 68

[85] Mishima, K., Hayashi, M., Yi, J., Lin, S. H., Selzle, H. L., and Schlag, E. W. *Phys. Rev. A* **66**, 033401 (2002). 73, 117

[86] Wörner, H. J., Niikura, H., Bertrand, J. B., Corkum, P. B., and Villeneuve, D. M. *Phys. Rev. Lett.* **102**, 103901 (2009). 75

[87] Cooper, J. W. *Phys. Rev.* **128**, 681 (1962). 75

[88] Lein, M., Corso, P. P., Marangos, J., and Knight, P. L. *Phys. Rev. A* **67**, 023819 (2003). 75

[89] Guhr, M., McFarland, B. K., Farrell, J. P., and Bucksbaum, P. H. *J. Phys. B: At. Mol. Opt. Phys.* **40**, 3745 (2007). 75

[90] Muller, H. G. *Laser Physics* **9**, 138 (1999). 76, 79

[91] Bauer, D. and Koval, P. *Computer Physics Communications* **174**, 396 (2006). 76

[92] Arfken, G. B. and Weber, H. J. *Mathematical methods for physicists*. Academic Press, New York, (1995). 78

[93] Schafer, K. J. and Kulander, K. C. *Phys. Rev. A* **42**, 5794 (1990). 81

[94] H.G.Muller, P.H.Bucksbaum, Schumacher, D. W., and Zavriyev, A. *J. Phys. B: At. Mol. Opt. Phys.* **23**, 2761 (1990). 83

[95] Meyer, M., Cubaynes, D., Glijer, D., Dardis, J., Hayden, P., Hough, P., Richardson, V., Kennedy, E. T., Costello, J. T., Radcliffe, P., Düsterer, S., Azima, A., Li, W. B., Redlin, H., Feldhaus, J., Taieb, R., Maquet, A., Grum-Grzhimailo, A. N., Gryzlova, E. V., and Strakhova, S. I. *Phys. Rev. Lett.* **101**, 193002 (2008). 83

[96] Mauritsson, J., Dahlstrom, J. M., Mansten, E., and Fordell, T. *J. Phys. B: At. Mol. Opt. Phys.* **42**, 134003 (2009). 83

[97] Protopapas, M., Kight, P., and Burnett, K. *Phys. Rev. A* **49**, 1945 (1994). 83

[98] Protopapas, M., Sanpera, A., Kight, P., and Burnett, K. *Phys. Rev. A* **52**, R2527 (1995). 83

[99] Maquet, A. and Taieb, R. *J. Mod. Opt* **54**, 1847 (2007). 83

[100] Shapiro, M. and Brumer, P. *J. Chem. Soc. Faraday Trans* **93**, 1263 (1997). 83

[101] Shapiro, M. and Brumer, P. *Phys. Rep.* **425**, 195 (2006). 83

[102] Schafer, K. J. and Kulander, K. C. *Phys. Rev. A* **45**, 8026 (1992). 83

[103] Schumacher, D. W., Weihe, F., Muller, H. G., and Bucksbaum, P. H. *Phys. Rev. Lett.* **73**, 1344 (1994). 83

[104] Watanabe, S., Kondo, K., Y.Nabekawa, Sagisaka, A., and Kobayashi, Y. *Phys. Rev. Lett.* **73**, 2692 (1994). 83

[105] Agostini, P. *Two-color and single-color above threshold ionization.* Kluwer Academic,Plenum, NY, (2001). 83

[106] Veniard, V., Taieb, R., and Maquet, A. *Phys. Rev. Lett.* **74**, 4161 (1995). 83, 89

[107] Antoine, P., L'Huillier, A., and Lewenstein, M. *Phys. Rev. Lett.* **77**, 1234 (1996). 84

[108] Hentschel, M., Kienberger, R., Spielmann, C., Reider, G. A., Milosevic, N., Brabec, T., Corkum, P., Heinzmann, U., Drescher, M., and Krausz, F. *Nature* **509**, 414 (2001). 84

[109] Drescher, M., Hentschel, M., Kienberger, R., Tempea, G., Spielmann, C., Reider, G. A., Corkum, P. B., and Krausz, F. *Science* **291**, 1923 (2001). 84

[110] Itatani, J., Quere, F., Yudin, G. L., Ivanov, M. Y., Krausz, F., and Corkum, P. B. *Phys. Rev. Lett.* **88**, 173903 (2002). 84

[111] Yudin, G. L., Patchkovskii, S., and Bandrauk, A. D. *J. Phys. B: At. Mol. Opt. Phys.* **40**, F93 (2007). 84

[112] Yudin, G. L., Patchkovskii, S., and Bandrauk, A. D. *J. Phys. B: At. Mol. Opt. Phys.* **41**, 045602 (2008). 84

[113] Ishikawa, K. *Phys. Rev. Lett.* **91**, 043002. 84

[114] Javanainen, J., Eberly, J. H., and Su, Q. C. *Phys. Rev. A* **38**, 3430 (1988). 84

[115] Su, Q. and Eberly, J. H. *Phys. Rev. A* **44**, 5997 (1991). 84

[116] Feit, M. D., A. Fleck, J., and Steiger, A. *J. Comput. Phys.* **47**, 412 (1982). 85

[117] Misra, B. and Sudarshan, E. C. G. *J. Math. Phys.* **18**(4), 756–763 (1977). 86

[118] Tannor, D. J. *Quantum Mechanics a time dependent perspective*. University Science books, USA, (2007). 87

[119] Bivona, S., Bonanno, G., Burlon, R., and Leone, C. *Laser Phys.* **20**, 2036 (2010). 97

[120] Lehtovaara, L., Toivanen, J., and Eloranta, J. *J. Comput. Phys.* **221**, 148 (2007). 100

[121] Čerkić, A., Hasović, E., Milošević, D. B., and Becker, W. *Phys. Rev. A* **79**, 033413 (2009). 104

[122] Faisal, F. H. M., Becker, A., and Muth-Bohm, J. *Laser Phys.* **9**, 115 (1999). 104

[123] Economou, E. N. *Green's Function in Quantum Physics*. Springer-Verlag, Berlin, (1983). Chapter 2. 107, 108, 109

[124] Bjorken, J. D. and Drell, S. D. *Relativistic Quantum Mechanics*. McGraw-Hill, New York, (1964). 110

[125] Holstein, B. R. *Topics in Advanced Quantum Mechanics*. Addison-Wesley, Redwood City, (1992). 110

[126] Goldberger, M. L. and Watson, K. M. *Collision Theory*. Dover, (2004). 110

[127] Bisgaard, C. Z. and Madsen, L. B. *Am. J. Phys.* **72**, 249 (2004). 112, 113, 114

[128] Ivanov, M. Y., Spanner, M., and Smirnova, O. *J. Mod. Opt.* **52**, 165 (2005). 117

[129] Mineo, H., Chao, S. D., Mishima, K., Nagaya, K., Hayashi, M., and Lin, S. H. *Phys. Rev. A* **75**, 027402 (2007). 117

[130] Abramowitz, M. and Stegun, I. A. *Handbook of Mathematical Functions*. Dover, New York, (1972). 118